Characterisation of Modified Glass-ionomer Cements for Medical Applications

Anthony John Turner

Thesis Presented for the Degree of Doctor of Philosophy

The University of Sheffield

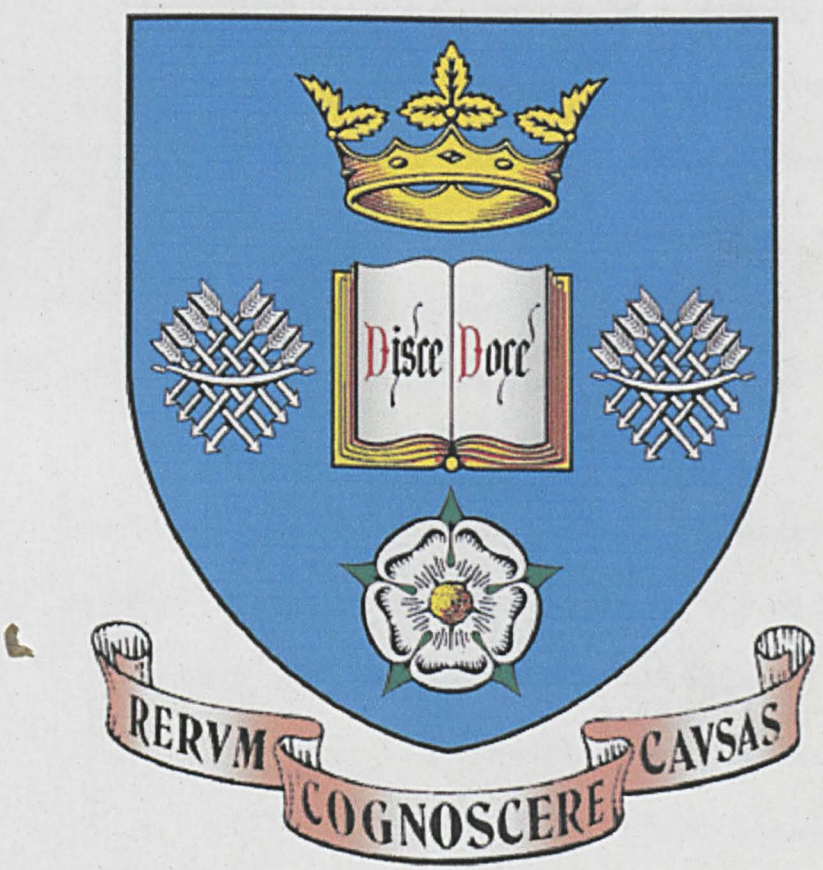

Department of Engineering Materials
The University of Sheffield
Sir Robert Hadfield Building
Mappin Street
Sheffield

April 2005

Acknowledgements

I would like to thank my supervisors Prof John Sharp and Prof Paul Hatton for all their help on this project. Their guidance and advice made this study a success. I would also like to thank Prof Ian Brook for his help and advice.

I am grateful for the support and enthusiasm shown by the technical staff of both the Engineering Materials Department and the School of Clinical Dentistry at Sheffield University. Special thanks are in order for Mr I Watts and Mr D Haylock for their expert help on glass manufacture and processing without which this project would have been not been a success. I would also like to thank Miss Beverly Lane for her extensive support and expertise with the thermal analysis of the ionomer glasses. Thanks to Mr B Keeley for helping with the XRD and Mrs J Mundy for advice and assistance on the biocompatibility studies.

Further thanks to the Centre For Analytical Sciences (Chemistry Department, Sheffield University) and its technicians for carrying out ICP of the ion release samples, Dr Fred Wilburn for his knowledge and help with further DTA analysis and understanding, and Mr W Simpson of Glassworks UK who supplied materials and helpful advice on the manufacture of coloured GICs. Finally I would like to thank Dr Adrian Brough (University of Leeds) for his enthusiasm and dedication to the NMR project.

Abstract

Medical-grade glass ionomer cements (GICs) are commercially available for surgical implantation in otology. GICs have advantageous properties as a bone replacement material, including the ability to bond to mineralised tissue such as bone and a good biocompatibility *in vivo*. However, cement compositions are largely based on the GIC dental cement compositions they were derived from and are not optimised for use in medical applications. The specific objective of this project was to produce improved GICs for surgical application in otology, based upon a commercially available bone cement and tailor the properties to the specific needs of the surgeon while preserving the beneficial properties of the original composition.

Novel GICs based on the substitution of calcium with either strontium, barium or a mixture of species in the ionomer glass component were fabricated and characterisation of the glass and cements undertaken in addition to NMR (nuclear magnetic resonance) analysis of the effect of additives in GICs setting reactions.

The substitution of strontium and barium ions produced cements with improved properties that compared favourably with the commercial material (SerenoCem®) used as a control in this study. Radiopacity and biocompatibility were enhanced without a significant negative effect on the cement properties. XRD (X-Ray Diffraction) of the heat-treated glasses identified Sr/Ba analogous phases present to those reported previously in the literature.

It was concluded that modified ionomer glasses based on the SerenoCem® medical cement composition, tailored for improved properties, will allow the material to accommodate the specific needs of the surgeon and therefore increase clinical viability in bone replacement surgery.

Abbreviations and Nomenclature

π	Pi.
λ	Wavelength.
Å	Angstroms.
°C	Degrees Celsius.
µm	Micrometers.
Ø	Diameter.
°	Degrees.
cm	Centimetres.
DTA	Differential Thermal Analysis.
EDS	Energy Dispersive Spectroscopy.
ENT	Ear, nose and throat.
g	Gram.
GIC/GICs	Glass Ionomer Cement/Glass Ionomer Cements.
GIC (**)	GIC prepared from Glass (**).
Glass (**)	Glass powder of the composition (**).
ICP-ES	Inductively coupled plasma – emission spectroscopy.
kHz	Kilohertz.
kV	Kilovolts.
mA	Milliamps
mg	Milligrams.
ml	Millilitres.
mm	Millimetres.
Mol%	Molar Percentage
MPa	Megapascals.

MTT	Methyl thiazolyl tetrazolium.
N	Newtons.
NMR	Nuclear magnetic resonance.
RMM	Relative Molecular Mass.
ROS cells	Rat osteosarcoma cells.
SEM	Scanning Electron Microscopy.
TEM	Transmission Electron Microscopy.
Tg	Glass Transition Temperature.
T_{X*}	Temperature of Crystallisation of phase X and of phase number *.
Wt%	Weight Percentage
XRD	X-Ray Diffraction.

Contents Page:

Heading	Page Number
Acknowledgements	ii
Abstract	iii
Abbreviations and Nomenclature	iv
Contents	vi
1. Introduction	1
2. Literature Survey	3
2.1 GICs	3
2.1.1 Dental Materials	4
2.1.2 GICs	8
2.1.2.1 Introduction and History	8
2.1.2.2 Setting Reaction	11
2.1.2.3 Structure and Properties	17
2.2 GICs in Medical Applications	20
2.3 Ionomer Glasses	24
2.3.1 Ionomer Glasses	24
2.3.2 Coloured Glasses	28
3. Experimental Procedures	30
3.1 Glass Preparation	30
3.1.1 Strontium Substituted Glass Compositions	31
3.1.2 Substituted Glasses Incorporating Ca, Sr and Ba	32
3.2 Glass Characterisation	34
3.2.1 Particle Size Analysis	34
3.2.2 XRD and DTA of the Prepared Glasses	35
3.2.3 Characterisation of the Heat Treated Glasses	36
3.2.4 TEM and EDS	36
3.3 Cement Characterisation	37
3.3.1 Gilmore Needle Indentation Test	38
3.3.2 Radiopacity	38
3.3.3 Flexural Strength	39
3.3.4 Ion Release	40
3.3.5 Biocompatibility	40

3.3.6 Coloured Ionomer Glass Compositions 41
3.3.7 NMR 43
4. Results 45
4.1 Glass Preparation 45
4.2 Glass Characterisation 46
4.2.1 Particle Size Analysis 46
4.2.1.1 Strontium Substituted Glasses 46
4.2.1.2 Substituted glasses incorporating Ca, Sr and Ba 51
4.2.2 XRD and DTA of the Prepared Glasses 57
4.2.3 Characterisation of the Heat Treated Glasses 65
4.2.4 TEM and EDS 81
4.3 Cement Characterisation 83
4.3.1 Gilmore Needle 83
4.3.2 Radiopacity 85
4.3.3 Flexural Strength 89
4.3.4 Ion Release 92
4.3.5 Biocompatibility 95
4.3.6 Coloured GICs 97
4.3.7 NMR 99
5. Discussion 104
5.1 Glass Preparation 104
5.2 Glass Characterisation 105
5.2.1 Particle Size Analysis 105
5.2.1.1 Strontium Substituted Glasses 106
5.2.1.2 Substituted glasses incorporating Ca, Sr and Ba 108
5.2.2 DTA, Heat treatment and XRD 108
5.2.3 Characterisation of the Heat Treated Glasses 112
5.2.3 TEM and EDS 114
5.3 Cement Characterisation 114
5.3.1 Gilmore Needle 114
5.3.2 Radiopacity 117
5.3.3 Flexural Strength 120
5.3.4 Ion Release 122
5.3.5 Biocompatibility 124
5.3.6 Coloured GICs 125
5.3.7 NMR 127
6. Conclusions 133

7. Further Work **135**
8. References **136**
9. Appendices **144**

1. Introduction

Medical-grade glass ionomer cements (GICs) are commercially available for surgical implantation in otology. GICs have advantageous properties as a bone replacement material, including the ability to bond to mineralised tissue such as bone and a good biocompatibility *in vivo*.

SerenoCem® (Corinthian Medical, UK), a commercial medical-grade glass ionomer cement (GIC), is currently used in Europe for reconstructive surgery of the middle ear. In addition, this material has recently received regulatory permission for use in the USA in 2001 [1]. The unique biological and physical properties of SerenoCem® have allowed the material to find a niche market in certain aspects of middle ear surgery.

While licensed for specific otological applications, the cements used are broadly similar in composition to many dental cements and not optimised for use in medical applications. Surgeons would appreciate a number of modifications to existing compositions in order to improve their clinical viability. Potential modifications include improved handling characteristics to aid placement and ease of use, coloured glasses to allow coloured cements for revision surgery, enhanced mechanical properties, and superior radiopacity to assist postoperative detection and care.

One potential modification is the substitution of calcium ions by strontium ions in the glass. While this approach has been employed in dental biomaterials to increase radiopacity, no Sr^{2+}-based medical GIC bone cements have been reported to date. Moreover, no reports of the effect of this substitution or the use of Ba^{2+} ions on cement properties have appeared in the literature.

The aim of this project was to produce commercially viable glass ionomer cements with improved properties over existing commercial GICs for surgical implantation in otology. The specific objectives of this project were to produce novel glass compositions based on the substitution of strontium, barium or a combination of the two species for calcium, and fully characterise their properties and those of the resultant cements. Secondary objectives were to obtain coloured ionomer glasses using colouring agents for use in cements for paediatric dentistry and further, to advance our understanding of the structure-property relationships involved in the setting reaction of a GIC using techniques such as NMR to follow the affect of tartaric acid on the set. All novel compositions were compared to a commercially available GIC bone cement, SerenoCem®.

2. Literature Survey

2.1 GICs

Glass-ionomer cements (GICs) have been used successfully in dental applications for over thirty years and are widely regarded as an effective restorative material [2]. GIC popularity amongst dental practitioners is based on a number of specific factors including adhesion to dentine and enamel, reasonable aesthetics, fluoride release *in vivo* and good biocompatibility. Fluoride ion release from GICs has been reported to inhibit caries and may provide increased resistance to acid attack on the tooth tissue surrounding the restoration [3].

Despite its advantageous properties, the glass-ionomer cement has limited oral application due to a weak diametral tensile (a clinically significant measurement of the stress undergone by the tooth or replacement material during chewing which involves three vectors of force) and flexural strength, dissolution of the immature cement on setting, poor translucency, and a degree of clinical variability (overcome by capsulation delivery systems).

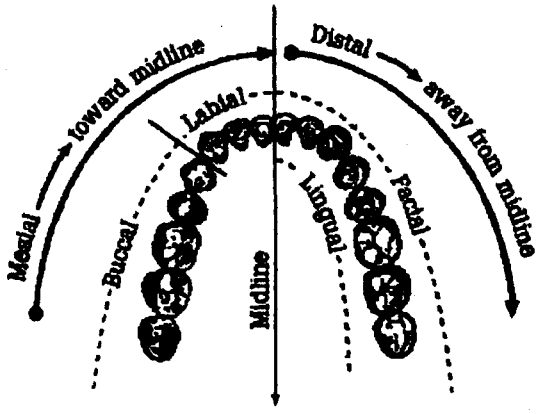

Figure 2.1: Dental positioning or surface terms [4].

These factors have led to the GIC being primarily used as non-load bearing restorations (Class V gingerval third of the labial, bucal, lingual or palatal surfaces of teeth), luting cements, and as adhesive liners for composite restoratives (for a general overview of tooth structure and spatial terms see *Figure 2.1* and *Figure 2.2*) [2]. Advances in materials and oral preparation have widened the use of GICs in dental applications, extending them to Class III (cavities originating on the proximal surfaces of incisors and canines and not involving the incisal angle), Class I restorations, and for core replacement under crowns.

Following the cements success as a dental restorative material, GICs found a niche in medical applications and are now used in Europe for reconstructive surgery of the middle ear and posses the potential for wider application in intensive medical areas such as bone cementation and reconstruction [1]. Additional properties that make the GIC attractive for use as a bone substitute include a negligible setting exotherm, adhesion to bone and metals, biomechanically matched formulations that may be easily moulded and shaped at the implant site with no shrinkage on setting, and bioactivity due to the release of osteoconductive ions (such as fluoride and aluminium).

2.1.1 Dental Materials

Mineralised tooth tissue is an integral part of the human digestive system, allowing the mastication of food into components that are easier to process by the body (*Figure 2.2*). Patient dentition is a significant factor in the aesthetics of the face and mouth, an increasingly prevalent aspect in modern dentistry. Tooth tissue, a mix of organic and mineral phases, may be damaged by a variety of mechanisms including mechanical

trauma including erosion, and disease. One of the most prominent causes of failure is by caries, a disease of the mineral and organic tissue, that form enamel and dentine.

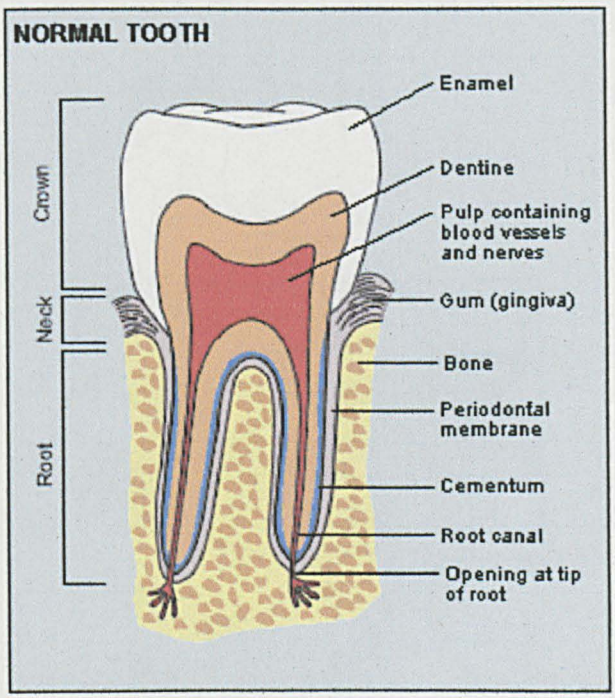

Figure 2.2: Structure of the tooth [5].

The general structure of a tooth consists of two important layers. Enamel forms the calcified surface layer of the tooth structure and is the most densely calcified tissue of the body, consisting of 96% by weight of the mineral phase hydroxyapatite ($Ca_{10}(PO_4)_6(OH)_2$). The remaining 4% is organic material and water. The prismatic structure of enamel is weak and may be sheared or fractured along its boundaries (*Figure 2.3*). Dentine is the inner layer of the tooth structure, protecting the sensitive pupal cavity. 20% of dentine is organic, providing a tough and slightly elastic material [2].

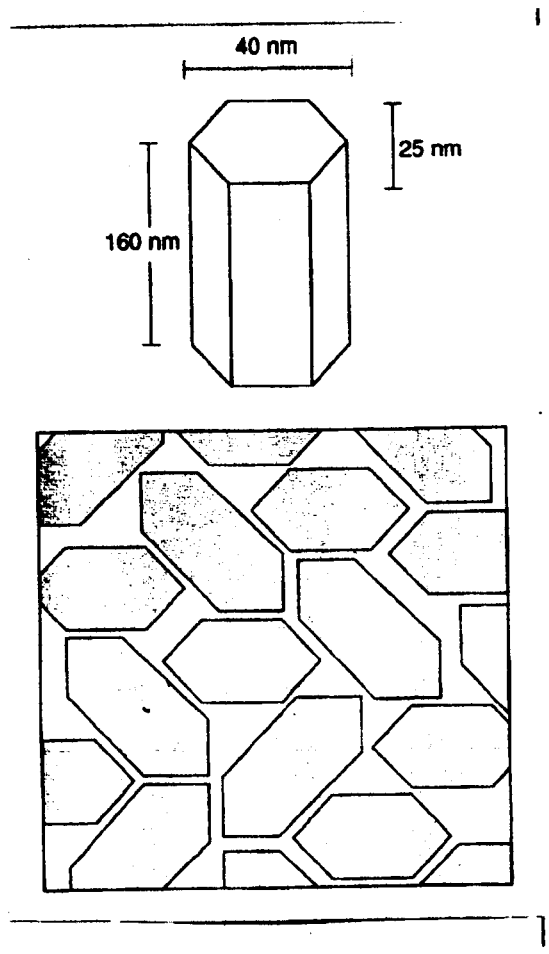

Figure 2.3: Schematic of the apatite crystal structure of enamel [2].

Dental caries effects the mineralised tissues of the tooth ultimately leading to demineralisation and disintegration of the mineral and organic components respectively. This process is initiated by the absorption of a mix of bacteria and their products (dental plaque) onto the enamel surface. The action of micro-organisms on fermentable carbohydrates leads to acidic metabolic bi-products and therefore, a decreased pH and eventual dissolution of the hydroxyapatite salt and loss of organic material [3]. Severe pain is associated with the percolation of harmful bacteria causing pupal inflammation. The increase in prominence of dental caries in the western world has led to a greater need for repair and restoration. The absence of a natural replacement for damaged or diseased tooth tissue dictates that synthetic materials must be utilised to fabricate an

effective dental restorative material. An ideal restorative material would combine strength, fluoride release capabilities, facile, better adhesion to bone, biocompatibility, and similar aesthetics to the host dentition.

Table 2.1: General overview of the materials used in dentistry.

Material	Advantages	Disadvantages
Ceramics	Good aesthetics, strong.	Wear, brittle fracture, poor bonding.
Metals	Strong and well understood.	Poor aesthetics, disputable biocompatibility, and expansion mismatch.
Polymers	Good aesthetics, cheap.	Poor mechanical properties, wear and suffer from biodegradation and leaching.
Composites	Tailored properties such as aesthetics and expansion coefficient.	Generally lack strength and are susceptible to wear.

A general list of properties for the basic subgroups of restorative materials can be found in *Table 2.1*. No single class of material can fulfil the many needs of the clinician and patient. Therefore, to fulfil these requirements, composites of the main material classes have been developed to tailor the material properties to the application.

Glass-ionomer cements have become one of the most researched groups of dental materials due to a number of advantageous properties including superior adhesion to enamel and dentine by hydrogen and ionic bonding, and the gradual release of fluoride

in vivo [2]. GICs can also be colour matched to enamel and radiopacity tailored with the incorporation of heavy metals. Despite these benefits, GICs have limited application due to their low tensile strength, brittle nature, and early susceptibility to water on setting. The following *Section 2.1.2* describes the GIC in further detail including its setting chemistry and structure.

2.1.2 GICs

2.1.2.1 Introduction and History

Polyalkenoate cements or glass-ionomer cements (GICs) were invented in 1969 at the Laboratory of the Government Chemist by Wilson and Kent. Original research stemmed from the dissatisfaction of dental practitioners with the common dental silicate cements [2]. Initial commercial acceptance was slow and the first commercial GIC product, termed ASPA (AluminoSilicate PolyAcrlyic) by De Trey, was released in 1976 to a mixed response from the dental community and was not a great success due to its limited handling characteristics [2].

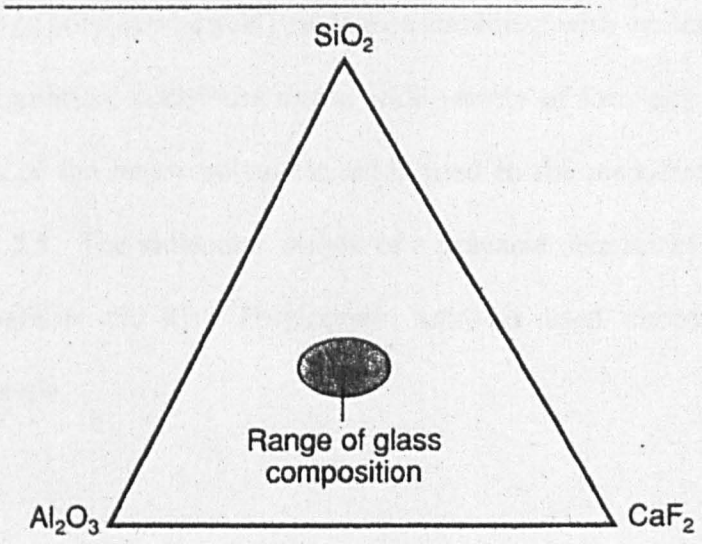

Figure 2.4: Range of ionomer glass compositions used in GICs [2].

Improvements to the original design of the cement have resulted in a large variation in the composition of current commercial materials. However, compositions are restricted to the region indicated in *Figure 2.4*. Glasses formed outside of this range tend to crystallise or phase separate upon quench cooling [2]. Initial improvements were hampered by a poor knowledge of their setting chemistry but recent studies, such as those by A.D.Wilson and J.W.Nicholson [7, 8], have improved understanding of the structure and property relationships inherent to the GIC. Comprehension of the setting chemistry of a GIC is crucial in predicting the microstructure and eventual properties of the cement.

A GIC is formed by two methods:

1. Mixing a glass powder with an aqueous solution of a poly(acrylic) acid.
2. Mixing a glass powder containing freeze-dried poly(acrylic) acid with water.

Polyalkenoate cements are available in a wide variety of customized forms that determination of their setting chemistry can be difficult [2, 8]. Variables include the glass composition and reactivity or the polyacid with which it reacts [2].

A large range of poly(acrylic acid) analogues combined with variations in molecular weight and configuration, contribute to the wide variety of formulations available for use. Schematics of the major polymeric acids used in the manufacture of GICs are shown in *Figure 2.5*. The molecular weight of a polyacid determines its viscosity and therefore handleability [2, 9]. Poly(acrylic acid) is used almost exclusively in commercial materials.

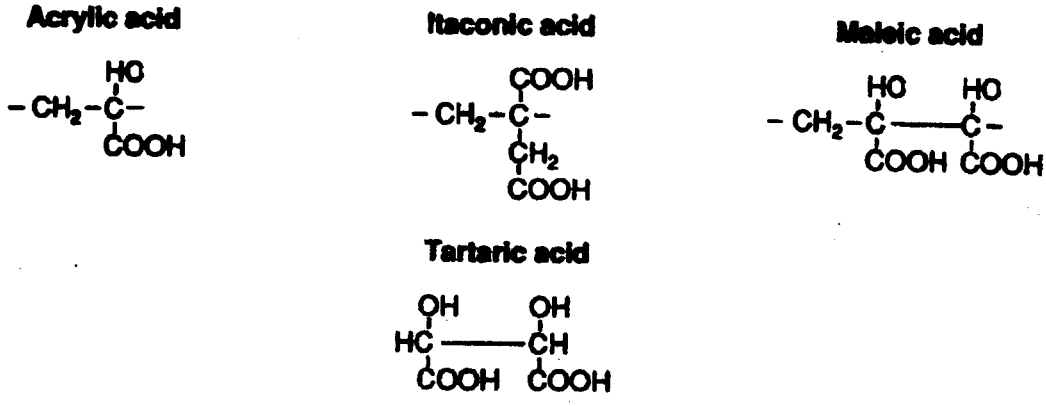

Figure 2.5: Some important polyacids and setting additives used in GICs [2].

Studies on polyacid copolymers have been noted in the literature. The copolymer poly(vinylphosphonic acid) was shown to have potential as a GIC component, improving the initial stability of the cement to hydrolytic attack [10, 11]. Maleic acid is an effective polymer or copolymer due to a high density of functional groups that give an increased crosslinking density. A higher crosslinking density provides better strength but a more brittle cement [8, 12]. Changes to the polymer component have been shown to increase GIC strength due to matrix failure being the significant cause of cement failure [13]. Further additions to the liquid component of the GIC have been studied. Tartaric acid is a major addition to the setting reaction of commercial GICs.

These will be discussed further in *Section 2.1.2.2.* Ionomer glasses used in the manufacture of GICs will be discussed in *Section 2.3.*

2.1.2.2 Setting Reaction

GICs set by an acid-base reaction between the acidic polymer and a basic glass. The following mechanism is based on the mixing a glass powder containing freeze-dried poly(acrylic acid) with water. Combining a glass powder with an aqueous solution of a poly(acrylic acid) uses the same mechanism but the polyacid has already dissociated prior to mixing. The setting reaction of glass-ionomer cements consist of three overlapping stages:

- Dissolution
- Gelation
- Hardening

The three distinct phases are a result of the varying release rates of the crosslinking species from the glass particles (calcium and aluminium ions) and the hardening of the polymer matrix with time [2]. Dissolution is the first stage of the setting reaction upon mixing of the cement constituents. Water liberates the hydrogen ions from the polymeric acid forming dissociated carboxyl groups. The hydrogen ions chemically attack the surface of the glass particles releasing the network cations (Ca^{2+}, Al^{3+}). The composition of the ionomer glass involved in the setting reaction can determine the rate of chemical attack and is further discussed in *Section 2.3.1.* To maintain electrical neutrality the hydrogen ions that are released diffuse into the glass and relieve the net negative charge. Therefore, elution of the aluminium and calcium ions from the surface

of the glass particles result in a cation-deficient zone, referred to as a siliceous hydrogel layer [4].

Conflicting papers on this subject contend that Si^{4+} is also leached from the glass network. This was suggested by Hatton and Brook (1992) who proposed the silicon ions were not confined to the outer depleted layer but were involved in crosslinking of the polycarboxylate following the discovery of Si in the matrix with EDS [6]. Matusya *et al* (1996) investigated the setting chemistry of GICs using NMR and infrared spectroscopy to further understand the structural change during hardening and confirm the role of the silica phase [14]. ^{27}Al NMR analysis showed Al^{3+} ions in a tetrahedral coordination with the oxygen in the original glass. As the setting reaction progressed towards completion a fraction of the Al^{3+} ions became octahedrally coordinated to form the Al polyacrylate gel. A chemical shift was observed in the ^{29}Si NMR spectra of the glass and cement during hardening. The shift was attributed to chemical variation and structural change in the silicate network and the silicate network was inferred to play a significant part in the increase in GIC strength after gel formation [14]. Nicholson (1998) agreed with Hatton and Brook and postulated that, since the acetates of calcium and aluminium are soluble, silicon and phosphorus are released to form an interpenetrating inorganic network of their own that contributes to the improved insolubility of the cement [8]. Nicholson referred to this stage as a large-scale dissolution rather than an ion exchange. This was contested by Maeda *et al* (1999) who used a SIMS technique to show that silica was only found in the silicious layer, a silica gel layer that surrounds the glass particle forming a 'halo' non-electron dense region [15].

Gelation is the second phase of the setting reaction and involves the initial set or 'gel' of the polymer matrix. Free cations (Ca^{2+} and Al^{3+}) form crosslinks or 'bridges'

between the dissociated carboxyl groups of the polycarboxylates. The initial set occurs within a few minutes. Calcium ions being divalent can diffuse quicker and are the initial crosslinking species to bridge the polymer matrix. Aluminium release and crosslinking is slower (being trivalent), although there is uncertainty in the role of aluminium in the setting reaction caused by the detection of aluminium ions early in the setting process. Nicholson speculated that the aluminium ions form complexes that are not immediately available for the reaction and extraction of discrete ions is expected to be slow [8].

The final stage involves the hardening of the cement and is marked by the formation of aluminium bridges between the carboxyl groups. A typical final setting time is considered to be between five and ten minutes, although, the cement gradually hardens over a longer period of time to its final set. Crosslinking of the trivalent aluminium ions results in stronger and more numerous bonds and a final set over time [2]. The setting reaction of a GIC is summarised in *Figure 2.6*. This theoretical structure was observed in the transmission electron microscope and described by Hatton and Brook in 1992 [6].

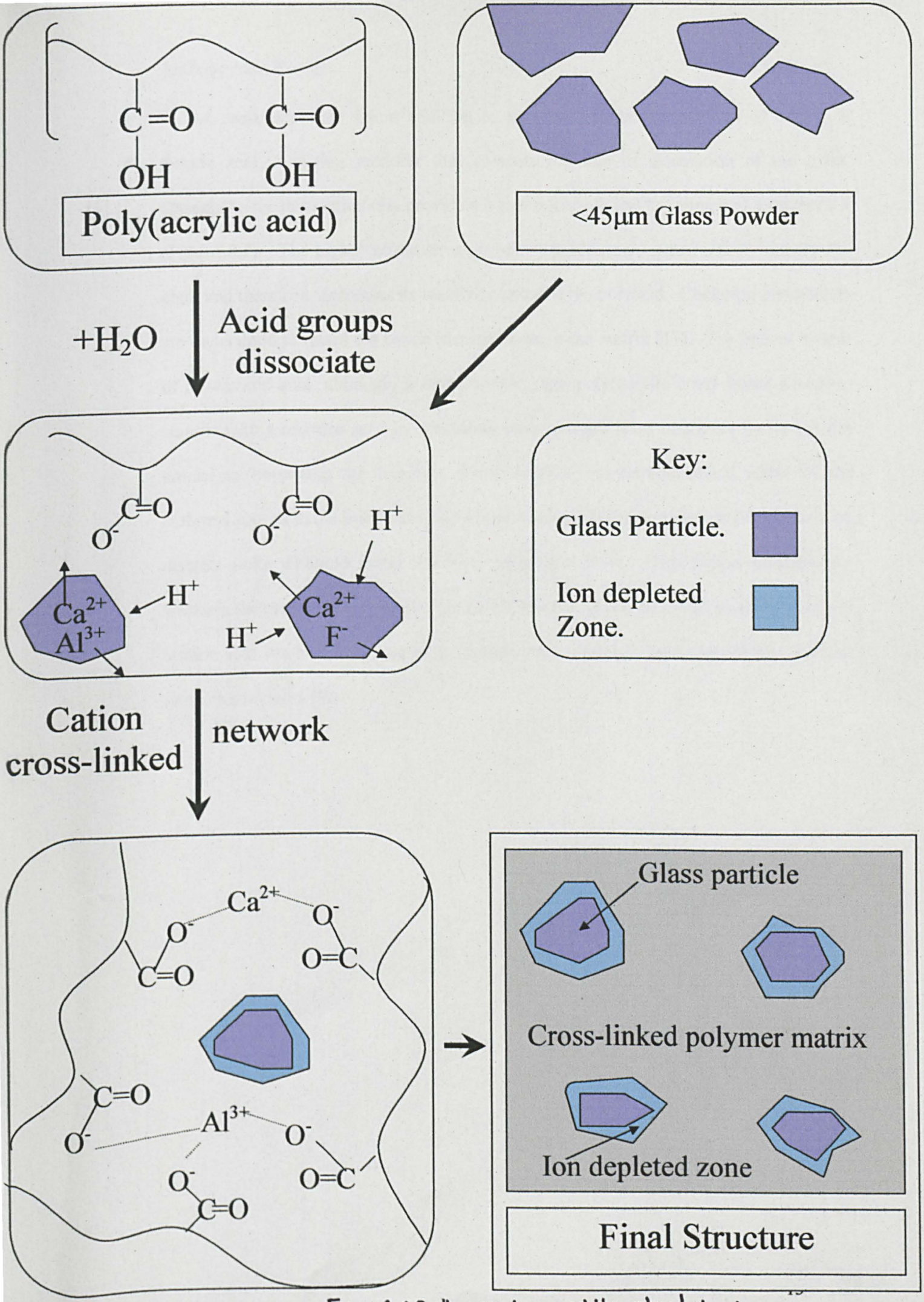

Figure 2.6 Setting reaction and theoretical structure of a GIC.

The most important liquid addition to the dynamic setting reaction of a GIC is tartaric acid, a setting modifier that controls the rate of dissolution of the glass. Changes to the dissolution rate provide a better initial clinical handling and a sharper set (*Figure 2.7*). The higher acidic strength of (+)-tartaric acid preferentially attacks the glass and therefore, decreases its reactivity towards the polyacid. Chelating compounds are understood to retard the cation incorporation in the matrix [17]. The optical isomer of (+)-tartaric acid, although, a stronger acid than poly(acrylic acid) forms a weaker cement with a retarded set. In conclusion acid strength is an important factor but not crucial to improving the handling characteristics. A stereochemical effect of the carboxyl groups in the isomer act as a bridge between polyanion chains and, by forming discrete units withhold metal ion from polyanion chain. This delays gelation and weakens the cement [18]. The compressive strength of cements with small additions of tartaric acid has also been shown to be improved, although, the origin of this increase remains a mystery [8].

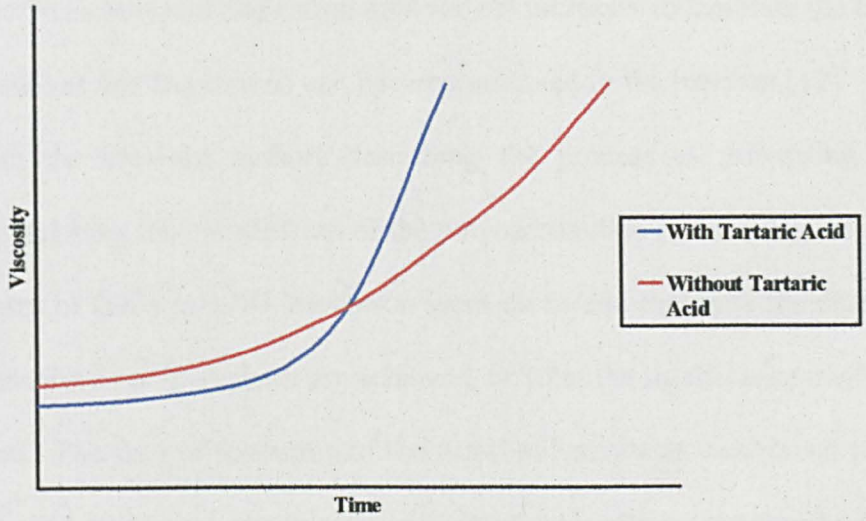

Figure 2.7: Clinical effect of tartaric acid on the setting profile of a GIC [2].

The initial work on chelating agents in GICs was done by A.D.Wilson *et al* in 1976 to improve the formula of the ASPA cement. Using a Gilmore Needle and oscillating rheometer Wilson *et al* surveyed a range of additives and measured their effect on the setting properties of the cement. Tartaric acid proved to be such a successful addition that it is still the major chelating agent in modern commercial systems [16]. The original studies concentrated on the potential improvements to the working and setting times of the cement, borne out of a clinical need. In 1981 Prossler *et al* further investigated additions to the cement by applying modern infrared spectroscopy techniques to determine how the chelating agents adapt the chemistry of the set [12]. The acid-base reaction was concluded to be modified by the acidity of the setting environment. In general the setting reaction could be slowed (basic additions) or accelerated (acidic additions), although, the authors suggested that stronger acids and bases do not necessarily have an increased effect on setting rates. Additives that extend the working time impair the extraction of cations and an extension in the setting time was attributed to the formation of base-polyacid complexes, which block crosslinking

reactions between polyacid and cation until the pH increases to facilitate the break down of the complexes and the cations can become involved in the reaction [12]. Crisp *et al* agreed with the previous authors describing the process as preventing premature gelation by delaying the crosslinking of the polycarboxylate chains [18]. In a review of the chemistry of GICs in 1998 Nicholson went on to add that how the changes to the rate of formation of polyacrylates are achieved, or what the significance might be, is not yet apparent. The time of formation of the metal polyacrylates was shown to vary with the addition of tartaric acid; the calcium salts form more slowly, but the aluminium ones form more rapidly [8]. However, the application of excess tartaric acid (approx >20%) retards and weakens the cement. Higher concentrations of acid reduces the cements resistance to aqueous attack and effects cement solubility [18]. Fluoride ions have also been shown to improve 'workability' and have an influence on the setting characteristics of fluoride containing GICs by the formation of aluminium fluoride complexes that aid extraction of the cations and prevent premature incorporation into the matrix [17]. Although, there is no direct evidence of such species and other structures and bonding patterns not yet apparent may occur [8].

2.1.2.3 Structure and Properties

The set GIC microstructure consists of a cation cross-linked polycarboxylate matrix surrounding alumino-silicate reacted glass particles, which act as a filler (*Figure 2.6*). The surface of the glass particles is cation deficient. This structure has been confirmed by Hatton and Brook using TEM [6]. The microstructure is a crucial factor in determining the properties of a GIC and its application.

Fluoride release is a beneficial dental property associated with glass-ionomer cements. Fluoride release *in vivo* is associated with an anticariogenic effect through a structural and metabolic process. Incidence rates for secondary caries in areas surrounding a GIC restorative have been studied and shown to be reduced [3]. The presence of fluoride has been shown to inhibit demineralisation resulting from caries by an ionic exchange with the hydroxide ion (OH^-) of hydroxyapatite. The resulting structure, known as fluorapatite, has increased resistance to dissolution, is less adhesive to cariogenic substances due to a lower surface energy, and exhibits a cariostatic effect [3]. Further studies have discussed the dependence of any anticariogenic effect and the amount of fluoride released but crucially the longevity of the fluoride elution [19]. The mechanism of fluoride release has been the focus of numerous studies for both long and short-term release [20-23]. Fluoride release is analogous to the majority of GIC properties and the cements dependence on a number of variable factors. Working and setting times, porosity, pH, environmental changes, and the initial fluoride content and structure of the glass are all important in the release of fluoride from the cement. Recharging the fluoride content of GICs using a NaF gel to simulate ion uptake orally after brushing have been successful, although, the improvement is limited [24].

Several hypotheses for the mechanism of fluoride release have been suggested. Tay and Braden (1987) concluded that there are two processes involved in fluoride elution, a rapid surface release and a slower bulk diffusion process [21]. De Witte *et al* (1999) carried out concentration studies of fluoride release and applied a weighted linear regression analysis of their findings, corroborated the mathematical analysis of Tay and Braden [23]. Fluoride is initially liberated from the glass structure during dissolution by the dissociated H^+ attack of the glass surface and as complexes with the aluminium as the cement hardens (*Section 2.1.2.2*). A significant initial rapid release or 'wash out' of

fluoride ions occurs as the ions are less tightly held in the matrix. The second phase of the release mechanism is limiting as fluoride ions diffuse greater distances to be released from the cement [21].

Other ions are released from GICs *in vivo*, however, they are less important in the oral environment. Ion release in medical applications is extremely important and a crucial factor in determining biocompatibility (for a more detailed discussion see *Section 2.2*)

The mechanical properties of a GIC are important in determining its application and effectivness *in vivo*. Numerous studies have been undertaken to examine the mechanical properties of GICs and suggest techniques to improve the cement strength for dental and medical applications [13, 25, 26]. Prosser *et al* commented that the most appropriate measure of strength of GICs is obtained with a flexural test as a GIC would only fracture at the atomic level by tensile or shear failure [27]. Xie *et al* investigated a number of mechanical properties and examined the fracture sufraces of the tested samples to ascertain the relationship between mechanical properties and microstructures of GICs [13]. Flexural strength measurements of 10-25 MPa were obtained for conventional GICs, however, resin modified GICs showed a significant improvement at approx 80 MPa. Cement failure was attributed to matrix fracture at the glass-matrix interface with the paths of crack propagation linking microstructural features. Microstructural factors such as the integrity of the glass-matrix interface, particle size, and the number of voids all contribute to the mechanical properties of a GIC [13].

2.2 GICs in Medical Applications

Improvements to the original material have allowed the GIC to become a successful dental material. With the glass-ionomers ability to bond to mineralised tissue (through hydrogen and ionic bonding of the polycarboxylate groups to the hydroyapatite surface [2]) and good biocompatibility it was ultimately considered a potential material for medical applications. Studies by Jonck (hip replacements), Brook (bone substitute for oral & maxillofacial surgery) and Geyer (otology) gave rise to optimism regarding the use of GICs for medical applications [28-33].

It was not until 1993 that evidence of problems with the surgical implantation of the glass-ionomer cements was reported. Renard *et al* reported cases of aluminium encephalopathy (accumulation of aluminium in the blood associated with Alzheimer's disease, a progressive, neurodegenerative disease characterised by loss of function and death of nerve cells [34]) after application of glass-ionomer bone cement Ionocem® (Ionos, Germany) in skull repair surgery [35]. Aluminium solubility is low at neutral pH but as pH increases and aluminium acts as a proton acceptor it is most likely released in the first few mins as discussed preciously. Exposure to water causes significant polymer loss and therefore, the ions released in the early stages of setting would be released *in situ*. One study measuring ionic release in the presence of water showed that the amount of aluminium ions locally was an order of magnitude greater than prefabricated implants [36]. Problems with this aluminium release from GIC during early water exposure led to a revision of the formulation of medical GICs, and the addition of many contraindications for use (e.g. skull-based surgery).

SerenoCEM® (Corinthian Medical Ltd, Nottingham, UK) medical bone cement was licensed for use in otological applications in 2001 [1]. SerenoCem® is available for

applications where aluminium release is not a critical factor. However, the risks associated with aluminium release *in vivo* need to be eliminated or reduced. Direct removal is not a viable alternative as aluminium and the Si:Al ratio is critical in determining cement properties (see *Section 2.3*)

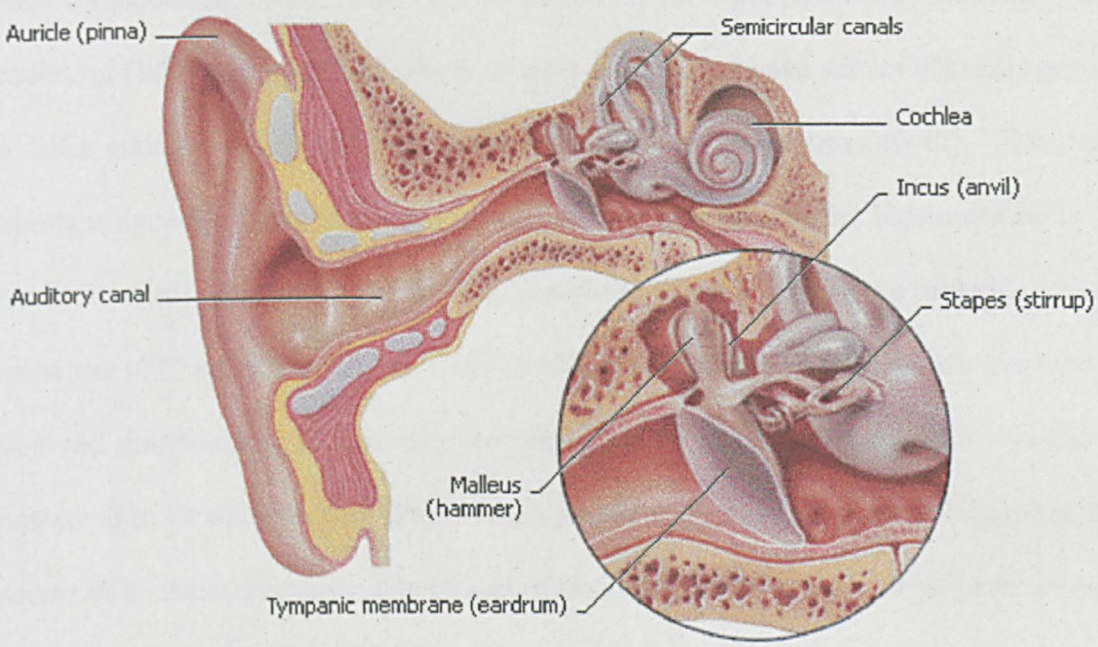

Figure 2.8: The structure of the human ear [37].

Despite the contraindications applied to GICs in medical applications, they have found a use in otology as surgical cements. Loss of function, the need for repair and reconstruction due to trauma and disease has increased the demands for materials in hard tissue replacement. SerenoCem® is used in non-weight bearing applications and ossiculoplasty procedures, such as fixation of cochlear implant electrodes and implantable hearing aids, repair of the intricate ossicular chain (malleus, incus and stapes) and in reconstruction of the canal wall (see *Figure 2.8*) [38]. GICs in medical applications offer improved properties to the surgeon such as the lack of an exotherm,

the ability to bond to bone or metallic implants (good mechanical cementation of implants), minimal shrinkage, and good bioactivity or biocompatibility.

The clinical success of a biomaterial in tissue replacement is the formation of a stable bone-implant interface and the ability to attract and bind bone cells. The surface of a GIC is hydrophilic and is able to bind factors that mediate the regulation of osteogenic (bone remodelling) cells. The GIC is therefore, an osteoconductive material [39]. Studies on GIC biocompatibility (both *in vitro* and *in vivo*) have shown that cells grown on GICs maintain cell phenotype and have 'bioactive' properties [40-42]. The most important dynamic factor relating the composition of a GIC to the biocompatibility *in vivo* is the release of ions. After the gelation phase of setting, there is a mobility of ions within the GIC and exchange with the *in vivo* environment. Ion release is dependant upon the composition of the ionomer glass. The application of 'wet' cement is considered to be toxic *in vivo* [35]. Glass particle size is another critical factor in the success of a cement implant. The causes of toxicity associated with larger particles size and higher powder liquid ratio *in vivo* are considered to be related with un-reacted acid and ongoing metallic ion release. Smaller sized particles have been shown to have a minor toxic effect on rat bone tissue with a later disturbance of adjacent bone formation [44].

Fluoride release in dental GICs is an important property but it is also affects the biocompatibility of a medical cements. Non fluoride based cements were shown to be less toxic *in vitro* but less osteoconductive *in vivo*. This led to research into the dose dependence effect of fluoride ions *in vivo*. High doses are detrimental to the dynamics of bone remodelling as the incorporation of fluoride into the hydroxyapatite mineral structure (in exchange with the OH^- groups) changes the unit cell size and has a toxic effect on the physiological environment. Changes to the mineral structure lead to a

bone structure of lower quality. Low doses have been shown to be beneficial to the local environment and aid implant incorporation by increasing bone formation (stimulating bone forming cells) and trabecular bone density as seen in an number of studies [43-48]. Strontium ion release *in vivo* has been investigated and found to be dose and distribution dependant with low doses depressing bone resorption and maintaining bone formation [49]. The combination of both fluoride and strontium ions on bone remodelling have led to research on the treatment of osteoporosis [45, 48]. Research into the effects of strontium based chemicals as a drug to aid osteoporosis is under investigation in a number of studies. Local strontium concentration in rats was found in low concentrations to interfere with bone formation at the level of cell differentiation, whereas at higher concentration it disturbed the mineralization process which is indicative of strontium interference with hydroxyapatite formation [50]. A recent study by Johal *et al* on a strontium-containing GIC was found to depress bone resorption and maintain bone formation while increasing trabaecular volume *in vivo*. The effect of strontium is dose dependant, however, the authors used a high proportion of the calcium substituted by strontium and found no deleterious effects [51]. A unique benefit of strontium release *in vivo* is the ability to use higher doses than available with calcium. This is due to the natural hormonal mechanism of control exhibited by the body over calcium under normal homeostatic control [52]. Recent studies on strontium hydroxyapatite implants in bone has shown a beneficial effect with strontium containing implants on bone tissue and show positive cytotoxicity and physiochemical results [53, 54]. Other groups have shown strontium hydroxyapatite implants to be osteoconductive, biocompatible and suitable for treating vertebral fractures [55, 56]. Aluminium release as discussed previously can be neurotoxic but there is evidence that

low doses can cause the proliferation of osteoblasts and new bone formation and interferes with the early stages of mineralization [39].

2.3 Ionomer Glasses

2.3.1 Ionomer Glasses

The ionomer glass component of a GIC can comprises a large variation in composition. The original glass compositions were calcium fluoroaluminosilicates [57]. The composition is largely restricted to a selective region, as the glasses tend to readily phase separate or crystallise upon cooling outside this region (see *Figure 2.2*) [2]. Current commercial compositions are based on the same basic composition but can include a number of other species to increase variation. Sodium and phosphorus are frequently used. Strontium or lanthanum additions are frequently applied in trace amounts to improve the radiopacity of the cement [7]. Despite its use as a radiopacifier in dental GICs, there are few studies concerning the effect of strontium on the glass science and material properties of the resulting GIC. A study by Johal *et al* suggested that strontium based GICs might prove useful as bone cements after examining the biocompatibility of a series of substituted glasses [51]. A study of a strontium oxide to poly(acrylic acid) was undertaken by Deb and Nicholson to determine the viability and cement setting characteristics of a strontium GIC. They concluded that except at low levels the oxide powder did not improve the compressive strength properties of the cements [58].

The structure of alkali silicate glasses can be described by the random network model of Zachariasen. SiO_4 tetrahedra form 5 to 8 membered rings with the network modifying alkali metal ions such as Ca^{2+} randomly occupy the interstitial holes in the rings (*Figure 2.9*) [59, 60]. A glass of purely [SiO_4] tetrahedra has electoneutrality and therefore, is immune to acidic attack and not viable as an ionomer glass in GICs. The addition of aluminium into the glass network disrupts the electroneutrality sufficiently to make the glass susceptible to acidic attack as the aluminium ions (3^+) are forced into 4-fold co-ordination disrupting the network. The Si:Al ratio in the glass is limited to a 1:1 ratio incorporation as aluminium is no longer forced into tetrahedral units above this ratio. The reactivity of the glass and its setting characteristics need to be balanced with the strength of a GIC, which increases proportionally to the concentration of aluminium ions [7, 8, 15]. Griffin and Hill tested a series of multi-component glasses including fluorine and phosphorus and found that the aluminium to silicon ratio did not have a significant influence on these glasses. The high phosphate content of the glasses was attributed to reducing this influence as a result of phosphorus locally balancing the four coordinate aluminium ions (less susceptible to acid attack) and forming hydrostable phosphorus-oxygen bonds [61]. The net negative charge from the addition of aluminium is balanced by the positive cations such as Ca^{2+} [7, 8]. The inclusion of species such as CaO in the glass leads to the development of non-bridging (structural units where oxygen bridges have been broken) oxygen units and is referred to as a network modifier [8].

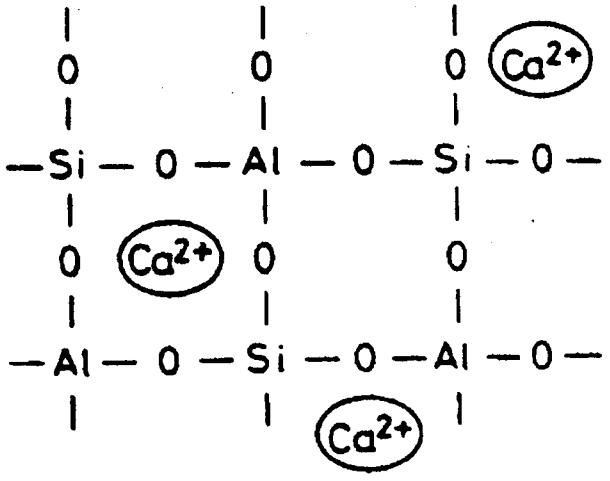

Figure 2.9: Typical glass network for a calcium-alumino-silicate glass [60].

The addition of fluorine, often added as CaF_2, into the glass structure decreases the temperature of glass fusion, can increase strength, improve handling by disrupting the glass network to increase acid susceptibility, and as discussed previously, fluorine has a role in inhibiting caries in dental applications. Fluorine lowers the refractive index of the glass and enables a match to the polysalt matrix giving rise to optically translucent cements [62]. There is evidence that the fluorine atoms are bound to the aluminium atoms of the glass network and forming non-bridging fluorines [63]. The addition of fluorine has been seen to decreases the glass transition temperature consistent with a network disrupting role.

Phosphate comprises a significant fraction of the glass phase in a number of ionomer glass compositions. PO_4 tetrahedra are found adjacent to AlO_4 tetrahedra in the glass network as a result of the charge balancing effect between the two ions. Studies by Mohialdin *et al* have demonstrated the presence of $AlPO_7$ species in ionomer glasses [64]. The addition of phosphate into the glass network modifies the acid resistance of the glass by changing the susceptibility of the Al-O-Si bonds to hydrolysis. Griffin and

Hill investigated the effect of phosphate on a series of ionomer glasses and concluded that phosphate content has a significant influence on resulting cement properties with low compositions benefiting working and setting, and slight improvements in compressive strength. Higher phosphate contents excessively disrupt the crosslinking process by competing with the carboylate groups for the metal cations [65].

Phase separation is known to occur in glass powders used in glass-ionomer cements causing batch variation, and is used in commercial systems to decrease the reactivity of the glass leading to increased setting times and strength. Controlling the glass structure could be applicable to controlling the setting properties of a GIC by 'deactivating' the reactivity of the glass. A surface crystallisation process can lead to a surface network that is less susceptible to acidic attack [7, 60]. Using appropriate heat treatments, crystallised CaF_2 from the glass and showed how the structure could stabilise fluorine and batch continuity, although this ties up the fluoride ion and therefore is unavailable for fluoride release.

Liquid-liquid phase separation is an important factor occurring on quenching into two separate phases, one rich in the residual alumino-silicate and one, which is rich in calcium and fluorine. The latter phase is attacked preferentially by the polyacid (non-uniform attack) and thus could have an important role in the setting reaction. Phase separation of glasses will occur when the geometrical effects or differences in charge (between the silica network and network modifiers) create a situation where the glass separates to decrease the free energy of the system [66]. This presents another commercially used process for reducing the reactivity of the glasses [7, 60]. Wood and Hill found the mechanism of phase separation in the studied glass to be by spinodal decomposition [60].

During studies of a suitable glass ($2SiO_2.Al_2O_3.CaO.CaF_2$), Wood and Hill determined that on crystallisation of non phosphate systems, CaF_2 was initially nucleated (Ca^{2+} and F^- are mobile in the glassy network) followed by anorthite at slightly higher temperatures (anorthite crystallisation requires bond breaking of the glass network and therefore occurs at temperatures greater than T_g). As anorthite ($CaAl_2Si_2O_8$) and CaF_2 have similar lattice parameters, CaF_2 probably nucleated the anorthite from the remaining glassy phase [60]. Phosphate containing glasses initially crystallise apatite most likely as fluorapatite with mullite as the second phase. High phosphate content will favour apatite formation over fluorite [67]. This was corroborated recently in a study by Hurrell-Gillingham *et al* [68].

2.3.2 Coloured Glasses

Colour is the light that transmits through or reflects off an object. The colour in glass comes from one, or a combination of factors or materials and is rarely a constant produced by a particular oxide in isolation. The arrangement of electrons surrounding atoms of a particular colouring material are affected by the light energy and by the magnetic energy of adjacent atoms. Oxidising or reducing atmosphere (furnace conditions) can have a significant effect as some of the colours can exist in the glass in more than one valence state. Several 'colouring oxides' can be added to create an overall colour i.e. 'black' is made up of oxides each affecting light transmission at different wavelengths:- blue, purple, grey, green, red etc. A mixing of oxides can produce a variety of different colours when combined together [69]. Coloured glasses could produce a variety of coloured cements for use as GICs. Although this has been marketed using resin modified glasses and more recently for a GIC in paediatric

dentistry, further research on its effect on glass structure and properties is required [70, 71]. Combining the differentiation of coloured cement from native tissue and the addition of radiopacifiers would give greater postoperative care and aid revision surgery.

3. Experimental Procedures

3.1 Glass Preparation

The chemicals used in batching of the glasses used in this project are listed in *Table 3.1*. Commercial SerenoCem® bone cement, batch no 079920-5 (Corinthian Surgical, UK), was used as the control in all experiments. Glass compositions for the various series are shown in the following *Sections 3.1.1* and *3.1.2*.

Table 3.1: Chemical reagents used in the manufacture of the glasses used in this study.

Material	Manufacturer	Purity (%)
SiO_2	Loch Aline Sand	>99
$Al(OH)_3$	Acros Organics, UK	>99
$CaHPO_4$	Fisher Scientific, UK	>96
$NH_4H_2PO_4$	Fisher Scientific , UK	100
CaF_2	Aldrich Chemical company, UK	99.0
$CaCO_3$	Fisher Scientific , UK	98
$SrHPO_4$	GFS Chemicals, USA	99.0
SrF_2	Aldrich Chemical company, UK	>99
$SrCO_3$	Aldrich Chemical company , UK	>98
BaF_2	Acros Organics , UK	99.0
$BaCO_3$	Acros Organics , UK	>99

The charge, to yield 150 g of glass, was placed in a sillimanite crucible (Al_2SiO_5) and an alumina (Al_2O_3) shield was used as a lid to prevent fluorine loss as silicon tetrafluoride during firing [61]. Sillimanite was used due to the tendency of alumina crucibles to undergo chemical attack by the high fluorine and phosphorus content of the glasses. Batches were heated at 2°C/min to 1050°C and held overnight, to avoid thermal shock of the aluminium silicate crucibles, and then transferred to an electric silicon carbide furnace at 1450°C for three hours.

At the conclusion of the melt, a small splat was taken for electron microscopy and the bulk of the glass quenched into water to prevent crystallisation on cooling. The resulting granular frit was air dried before being milled in a 1-litre porcelain ball mill with alumina balls to decrease contamination, and sieved to a <45 μm powder. Both the crucible and batch/glass were weighed prior to and after melting to allow calculation of the weight lost during the melt process.

On melting, any interaction of the glass with the crucible was noted. To ascertain if this was a form of chemical attack, the crucibles were cross-sectioned and prepared in the usual manner for optical microscopy. Samples were examined using an Olympus CH2 optical microscope with a digital camera attachment.

3.1.1 Strontium Substituted Glass Compositions

A systematic substitution of strontium for calcium compounds was undertaken based on the parent glass composition of SerenoCem® ($4.5SiO_2{\cdot}3Al_2O_3{\cdot}1.5P_2O_5{\cdot}3CaO{\cdot}2CaF_2$) bone cement. To provide a second control material, a direct copy of SerenoCem® was produced using the parent glass composition but manufactured using the chemical reagents in *Table 3.1*. Batch calculations for the substituted glass compositions are

given in *Appendix I*, and the series of compositions produced given as *Table 3.2*. The molar ratio substitution was of the form $4.5SiO_2 \cdot 3Al_2O_3 \cdot 1.5P_2O_5 \cdot (3-x)CaO \cdot (2-y)CaF_2 \cdot (x)SrO \cdot (y)SrF_2$, where x=0-3 and y=0-2. Due to safety considerations a calcium hydrogen orthophosphate was used in the batch instead of phosphorus pentoxide to provide the required phosphate content of the glass. The six experimental glass compositions were given the nomenclature Glass (**), where (**) refers to the composition used (Ca or Sr1-5), as shown in *Table 3.2*.

Table 3.2: Glass compositions of the strontium substituted and control glasses.

Glass Composition	Mol % of Components in the Glass						
	SiO_2	Al_2O_3	P_2O_5	CaO	SrO	CaF_2	SrF_2
SerenoCem®	32.0	21.3	10.9	21.5	0	14.3	0
Glass (Ca)	32.0	21.2	10.9	21.8	0	14.2	0
Glass (Sr1)	32.0	21.2	10.9	21.8	0	7.1	7.1
Glass (Sr2)	32.0	21.2	10.9	21.8	0	0	14.2
Glass (Sr3)	32.0	21.2	10.9	14.5	7.3	0	14.2
Glass (Sr4)	32.0	21.2	10.9	7.3	14.5	0	14.2
Glass (Sr5)	32.0	21.2	10.9	0	21.8	0	14.2

3.1.2 Substituted Glasses Incorporating Ca, Sr and Ba

To broaden the work of detailed in *Section 3.1.1* a mixed Group II ion affect was undertaken. A systematic substitution of strontium and barium for calcium compounds was undertaken based on the parent glass composition of SerenoCem® bone cement.

Batch calculations for the compositions for the substituted glasses are given in *Appendix I*, and the series of compositions produced given as *Table 3.3*. The molar ratio substitution was of the form $4.5SiO_2 \cdot 3Al_2O_3 \cdot 1.5P_2O_5 \cdot 3xO \cdot yF_2$, where x=calcium, strontium or barium and y=calcium, strontium or barium compounds to be substituted into the commercial composition. The six experimental glass compositions were given the nomenclature Glass (XY), where (XY) refers to the composition used (*i.e.* Glass (CaSr) would represent a glass where X=Ca and Y=Sr) as shown in *Table 3.3*. It is worth noting that Glass (CaSr) and Glass (SrSr) are the same compositions as Glass (Sr2) and Glass (Sr5) respectively. However, Glass (CaSr) and Glass (SrSr) are manufactured using an ammonium dihydrogenphosphate and a Group II A oxide to provide the phosphate and Group II A ion respectively.

Table 3.3: Glass compositions of the substituted and control glasses.

Glass Composition	Mol % of Components in the Glass								
	SiO_2	Al_2O_3	P_2O_5	CaO	SrO	BrO	CaF_2	SrF_2	BrF_2
SerenoCem®	32.0	21.3	10.9	21.5	0	0	14.3	0	0
Glass (CaCa)	32.0	21.2	10.9	21.8	0	0	14.2	0	0
Glass (CaSr)	32.0	21.2	10.9	21.8	0	0	0	14.2	0
Glass (CaBa)	32.0	21.2	10.9	21.8	0	0	0	0	14.2
Glass (SrCa)	32.0	21.2	10.9	0	21.8	0	14.2	0	0
Glass (SrSr)	32.0	21.2	10.9	0	21.8	0	0	14.2	0
Glass (SrBa)	32.0	21.2	10.9	0	21.8	0	0	0	14.2
Glass (BaCa)	32.0	21.2	10.9	0	0	21.8	14.2	0	0
Glass (BaSr)	32.0	21.2	10.9	0	0	21.8	0	14.2	0
Glass (BaBa)	32.0	21.2	10.9	0	0	21.8	0	0	14.2

3.2 Glass Characterisation

3.2.1 Particle Size Analysis

Particle size analysis was used to verify the range of particle sizes achieved after ball milling of the as-cast glasses. Scanning electron microscopy (SEM) and laser particle size analysis was used to allow qualitative and quantitative analysis respectively.

Quantitative examination of the glasses was carried out using a Coulter LS130 particle size analyser (Coulter Electronics Inc, USA). Glass powder (<45 μm) was

dispersed into two litres of water and the particle size distribution was determined using the Fraunhofer optical model.

Powdered samples (<45 μm) of the unreacted glasses were viewed in an SEM to give an indication of the glass morphology and a qualitative representation of the laser particle size data. Powders were placed evenly on sticky carbon disks attached to metal stubs and gold splutter coated (SC500A EM scope) for 4 minutes prior to use. A CamScan (CamScan Electron Optics Ltd, USA) was used at an operating voltage of 10 kV for powdered samples. Secondary electron images were taken at 150, 250, 500, 1000 and x1500 magnification.

3.2.2 XRD and DTA of the Prepared Glasses

To determine the extent of crystallisation on cooling, the as-cast glass compositions were analysed using a Siemens D500 (Siemens, Germany) X-ray diffractometer. All XRD (X-ray diffraction) was carried out using copper Kα radiation (λ = 1.540562 Å) from 5 to 70°2θ, with angular increments of 0.01° and a scan speed of 2°2θ/min. XRD analysis on the samples was undertaken using an operating voltage of 40 kV and of 30 mA.

Differential thermal analysis (DTA) was carried out on the glasses to ascertain the glass transition temperature (T_g) and any crystallisation events (T_x) that take place on heating. 35 mg powdered samples (<45 μm) were placed in a Perkin-Elmer DTA 7 (Perkin-Elmer, USA) and heated against an inert reference (fired alumina) at 10°C/min to 1050°C under a flowing 100% argon atmosphere to avoid chemical attack of the platinum crucibles. Data was collected by a PC and displayed graphically.

Determination of the glass transition temperature from the DTA traces was found to be reproducible but difficult to resolve with sufficient accuracy. It was decided to repeat the DTA experiments using a variation of the method suggested by Wilburn [72]. The strontium substituted series of glasses and the commercial GIC SerenoCem® were subjected to a prior heat-treatment. Samples were heated at 10°C/min to within 50°C of the T_g given in the previous method, held for one hour and then cooled at 5°C/min to room temperature. Samples were then heated 10°C/min to 1050°C as before. Data was collected by a PC and displayed graphically.

3.2.3 Characterisation of the Heat Treated Glasses

To complement the data obtained from the DTA traces and to determine the crystalline phases represented by T_{X1} and T_{X2}, controlled heat treatments of the glasses at 700, 800, 900 and, in some instances, 1000 °C were carried out in a Lenton tube furnace (Lenton, UK). Samples were heated at 5°C/min to the required temperature and held for 120 minutes before being slow cooled at 5°C/min to room temperature. The resulting crystalline phases were identified using the Siemens D500. Identification of the crystalline phases was undertaken using JCPDS cards on CD-ROM [73].

3.2.4 TEM and EDS

Transmission electron microscopy (TEM) was used to determine if any phase separation or crystallisation had occurred upon cooling of the Glasses (Sr1-Sr5). Since XRD would detect the formation of major crystal phases, TEM was used to ascertain if micro-crystalline phases were present. Glass powders (<45 μm) were placed on sticky carbon

grids and observed in a TEM (Philips EM400, Philips, USA) at an accelerating voltage of 120 kV. Energy dispersive spectroscopy (EDS) via a link system was used to verify the elements present in the nano-glass particles observed in the TEM and detect differences in any phase-separated areas found.

3.3 Characterisation of Cements

Cements were made using mercaptan-free poly(acrylic acid), batch number 079915-2 (Advanced Healthcare, Tonbridge, Kent, UK), with a mean molecular weight of 52,000, and the ionomer glasses described in *Sections 3.1.1* and *3.1.2*. The ratio of components used was X g (X=1 g in commercial samples) of glass to 0.2 g poly (acrylic acid) to 0.3 g 10% tartaric acid solution (L(+)Tartaric acid, Sigma-Aldrich, Dorset, UK) in all experiments and the cements were hand mixed prior to use in accordance with the 'manufacturer's instructions on the mixing of SerenoCem® bone cement (where X is the molar equivalent weight of the novel glasses compared to the SerenoCem® glass, calculations are shown in *Appendix II*).

Where required, discs of the GICs were formed using a silicone rubber mould with impression dimensions of 9±0.5 mm in diameter and 2±0.2 mm thickness. All cements were given nomenclature similar to the parent glasses, *e.g* Glass (SrCa) becomes GIC (SrCa).

3.3.1 Gilmore Needle Indentation Test

The Gilmore Needle indentation test was used to determine the working and setting times of SerenoCem®, and the novel ionomer glass systems, according to the British dental material standard (BS EN29917 & 6039) [74, 75].

The samples (n=5) to be tested were mixed according to both the manufacturer's instructions and the dental material standards before being initially subjected to a 28 g indenter. The working time was recorded when the cement resisted this initial weight. The setting time was determined when the larger 400 g indenter was resisted. Both tests were carried out at ambient temperature 23±1°C (British Standard setting time is normally carried out at 37°C). A study of the effect of tartaric acid (5-15%) concentration on the setting characteristics of SerenoCem® and GIC (Sr5) cement was also carried out under the above conditions.

3.3.2 Radiopacity

Radiopacity measurements of the prepared cements were carried out on a dental X-ray unit, Siemens Heliodent MD (Siemens, Germany). Discs of GIC (Sr1-5), GIC (CaCa) GIC (SrSr), GIC (BaBa) and the SerenoCem® control were prepared as described in *Section 3.3* and aged for one day in a humid environment (100%) to prevent desiccation. Radiographs of the cement compositions were taken against an aluminium step-wedge and processed by an automated film-developing unit. All radiographs were taken with an exposure time of 0.1 seconds at 60 kV and a working distance from the aperture of 6 cm on to Kodak Dental Occlusal film (Kodak, USA).

3.3.3 Flexural Strength

Ten rods of each cement were prepared to dimensions of >25 mm in length and 4.6±0.05 mm in diameter. After 1 day, five rods from each composition were subjected to a 3-point bend study on a Hounsfield tester (Hounsfield, UK) and both the force and elongation to failure measured and displayed graphically by a PC. The test conditions used were Load range – 30 N, Extension – 5 mm, Test Speed – 1mm/min, Test End Point – 4.5 mm, Preload – 2 N, and Span – 25 mm. Flexural strength measurements were calculated from the measured force readings obtained from the 3-point bend test using *Equation 1*. Flexural Strength (FS) is given by

$$FS = \frac{Force \times Span}{\pi \times radius^3} \qquad (1)$$

This test was repeated again after a period of 28 days. To determine the mode of failure at 24 hours after mixing, fractured cements of SerenoCem®, GIC (CaCa), GIC (SrSr) and GIC (BaBa) were mounted on stubs, gold coated for 4 minutes (SC500A EM scope) and secondary electron images viewed in a CamScan (CamScan Electron Optics Ltd, USA) SEM at an operating voltage of 20 kV. Digital images were taken at x500 magnification. 28 day samples of all cements were mounted and examined in the SEM using the same process.

3.3.4 Ion Release

Discs of each cement (n=6) were mixed and placed in to 25 ml of deionised water contained in a plastic screw top beaker. All samples were stored in a 37°C incubator (100% humidity) and refreshed when a sample of the solution submerging the GIC was taken. The samples were refreshed to provide the optimum kinetic conditions for the release of the ions from the cement. Fluoride ion release was measured over a four week time period (samples were taken at 1, 7, 14 and 28 days respectively) using a fluoride ion selective electrode (Orion Research Inc, UK). 1 ml of TISAB (Orion Research Inc, UK) was added prior to measuring to ensure complete dissociation of the fluoride ions.

1 ml of hydrochloric acid (Sigma, UK) was added to the 9 ml samples taken after one week to ensure complete dissociation of the ions in solution. Further elemental release (Al, Si, P, Ca, Sr, Ba) was measured using ICP-ES (inductively coupled plasma - emission spectroscopy) on samples taken from the solutions after one week. Data courtesy of the Centre For Analytical Sciences (Chemistry Department, Sheffield University).

3.3.5 Biocompatibility

Biocompatibility of GIC (CaCa), GIC (SrSr) and GIC (BaBa) was investigated using rat osteosarcoma (ROS 17/2.8, Merck Inc) cells seeded into 24 well plates containing the test specimens and a cell density of 1.25×10^4 cells/ml. A tissue culture plastic control was included for comparison. The plates were incubated at 37°C in a 5% CO_2 atmosphere for 72 hours. Total protein assay was performed on cultures using the

Biruet method (n=5). A MTT (methyl thiazolyl tetrazolium) assay was also performed (n=5) on each composition. Scanning electron microscopy (SEM) was used to observe cell morphology and give a qualitative indication of the protein and MTT assays. A CamScan (CamScan Electron Optics Ltd, USA) was used at an operating voltage of 20 kV. These methods have been reported previously for the evaluation of *in vitro* biocompatibility of GICs [47, 68].

3.3.6 Coloured Ionomer Glass Compositions

Coloured ionomer glasses were made based on the SerenoCem®, glass ionomer bone cement composition (4.5SiO2·3Al2O3·1.5P2O5·3CaO·2CaF2) with 0.2 and 1.0 wt% additions of each colouring agent. The various methods used in colouring the ionomer glasses are described below. Colouring agents and blended glass used in this study were courtesy of Mr W. Simpson (Glassworks, UK) and are shown in *Table 3.4*.

Table 3.4: Glass colouring agents used in this study.

Colouring Agent	Expected Glass Colour
Cobalt carbonate	Blue
Manganese oxide	Purple
Erbium nitride	Pink
Neodymium oxide	Blue/mauve
Cerium oxide	Yellow/gold
Powdered lime green glass (K2021)	Lime green

No colouring agent	Colourless

The following steps were taken:

•Ionomer glasses were made based on the SerenoCem®, glass ionomer bone cement composition $4.5SiO_2 \cdot 3Al_2O_3 \cdot 1.5P_2O_5 \cdot 3CaO \cdot 2CaF_2$ with 0.2 and 1.0 wt% additions of all six colouring agents. A batch without any addition was used as a control sample.

Batched raw materials were placed in a silliminite (Al_2SiO_5) crucible and preheated to 1400°C, increasing the temperature by 2°C/minute to prevent damage to the crucible through thermal shocking. The crucible and contents were then placed in a gas furnace using an oxidising atmosphere and melted at 1400°C. After 3 hours, pouring of the glasses was attempted. However, this was not possible as the bases of all crucibles except that containing no colouring agent had undergone chemical attack, resulting in loss of their contents. It was assumed that chemical attack of the crucibles was due to the presence of the colouring agents.

•Production of ionomer glasses was attempted using the same SerenoCem® composition described above, but using a lower percentage of the colouring agents (0.02 wt%). Although no chemical attack of the crucibles occurred, the glasses produced were colourless. This suggested there was a complex interaction occurring between the colouring agents and the ionomer glasses.

•Therefore, to produce coloured glasses, greater than 0.02 wt% of each colouring agent was required. This was achieved by omitting phosphate and fluoride ions from the glass to produce a simpler glass composition and prevent these species from interacting with the colouring agents and hence chemically attacking the crucible during melting. Glasses were melted at 1400°C using the basic fluoride free composition shown in *Table 3.5* with 0.2 and 1 wt% colouring agent added to the batches. After 3 hours, the

glasses had not completely melted although the charge was obviously coloured. This is likely to be due to the lack of fluoride in the melt, which lowers the fusion temperature of the glass allowing the melting temperature to be reduced.

Table 3.5: Fluoride and phosphate free GIC composition [46].

Raw Material	Amount for 100 g
SiO_2	35.90
$Al(OH)_3$	46.82
$CaCO_3$	59.78

•Complete melting was achieved by reintroducing increasing amounts of fluoride into the glass until a composition with 10 wt% fluoride was produced. The glasses were also melted at 1550°C. This GIC composition is suitable for dental applications. The resultant glasses were ground for 3 hours in a porcelain ball-mill to produce a glass powder, which could pass through a 45 μm sieve. Glasses were mixed with poly(acrylic acid) and coloured cements formed.

3.3.7 NMR

A series of cement discs (n=10) of five increasing concentrations of tartaric acid (0, 5, 10, 20 and 30 wt% L(+)tartaric acid) were produced using the SerenoCem® GIC glass composition. Five discs were allowed to mature for a day before testing and a further five discs were matured for seven days before testing. This procedure allowed both

aged and un-aged cements to be investigated in addition to the effect of tartaric acid on the setting reaction. Both sample sets were stored in a humid environment (100%) at 37°C during maturation. Prior to testing, cement samples were crushed in a percussion mortar to produce a <45 μm powder.

^{27}Al and ^{29}Si NMR was applied to the samples using a Varian InfinityPlus 300 wideline NMR (nuclear magnetic resonance) spectrometer equipped with Chemagnetics style magic angle spinning (MAS) probes. All spectra were acquired using MAS and proton decoupling to obtain the relevant spectra. ^{27}Al NMR was undertaken at a spinning speed of 6 kHz using a 6 mm probe, and ^{29}Si NMR at a spinning speed of 4 kHz using a 9 mm probe. Data was processed using the spectrometer's Spinsight software and further analysis carried out with the Igor data analysis package supplied by Wavemetrics, (Oregon, USA) to allow deconvolution and interpretation of the collected data. All work was carried out at the Department of Civil Engineering (University of Leeds) under the expert supervision of Dr Adrian Brough.

4. Results

4.1 Glass Preparation

All novel GIC compositions formed glasses that had an amorphous appearance upon quench cooling. This indicated that no significant bulk or surface nucleation of crystals had occurred within the glass. Strontium and barium-based glasses appeared to be less viscous and more 'glass-like' upon pouring than the calcium-based glass compositions. Both the crucible and contents were weighed pre- and post- melting to calculate any loss during this process. All the glasses had undergone less than 5% loss by weight.

Crucibles were sectioned and viewed in an optical microscope to determine if any chemical attack had occurred during the melt. *Figure 4.1* shows a cross-sectional image of a crucible pre- and post- melting of Glass (Sr3). The presence of glass in the pores at the crucible surface suggested that some form of chemical attack may have occurred. These observations are discussed in detail in *Section 5.1*. However, this feature was only observed to a depth of 5-10 μm.

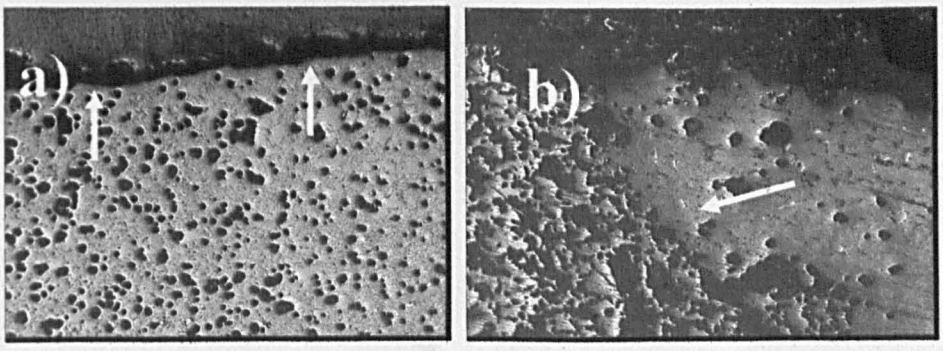

Figure 4.1: Optical images of a) Pre-melt crucible cross-section and b) Cross-section of a crucible chemically attacked by Glass (Sr3). Both images are x165 magnification (*i.e.* 1 cm = 60 μm). Arrows indicate the zone of glass attack of the crucible.

4.2 Glass Characterisation

4.2.1 Particle Size Analysis

4.2.1.1 Strontium Substituted Glasses

Scanning electron microscopy of the glass powders was undertaken to examine the morphology of the glasses and to complement the data obtained by laser particle size analysis. The laser particle size data and corresponding SEM (x250 and x500 magnification) images for the seven glass compositions are shown in *Figures 4.2 to 4.8*. *Table 4.1* shows the mean particle sizes of the substituted glasses.

Table 4.1: Laser particle size analysis data for the strontium substituted glass compositions showing the mean particle sizes and percentage of particles less than 45 μm in diameter.

Glass Composition	Particle Size Results	
	Mean Particle Size (μm)	<45 μm (%)
SerenoCem®	18.27	97
Glass (Ca)	25.91	98
Glass (Sr1)	23.85	85
Glass (Sr2)	20.79	90
Glass (Sr3)	26.46	85
Glass (Sr4)	20.11	95
Glass (Sr5)	26.18	85

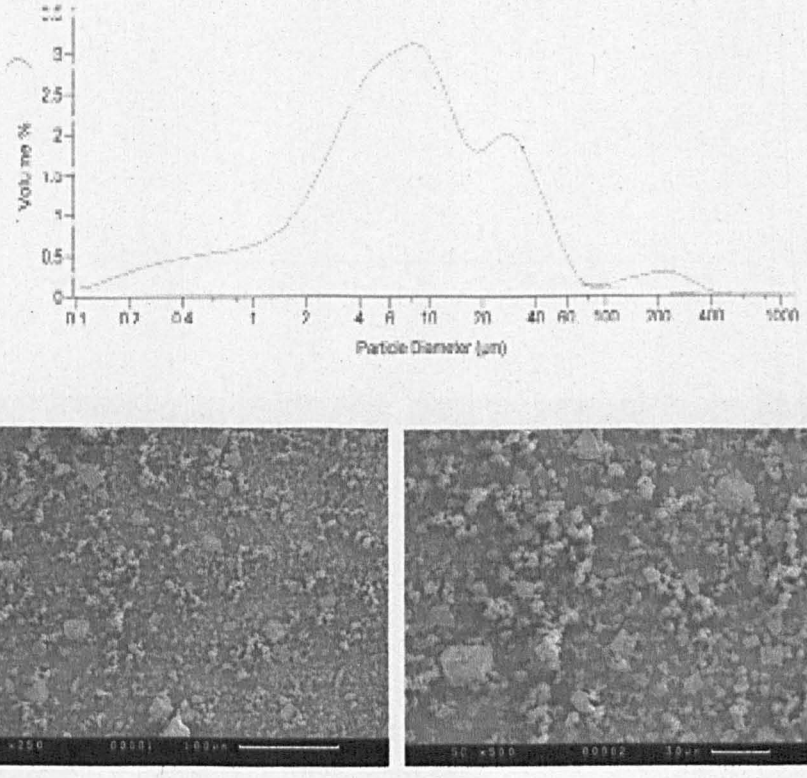

Figure 4.2: Particle size data for SerenoCem®.

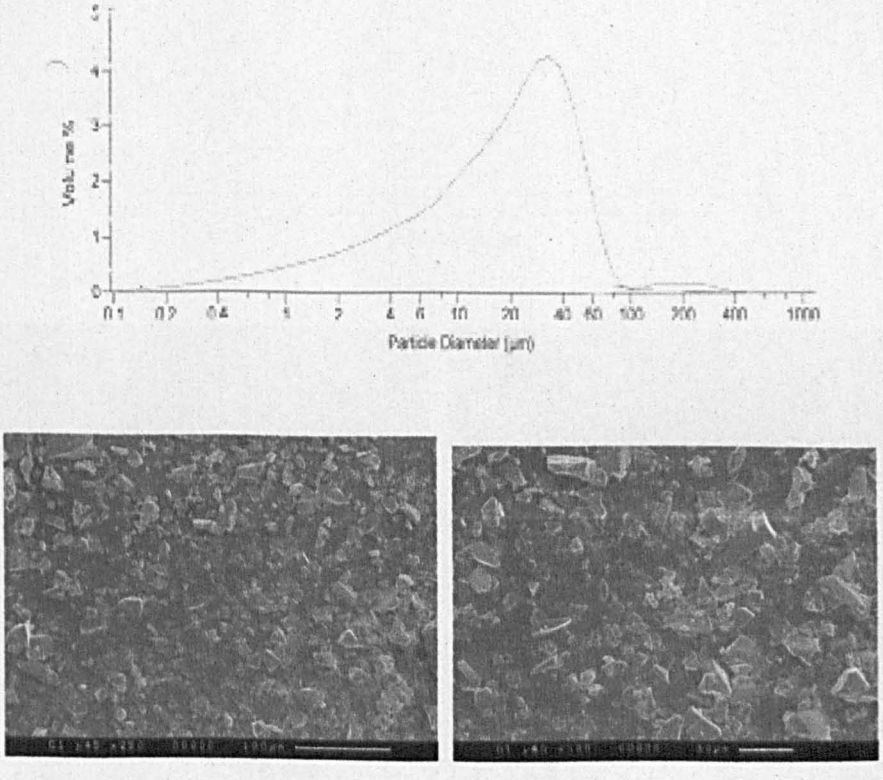

Figure 4.3: Particle size data for Glass (Ca).

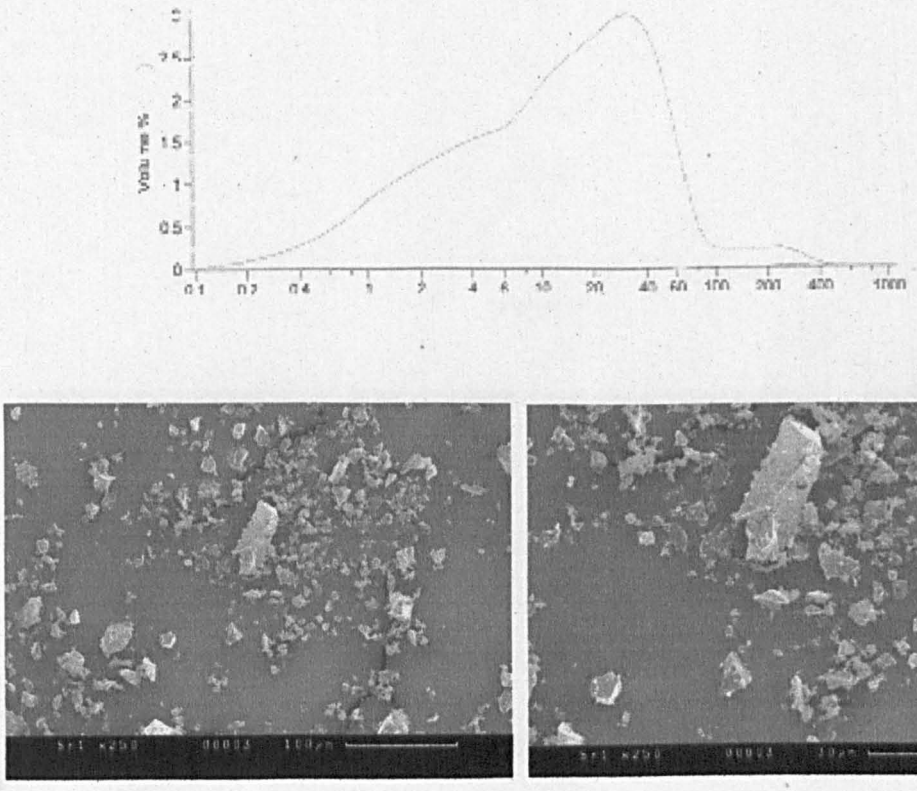

Figure 4.4: Particle size data for Glass (Sr1).

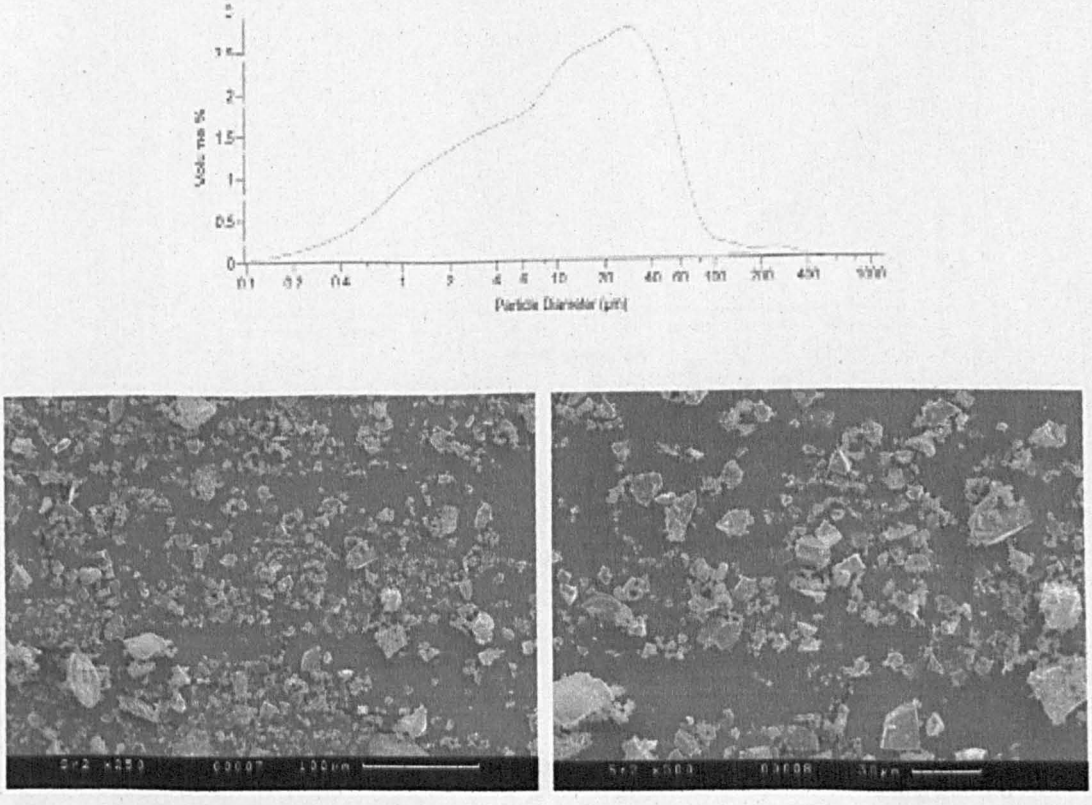

Figure 4.5: Particle size data for Glass (Sr2).

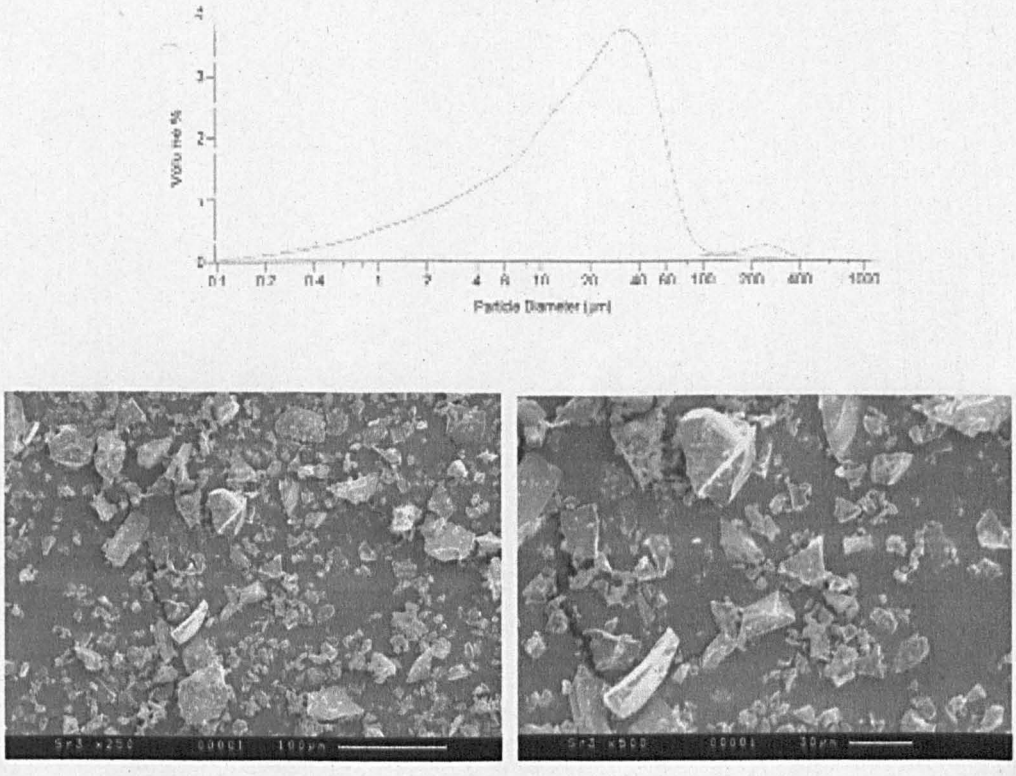

Figure 4.6: Particle size data for Glass (Sr3).

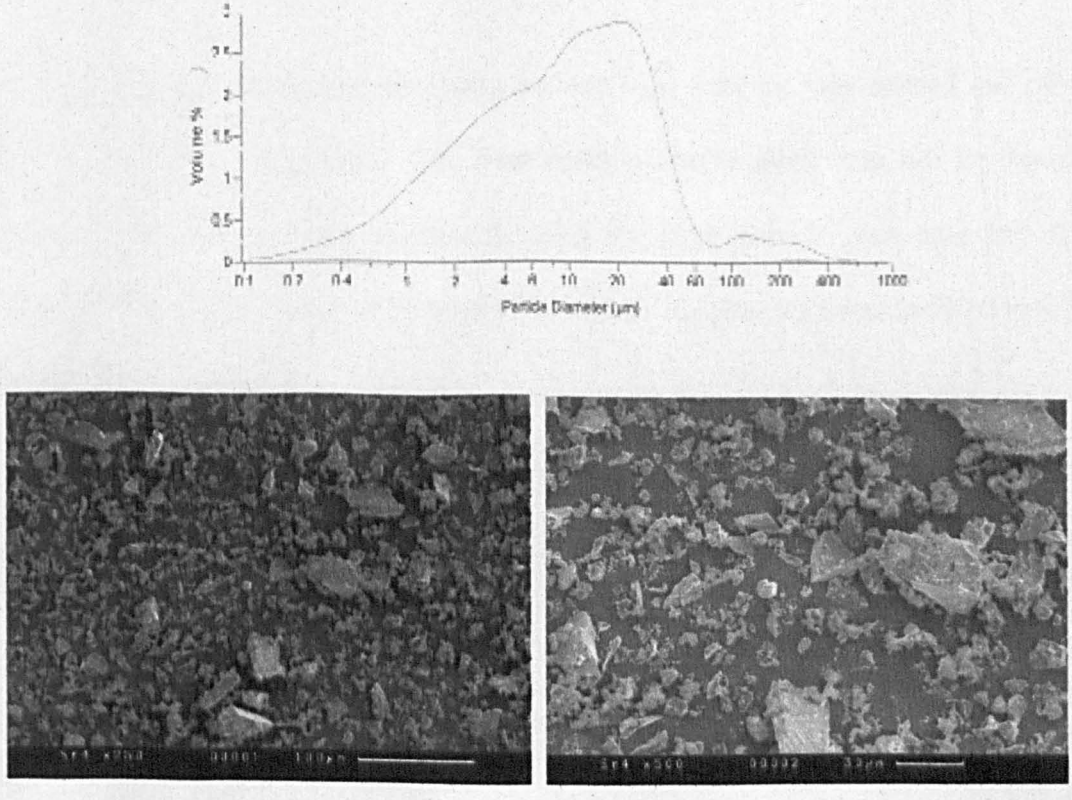

Figure 4.7: Particle size data for Glass (Sr4).

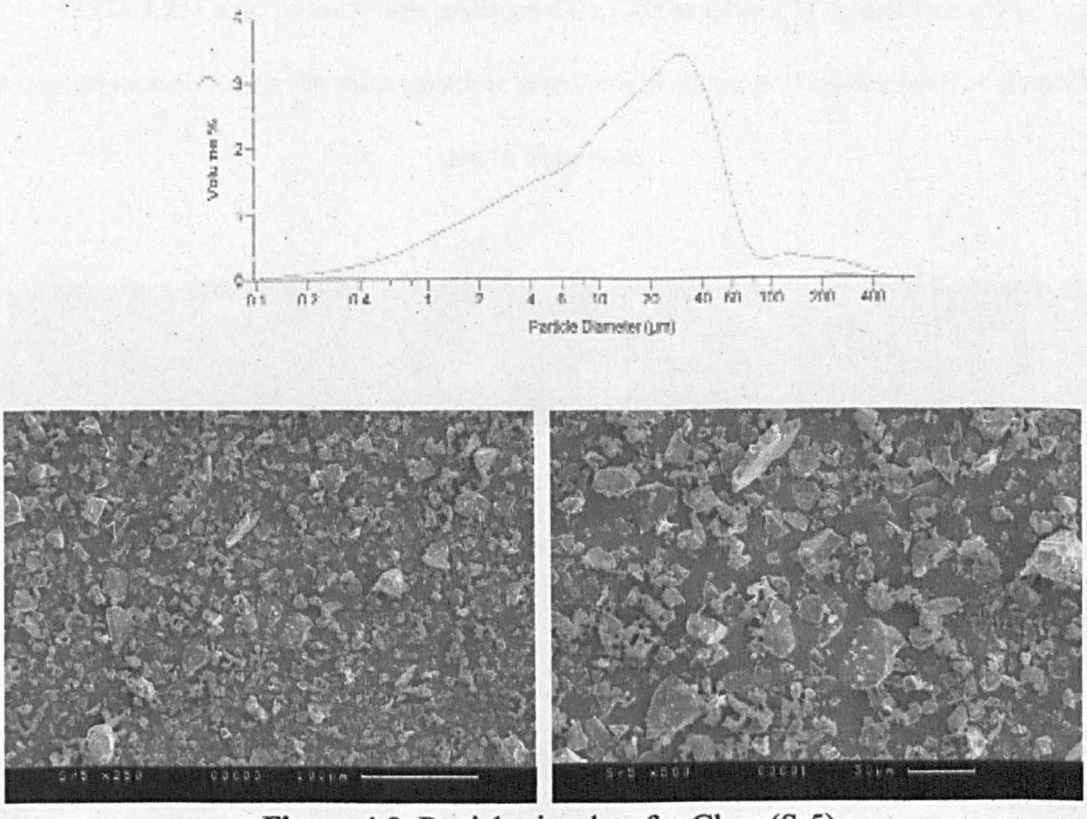

Figure 4.8: Particle size data for Glass (Sr5).

4.2.1.2 Substituted Glasses Incorporating Ca, Sr and Ba

Scanning electron microscopy and laser particle size analysis was carried out on the Group II A substituted glasses. The laser particle size analysis data can be found in table form in *Table 4.2* and graphically with the laser particle size data and SEM photomicrographs (x150 and x500 magnification) of the glass particles in *Figures 4.9* to *4.17*.

Table 4.2: Laser particle size analysis data for the Group II substituted glass compositions showing the mean particle sizes and percentage of particles less than 45 μm in diameter.

Glass Composition	Particle Size Results	
	Mean Particle Size (μm)	<45 μm (%)
SerenoCem®	18.27	97
Glass (CaCa)	17.81	98
Glass (CaSr)	21.05	97
Glass (CaBa)	20.82	97
Glass (SrCa)	18.75	97
Glass (SrSr)	18.46	98
Glass (SrBa)	21.10	97
Glass (BaCa)	18.11	98
Glass (BaSr)	14.27	99
Glass (BaBa)	19.11	98

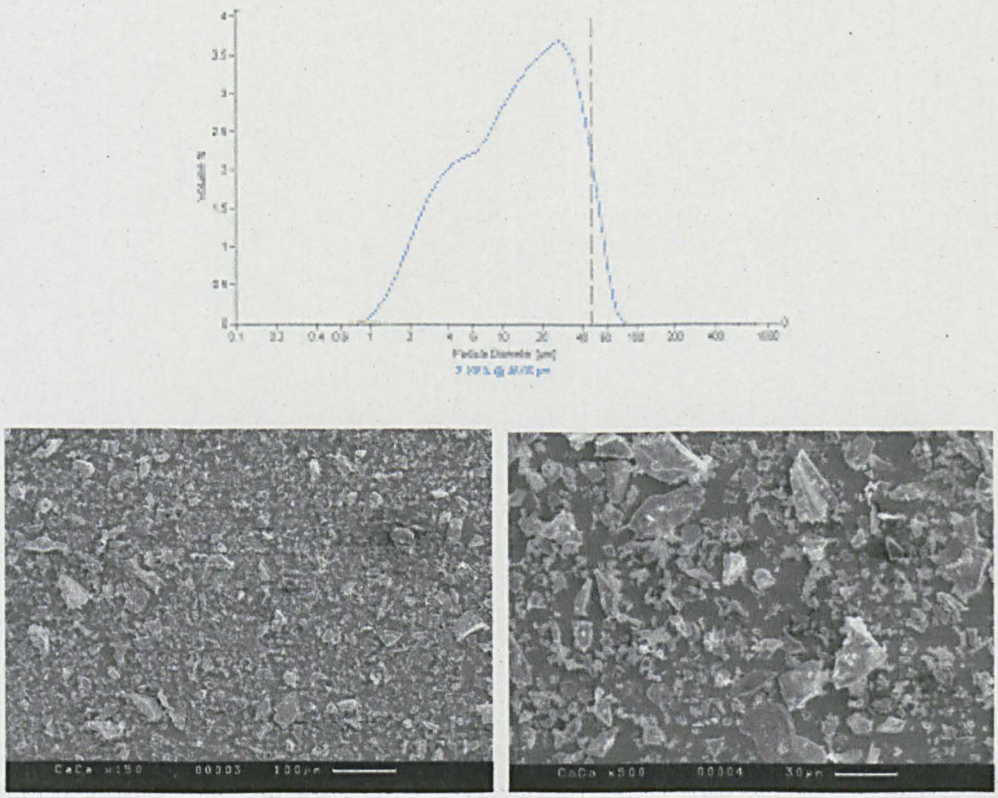

Figure 4.9: Particle size data for Glass (CaCa).

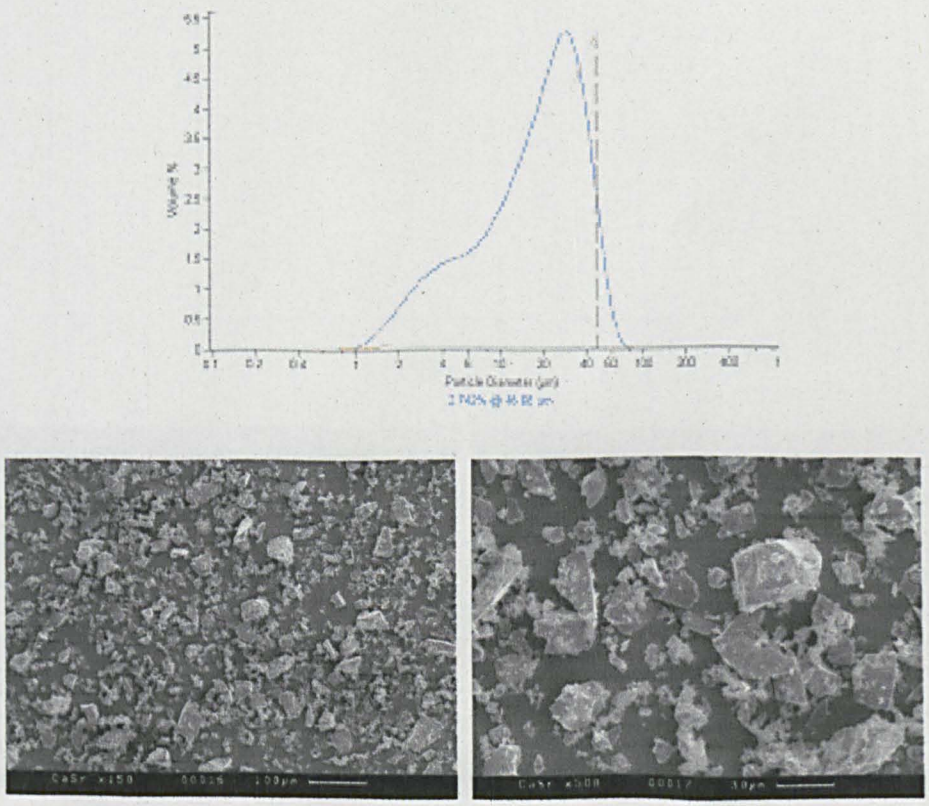

Figure 4.10: Particle size data for Glass (CaSr).

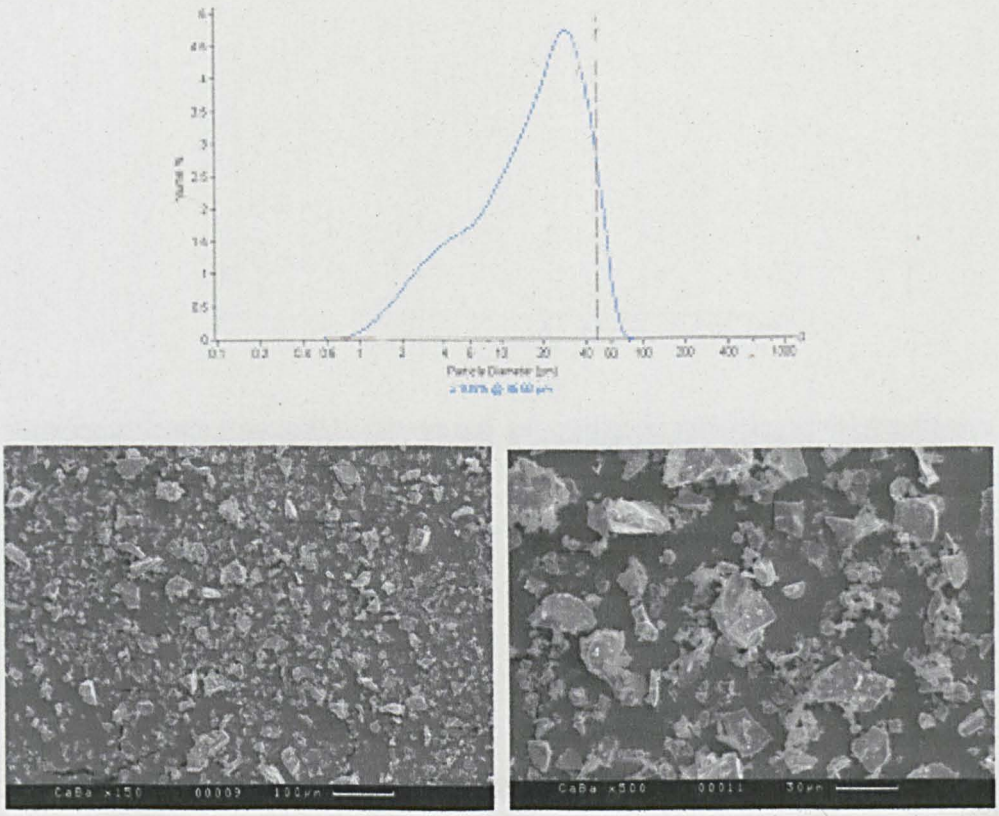

Figure 4.11: Particle size data for Glass (CaBa).

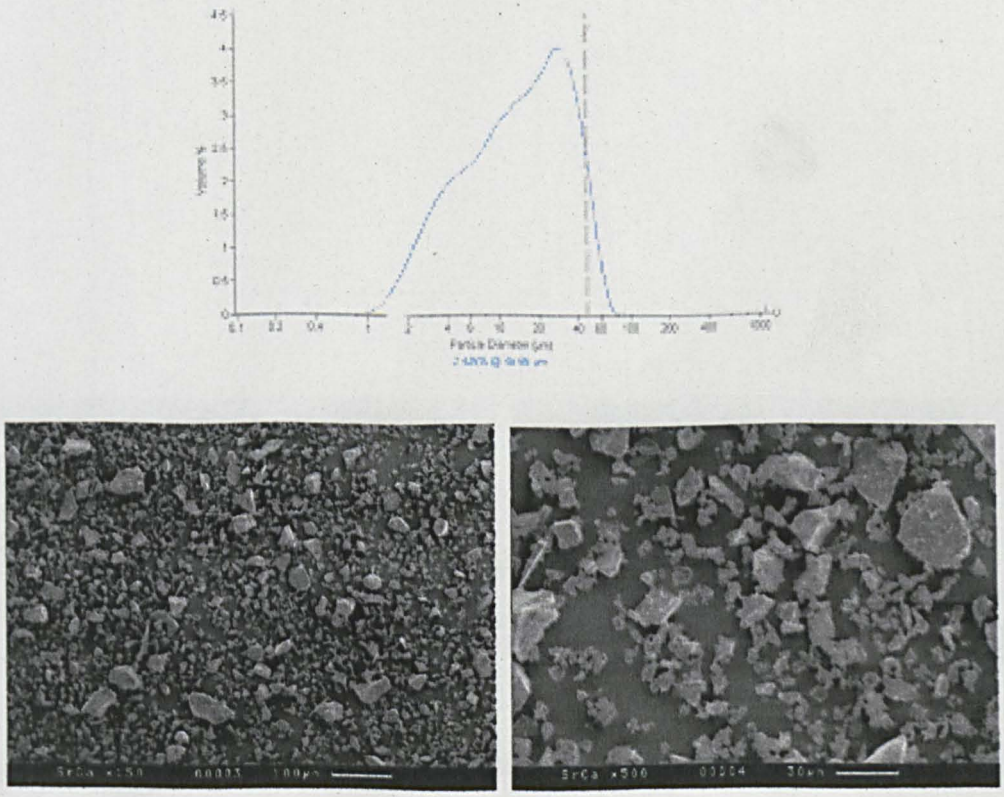

Figure 4.12: Particle size data for Glass (SrCa).

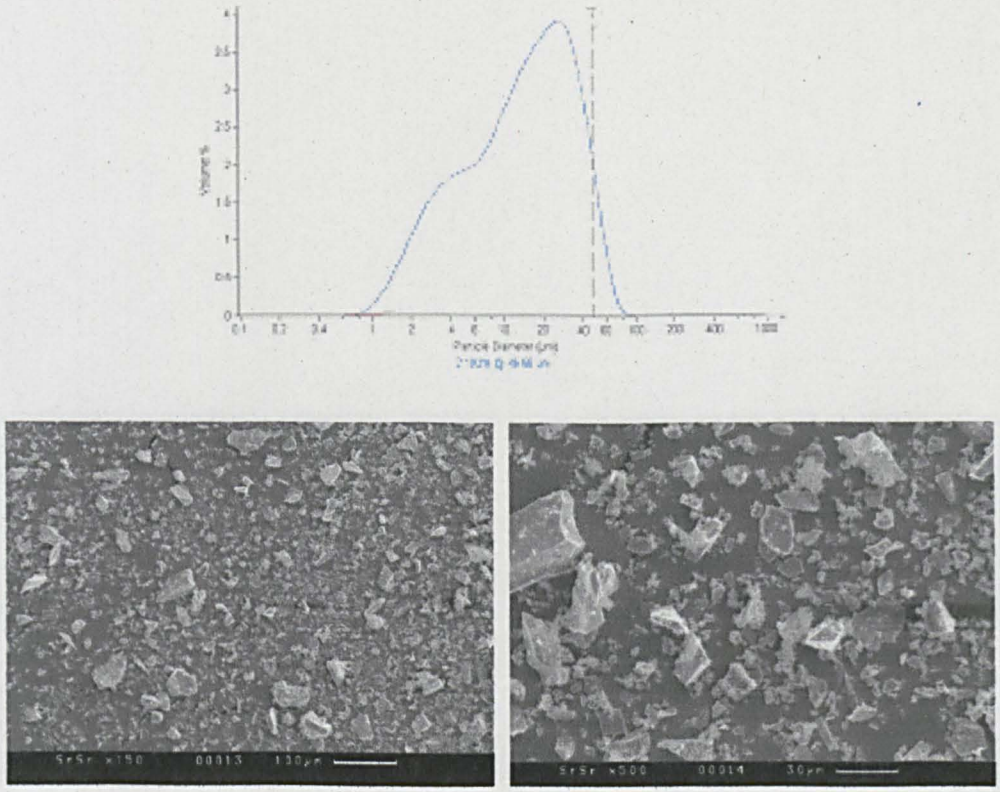

Figure 4.13: Particle size data for Glass (SrSr).

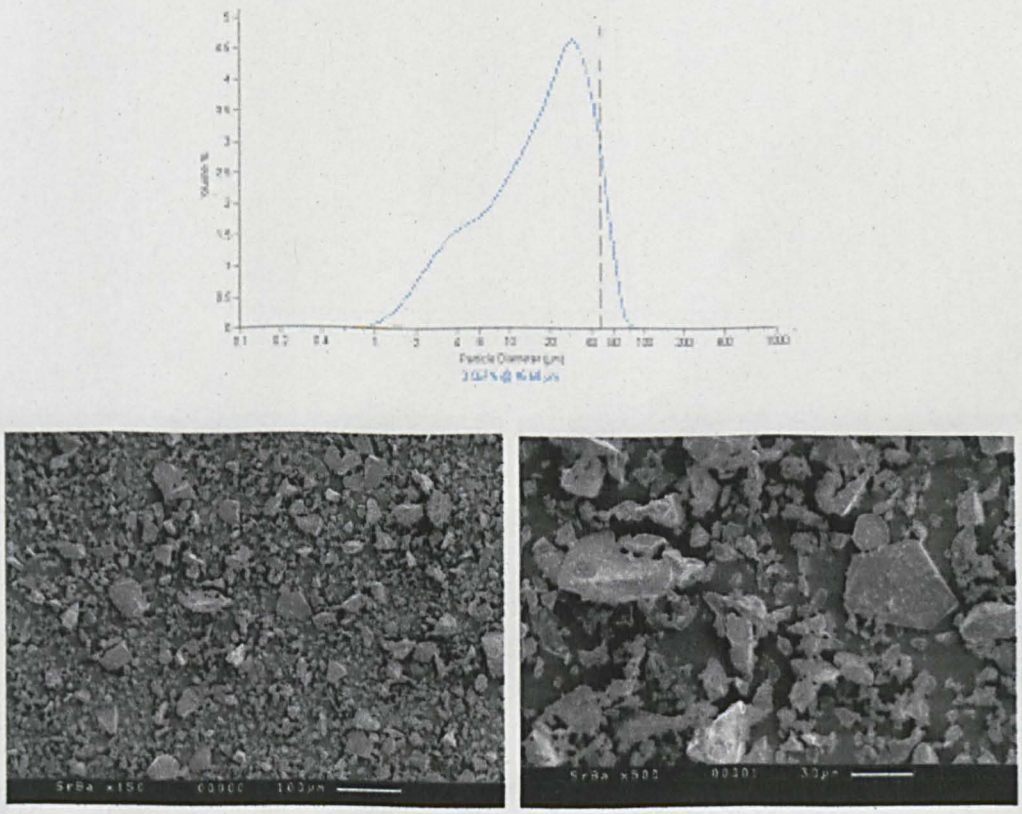

Figure 4.14: Particle size data for Glass (SrBa).

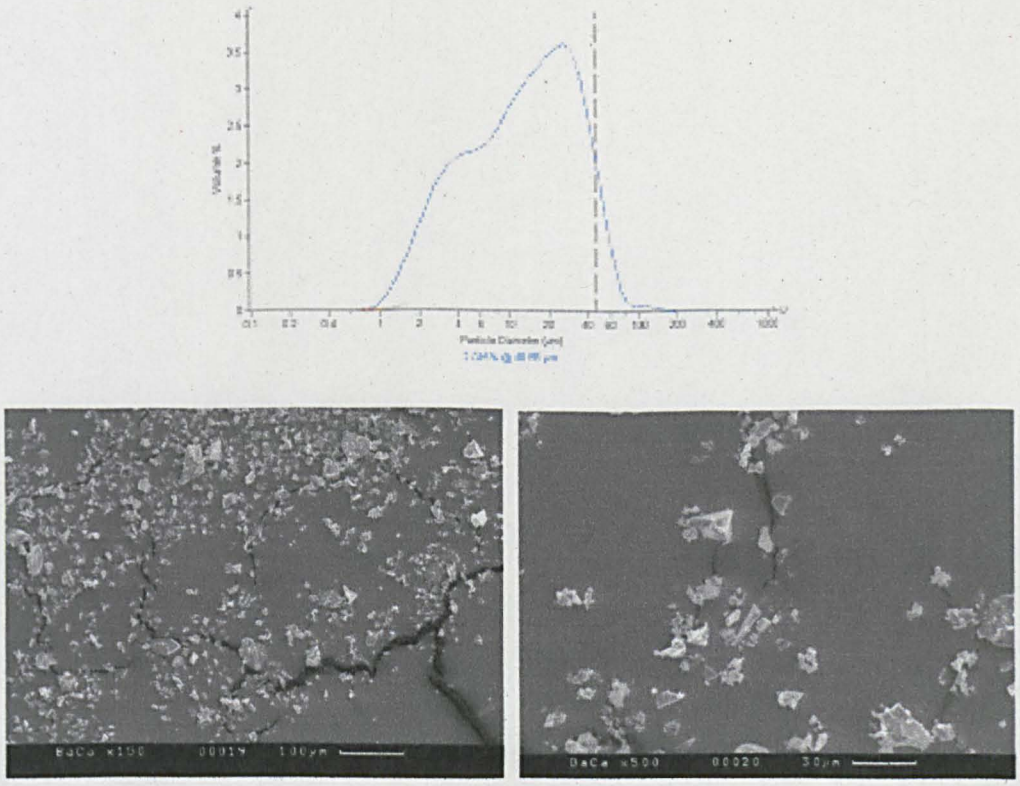

Figure 4.15: Particle size data for Glass (BaCa).

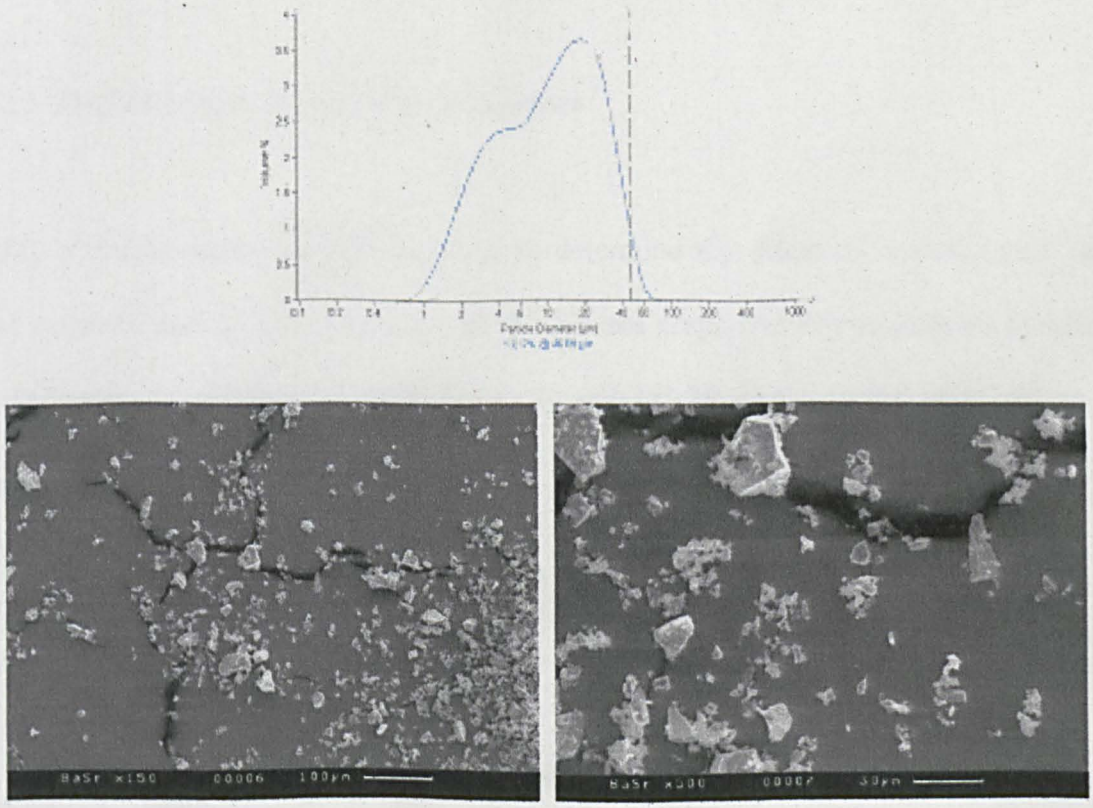

Figure 4.16: Particle size data for Glass (BaSr).

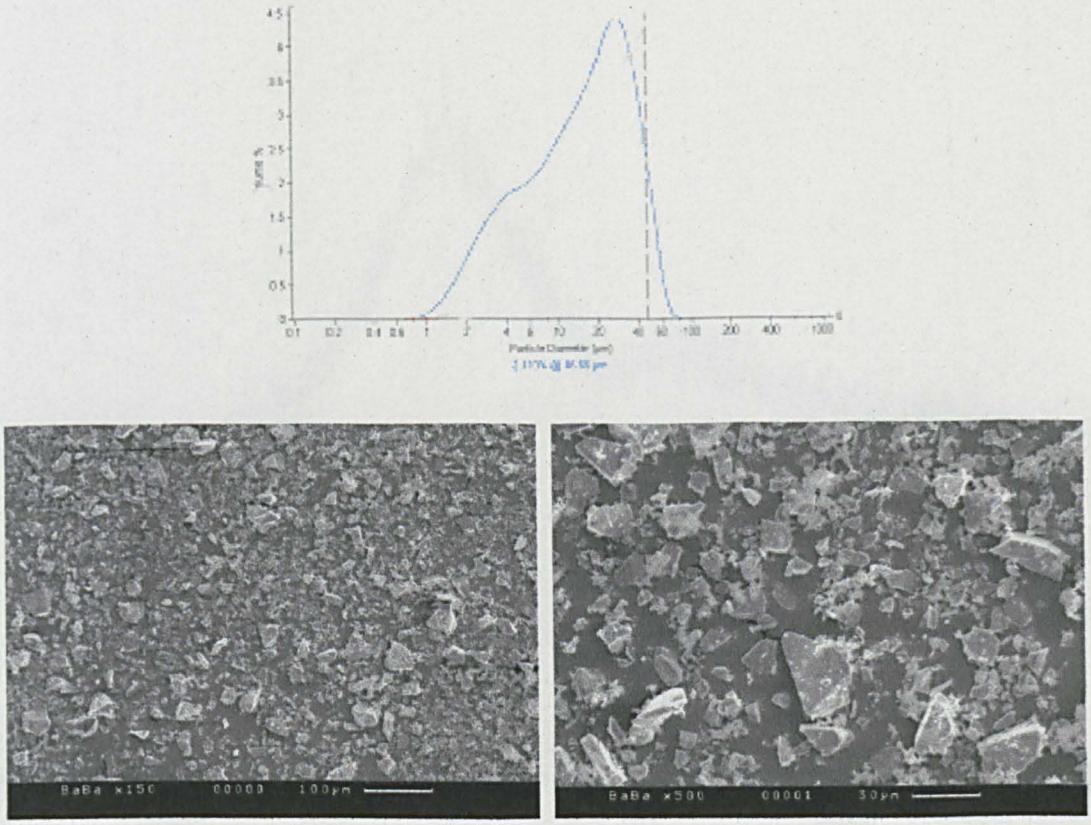

Figure 4.17: Particle size data for Glass (BaBa).

4.2.2 XRD and DTA of the Prepared Glasses

XRD of the quenched glasses was used to determine the extent of crystallisation that had occurred during rapid cooling. All the glasses prepared were amorphous to XRD, as indicated by the glassy hump between 20 and 35° 2θ. An example XRD pattern is displayed in *Figure 4.18*.

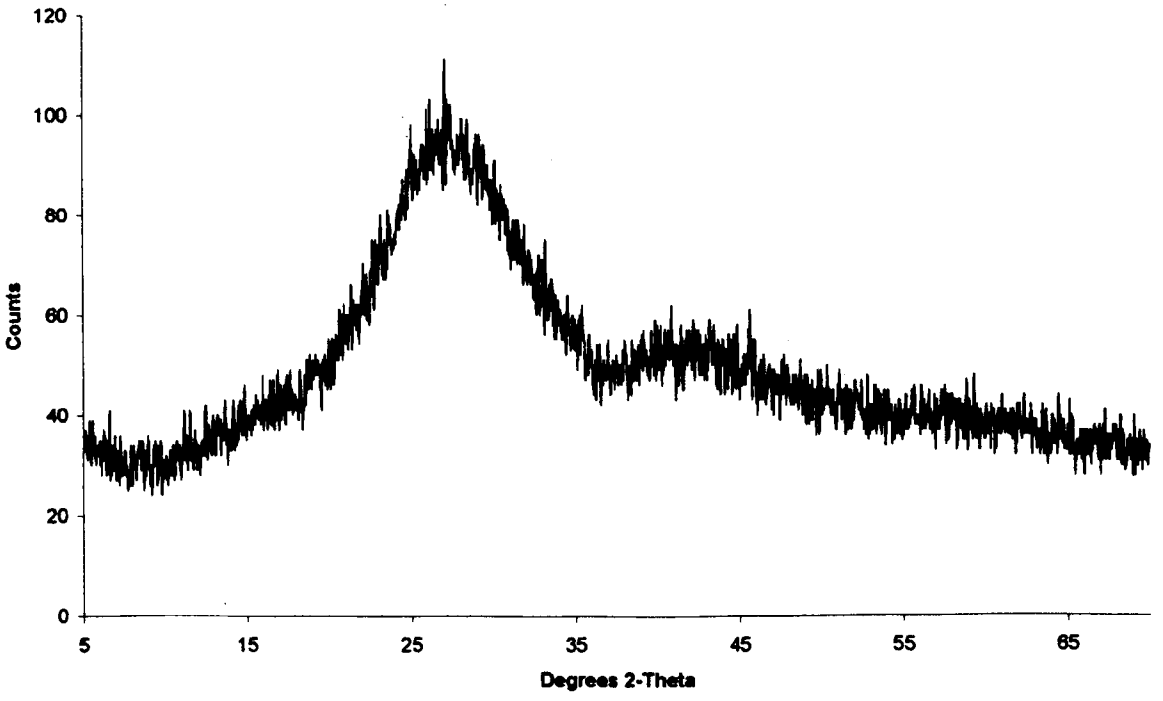

Figure 4.18: XRD trace of Glass (Sr3) showing the amorphous hump between 20 and 35 °2θ.

The profiles for the thermal events of the milled glasses are given in *Figure 4.19* for the strontium substituted series, *Figure 4.20* for the three 100% substitutions, and for the series of substituted glasses incorporating Ca, Sr and Ba in *Figures 4.21 to 4.23*. The glass transition and crystallisation temperatures obtained by DTA are tabulated in *Table 4.3*.

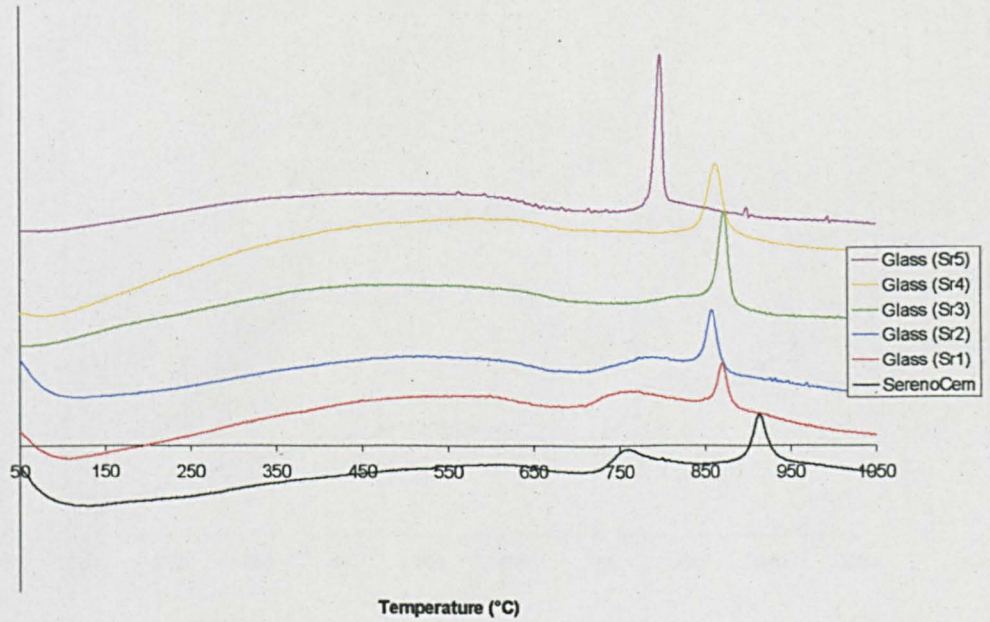

Figure 4.19: DTA trace of SerenoCem® and Glasses (Sr1-5) displayed offset to highlight the decrease in glass transition temperature and changes to the crystallisation temperatures with increasing strontium substitution. Y axis represents *x* °C.

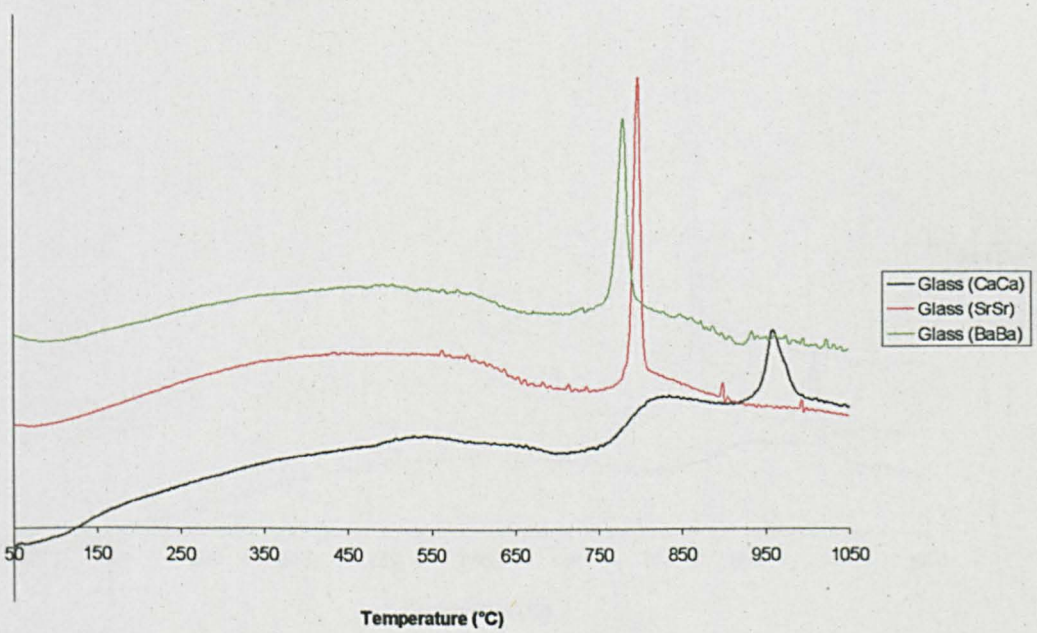

Figure 4.20: DTA traces of Glass (CaCa), Glass (SrSr) and Glass (BaBa) displayed offset to highlight changes in the glass transition and crystallisation temperatures. Y axis represents *x* °C.

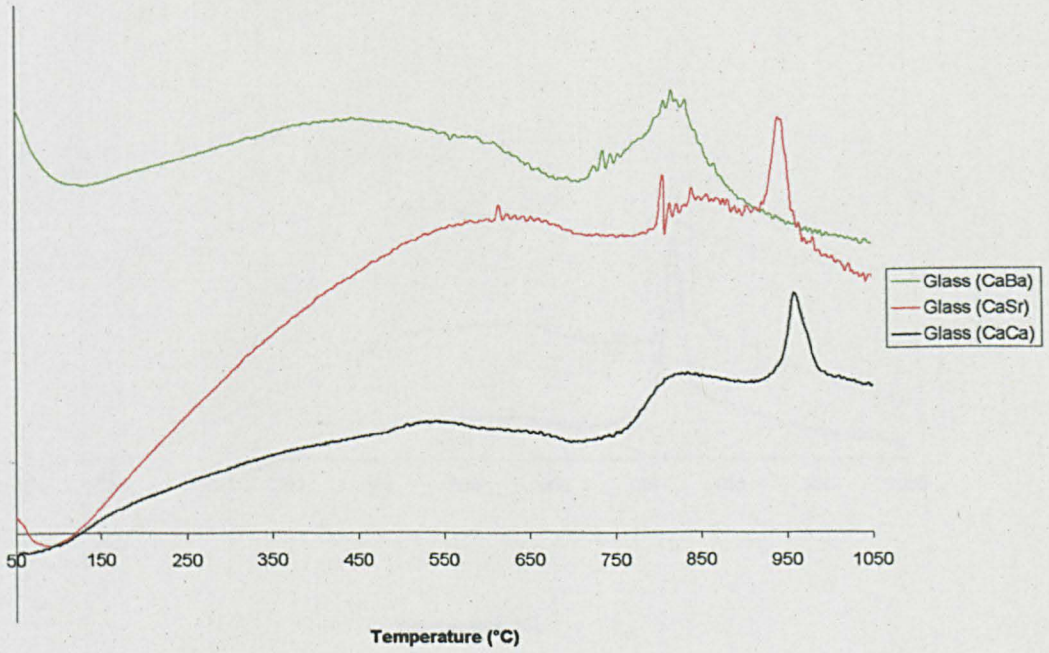

Figure 4.21: DTA traces of Glass (CaCa), Glass (CaSr) and Glass (CaBa) displayed offset to highlight changes in the glass transition and crystallisation temperatures. Y axis represents *x* °C.

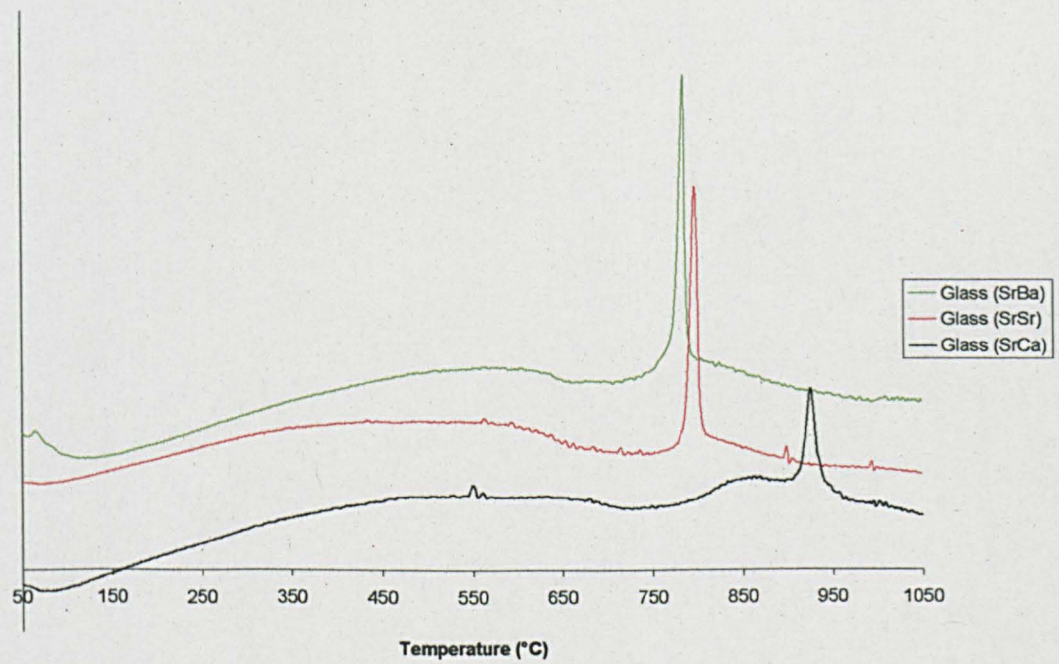

Figure 4.22: DTA traces of Glass (SrCa), Glass (SrSr) and Glass (SrBa) displayed offset to highlight changes in the glass transition and crystallisation temperatures. Y axis represents *x* °C.

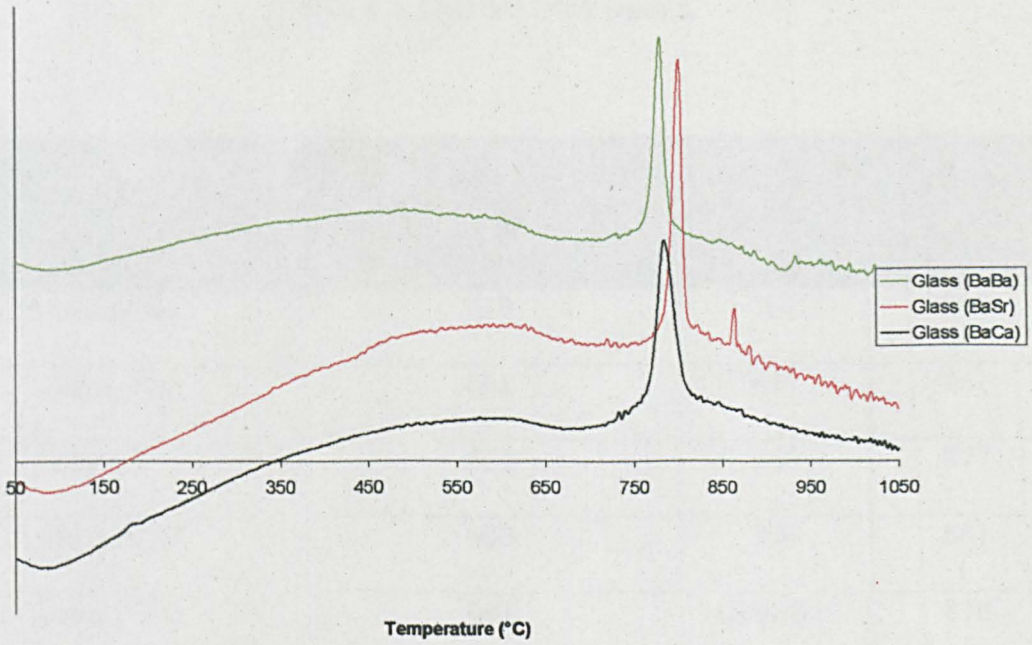

Figure 4.23: DTA traces of Glass (BaCa), Glass (BaSr) and Glass (BaBa) displayed offset to highlight changes in the glass transition and crystallisation temperatures. Y axis represents *x* °C.

Table 4.3: Derived DTA results.

Glass Composition	DTA Results		
	Tg (°C)	T_{N1} (°C)	T_{N2} (°C)
SerenoCem®	619	763	914
Glass (Ca)	661	831	961
Glass (Sr1)	593	769	877
Glass (Sr2)	600	795	861
Glass (Sr3)	631	Obscured	878
Glass (Sr4)	621	864	-
Glass (Sr5)	590	799	-
Glass (CaCa)	661	831	961
Glass (CaSr)	655	840	946
Glass (CaBa)	617	818	-
Glass (SrCa)	680	860	925
Glass (SrSr)	598	799	-
Glass (SrBa)	627	786	-
Glass (BaCa)	608	786	-
Glass (BaSr)	633	802	-
Glass (BaBa)	587	781	-

Accurate determination of the T_g of the ionomer glasses used in this project was difficult. To improve the definition of the glass transition temperature the glasses Glass (Sr1-5) and the commercial material were heat treated as described in *Section 3.2.2*. *Figure 4.24* shows two curves, one pre- and one post- heat treatment. The difference in

the glass transition and crystalline temperatures given by both methods is shown in *Table 4.4* and discussed in *Section 5.2.2*.

Table 4.4: DTA data for the commercial and novel strontium glasses. [R] denotes the repeat. A, represents the peak being absent or hidden by the larger T_{X2} peak.

Glass Composition	DTA Results					
	Tg (°C)	Tg [R] (°C)	T_{X1} (°C)	T_{X1} [R] (°C)	T_{X2} (°C)	T_{X2} [R] (°C)
SerenoCem®	619	639	763	763	914	914
Glass (Sr1)	593	619	769	759	877	874
Glass (Sr2)	600	623	795	776	861	860
Glass (Sr3)	631	647	A	A	878	890
Glass (Sr4)	621	650	A	A	864	866
Glass (Sr5)	590	615	A	A	799	806

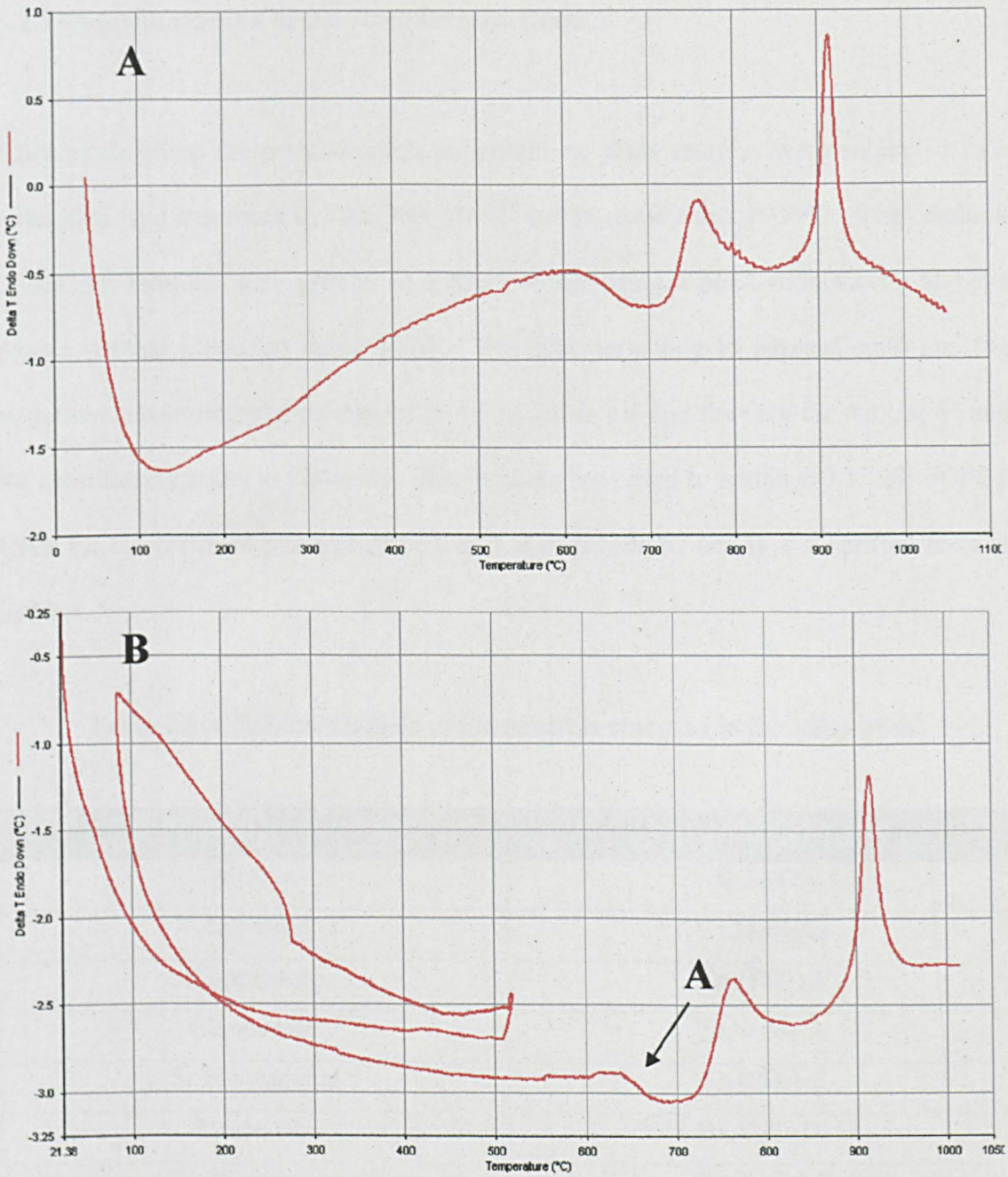

Figure 4.24: Two DTA traces for SerenoCem®. The first trace represents the results obtained prior to heat treatment and the second trace, post heat treatment. Note the more clearly defined glass transition temperature (A).

4.2.3 Characterisation of the Heat Treated Glasses

After establishing the crystallisation temperatures, glass samples were subjected to a controlled heat treatment to 700, 800, 900°C and in some cases 1000°C. The resultant crystalline samples were ground to a fine powder using a percussion mortar and the phases present identified using XRD. The data pertaining to SerenoCem® and the strontium substituted glasses can be found in *Table 4.6* and the data for the Ca, Sr and Ba substituted glasses in *Table 4.7*. Phases were identified to within ± 0.3° 2θ. JCPDS cards for the pertinent phases can be found in *Appendix III* and in a simplified form in *Table 4.5*.

Table 4.5: Chemical formula of the minerals observed in the XRD study.

Mineral Observed	Chemical Formula
Mullite	$Al_6Si_2O_{13}$
Anorthite	$CaAl_2Si_2O_8$
Fluorapatite	$Ca_5(PO_4)_3F$
Slawsonite	$SrAl_2Si_2O_8$
Sr Fluorapatite	$Sr_5(PO_4)_3F$
Paracelsian	$BaAl_2Si_2O_8$
Ba Fluorapatite	$Ba_5(PO_4)_3F$

Table 4.6: Crystalline phases identified by XRD after heat-treatment of SerenoCem® and the strontium substituted glasses, Glass (Sr1-5).

Material	Heat Treatment	$Angle_{Intensity}$	Phase(s)
SerenoCem®	As Cast	-	Amorphous
	700°	25.74_{100} 32.24_{76}	Mullite (15-776) Fluorapatite (15-876)
	800°	33.02_{99} 26.03_{63} 33.18_{63}	Fluorapatite Mullite Fluorapatite
	900°	28.14_{100} 32.08_{96} 32.01_{91} 21.74_{54} 26.09_{54}	Anorthite (41-1486) Fluorapatite Fluorapatite Anorthite Mullite
	1000°	28.16_{100} 32.02_{81} 33.18_{49} 21.67_{46} 25.98_{41}	Anorthite Fluorapatite Fluorapatite Anorthite Mullite
Glass (Sr1)	As Cast	-	Amorphous
	700°	31.85_{100} 32.68_{77}	Fluorapatite Fluorapatite

	800°	31.59_{100}	Fluorapatite
		32.76_{63}	Fluorapatite
		25.54_{52}	Fluorapatite
		32.84_{48}	Fluorapatite
	900°	31.93_{100}	Fluorapatite
		33.14_{51}	Fluorapatite
		26.45_{45}	Mullite
		25.89_{43}	Mullite
		49.44_{42}	Fluorapatite
		28.13_{33}	Anorthite
Glass (Sr2)	As Cast	-	Amorphous
	700°	-	Amorphous
	800°	31.75_{98}	Fluorapatite
		27.77_{68}	Anorthite
		21.82_{62}	Anorthite
		25.75_{62}	Fluorapatite
		32.96_{62}	Fluorapatite
		35.31_{45}	Mullite
	900°	27.74_{100}	Anorthite
		31.86_{81}	Fluorapatite
		21.76_{67}	Anorthite
		35.41_{60}	Mullite
		26.03_{51}	Mullite
		33.04_{48}	Fluorapatite
Glass (Sr3)	As Cast	-	Amorphous

	700°	-	Amorphous
	800°	27.65_{100}	Slawsonite (37-462)
		27.91_{96}	Anorthite
		27.44_{92}	Slawsonite
		26.01_{71}	Mullite
		35.2_{69}	Mullite
		31.76_{62}	Fluorapatite
		23.76_{57}	Slawsonite
		32.73_{50}	Fluorapatite
	900°	27.45_{99}	Slawsonite
		35.13_{65}	Mullite
		25.87_{64}	Fluorapatite
		21.69_{58}	Anorthite
		31.62_{51}	Sr Fluorapatite (17-609)
		23.64_{49}	Slawsonite
		32.41_{43}	Fluorapatite
Glass (Sr4)	As Cast	-	Amorphous
	700°	-	Amorphous
	800°	27.47_{92}	Slawsonite
		27.81_{73}	Anorthite
		25.94_{61}	Mullite
		35.11_{58}	Mullite
		23.73_{54}	Slawsonite
		30.07_{45}	Anorthite

	900°	27.68_{98}	Slawsonite
		26.14_{70}	Mullite
		35.42_{61}	Mullite
		23.97_{47}	Slawsonite
		32.78_{47}	Fluorapatite/ Sr Fluorapatite
		51.33_{44}	Fluorapatite
		21.94_{44}	Anorthite
Glass (Sr5)	As Cast	-	Amorphous
	700°	27.13_{100}	Sr Fluorapatite
		27.87_{94}	Slawsonite
		25.84_{86}	Mullite
		34.95_{78}	Mullite
		29.54_{76}	Slawsonite
		41.02_{68}	Mullite
	800°	27.32_{97}	Slawsonite
		25.88_{64}	Mullite
		30.08_{59}	Slawsonite
		35.14_{58}	Mullite
		23.66_{52}	Slawsonite
		30.80_{40}	Sr Fluorapatite

	900°	27.55_{92}	Slawsonite
		26.02_{78}	Mullite
		35.24_{68}	Mullite
		23.79_{62}	Slawsonite
		30.13_{54}	Sr Fluorapatite
		51.24_{42}	Slawsonite
		30.99_{41}	Sr Fluorapatite
	1000°	27.53_{97}	Slawsonite
		35.31_{76}	Mullite
		26.06_{62}	Mullite
		30.19_{41}	Sr Fluorapatite
		30.98_{41}	Sr Fluorapatite
		23.80_{41}	Slawsonite

Table 4.7: Crystalline phases identified by XRD after heat-treatment of SerenoCem® and the Group II A substituted glasses.

Material	Heat Treatment (°C)	$Angle_{Intensity}$	Phase(s)
Glass (CaCa)	As Cast	-	Amorphous
	700°	-	Amorphous
	800°	32.02_{90}	Fluorapatite
		32.23_{80}	Fluorapatite
		25.86_{74}	Fluorapatite
		33.01_{59}	Fluorapatite
		49.48_{46}	Fluorapatite
	900°	27.84_{100}	Anorthite
		27.54_{96}	Anorthite
		31.63_{99}	Fluorapatite
		27.99_{78}	Anorthite
		35.35_{77}	Mullite
		32.81_{74}	Mullite
		26.15_{73}	Fluorapatite
		21.77_{68}	Anorthite

	1000°	31.94_{95}	Fluorapatite
		33.23_{60}	Fluorapatite
		26.00_{59}	Mullite
		28.04_{54}	Anorthite
		21.73_{53}	Anorthite
		49.63_{52}	Fluorapatite
Glass (CaSr)	As Cast	-	Amorphous
	700°	-	Amorphous
	800°	27.73_{88}	Anorthite
		31.61_{78}	Fluorapatite
		36.21_{65}	Mullite
	900°	27.86_{93}	Anorthite
		31.86_{59}	Fluorapatite
		21.74_{58}	Anorthite
		35.37_{51}	Mullite
		25.81_{50}	Fluorapatite
	1000°	27.52_{90}	Slawsonite
		31.63_{69}	Sr Fluorapatite
		21.51_{61}	Anorthite
		35.16_{49}	Mullite
		25.66_{49}	Fluorapatite
Glass (CaBa)	As Cast	-	Amorphous
	700°	-	Amorphous

	800°	22.34_{100}	Paracelsian (10-352)
		29.90_{91}	Paracelsian
		33.72_{72}	Paracelsian
		31.81_{65}	Fluorapatite
		25.69_{63}	Fluorapatite
	900°	22.34_{94}	Paracelsian
		26.43_{88}	Ba Fluorapatite (71-1316)
		29.96_{84}	Paracelsian
		25.63_{82}	Fluorapatite
		31.76_{73}	Fluorapatite
		21.68_{67}	Anorthite
		40.90_{63}	Mullite
Glass (SrCa)	As Cast	-	Amorphous
	700°	-	Amorphous
	800°	31.55_{98}	Sr Fluorapatite
		27.73_{96}	Anorthite
		27.30_{92}	Slawsonite
		25.58_{75}	Fluorapatite
		25.29_{72}	Fluorapatite
		32.83_{66}	Fluorapatite/ Sr Fluorapatite
		35.51_{64}	Mullite
		48.47_{55}	Fluorapatite

	900°	30.79_{100}	Sr Fluorapatite
		27.46_{58}	Slawsonite
		27.35_{54}	Slawsonite
		27.73_{46}	Anorthite
		35.22_{43}	Mullite
	1000°	27.68_{100}	Slawsonite
		31.50_{100}	Sr Fluorapatite
		27.54_{96}	Slawsonite
		27.80_{83}	Anorthite
		25.99_{76}	Mullite
		35.24_{74}	Mullite
		32.64_{72}	Fluorapatite
		35.16_{69}	Mullite
Glass (SrSr)	As Cast	-	Amorphous
	700°	-	Amorphous
	800°	30.74_{100}	Sr Fluorapatite
		27.32_{85}	Slawsonite
		27.27_{79}	Slawsonite
		35.16_{56}	Mullite
		26.09_{54}	Mullite
	900°	30.62_{100}	Slawsonite
		27.23_{51}	Slawsonite
		25.92_{44}	Mullite
		27.54_{42}	Slawsonite
		35.08_{41}	Mullite

Glass (SrBa)	As Cast	-	Amorphous
	700°	-	Amorphous
	800°	26.68_{100}	Ba Fluorapatite
		30.51_{97}	Sr Fluorapatite
		25.84_{78}	Mullite
		21.72_{77}	Anorthite
		29.87_{68}	Paracelsian
	900°	30.56_{100}	Slawsonite
		26.74_{81}	Ba Fluorapatite
		25.78_{56}	Mullite
		32.43_{46}	Paracelsian
		29.84_{40}	Paracelsian
Glass (BaCa)	As Cast	-	Amorphous
	700°	-	Amorphous
	800°	22.40_{100}	Paracelsian
		25.70_{90}	Fluorapatite
		26.33_{95}	Mullite
		29.56_{84}	Paracelsian
		34.47_{72}	Fluorapatite
		29.99_{70}	Paracelsian
		27.59_{57}	Anorthite

	900°	26.50_{100}	Mullite
		25.75_{83}	Fluorapatite
		25.84_{74}	Fluorapatite
		29.64_{72}	Paracelsian
		34.62_{53}	Paracelsian
		24.98_{50}	Ba Fluorapatite
Glass (BaSr)	As Cast	-	Amorphous
	700°	-	Amorphous
	800°	26.57_{100}	Ba Fluorapatite
		25.79_{87}	Mullite
		34.53_{69}	Paracelsian
		23.36_{72}	Paracelsian
		22.51_{67}	Slawsonite
		30.32_{59}	Ba Fluorapatite
	900°	26.56_{98}	Ba Fluorapatite
		22.43_{94}	Slawsonite
		30.41_{86}	Ba Fluorapatite
		29.64_{72}	Paracelsian
		29.98_{74}	Paracelsian
		25.68_{74}	Mullite
Glass (BaBa)	As Cast	-	Amorphous

	700°	26.62_{100}	Ba Fluorapatite
		27.30_{83}	Anorthite
		28.03_{80}	Anorthite
		32.83_{78}	Paracelsian
		33.93_{83}	Anorthite
	800°	26.35_{100}	Mullite
		25.77_{60}	Mullite
		41.53_{58}	Paracelsian
		34.47_{56}	Paracelsian
		29.53_{54}	Ba Fluorapatite
		23.27_{51}	Ba Fluorapatite
	900°	26.44_{99}	Mullite
		36.85_{97}	Ba Fluorapatite
		29.65_{69}	Paracelsian
		29.53_{65}	Ba Fluorapatite
		25.68_{64}	Mullite
		34.47_{51}	Paracelsian

The following XRD curves of the heat-treated glass samples highlight the 'as cast', 800 and either 900 or 1000°C and the corresponding major phases present at those temperatures. *Figure 4.25* represents the SerenoCem® ionomer glass, *Figure 4.26* Glass (Sr3), and *Figure 4.27* Glass (Sr5). *Figure 4.28* Glass (CaCa), *Figure 4.29* Glass (SrSr), and *Figure 4.30* Glass (BaBa) provide a comparison of the phases present in the fully substituted calcium, strontium and barium ionomer glasses respectively.

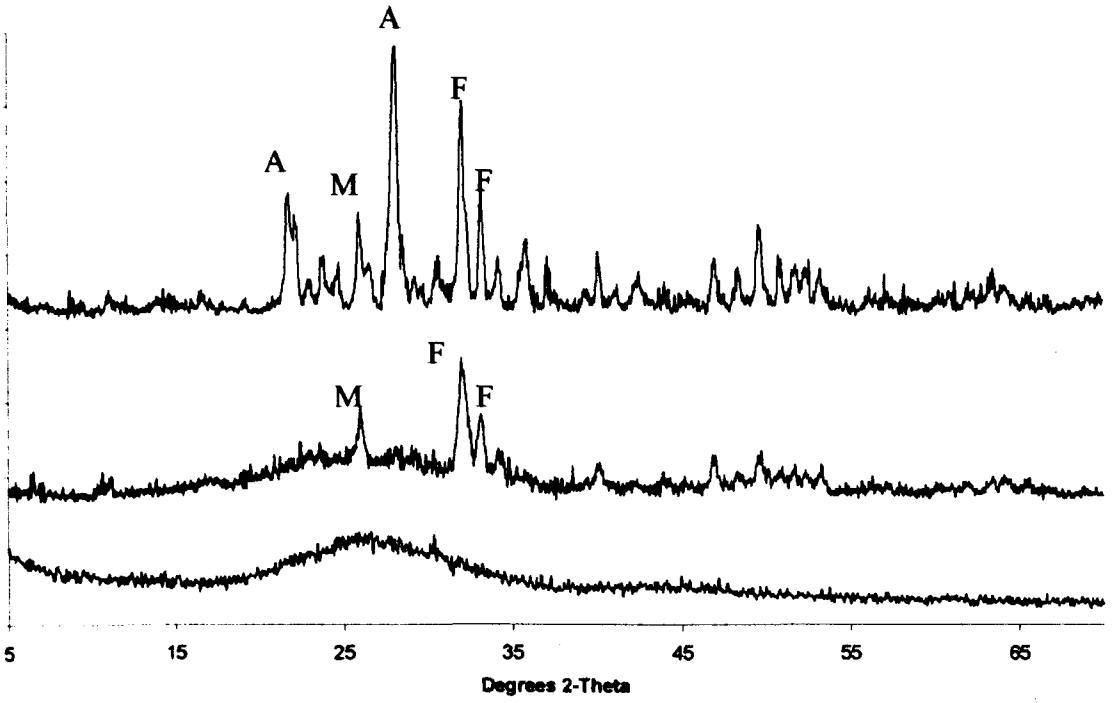

Figure 4.25: XRD curves for the as cast, 800 and 1000 °C heat-treated SerenoCem® ionomer glass samples. **F** represents fluorapatite, **M** mullite and **A** anorthite.

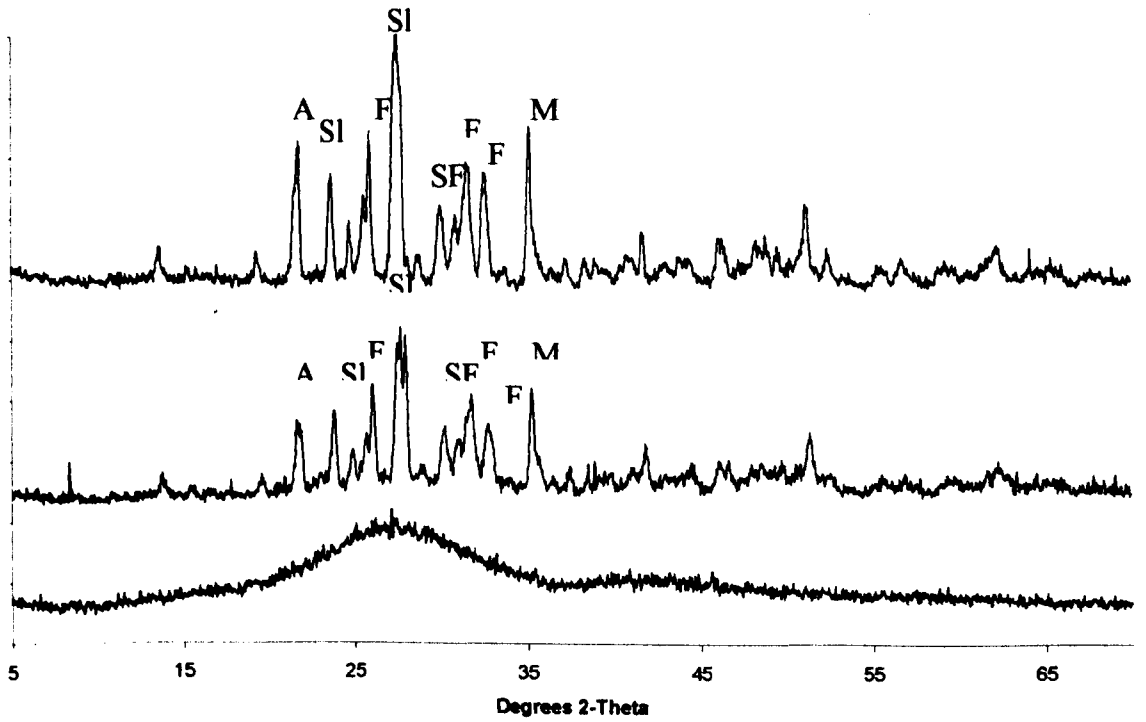

Figure 4.26: XRD curves for the as cast, 800 and 900 °C heat-treated Glass (Sr3) ionomer glass samples. **SL** represents slawsonite and **SF** strontium fluorapatite.

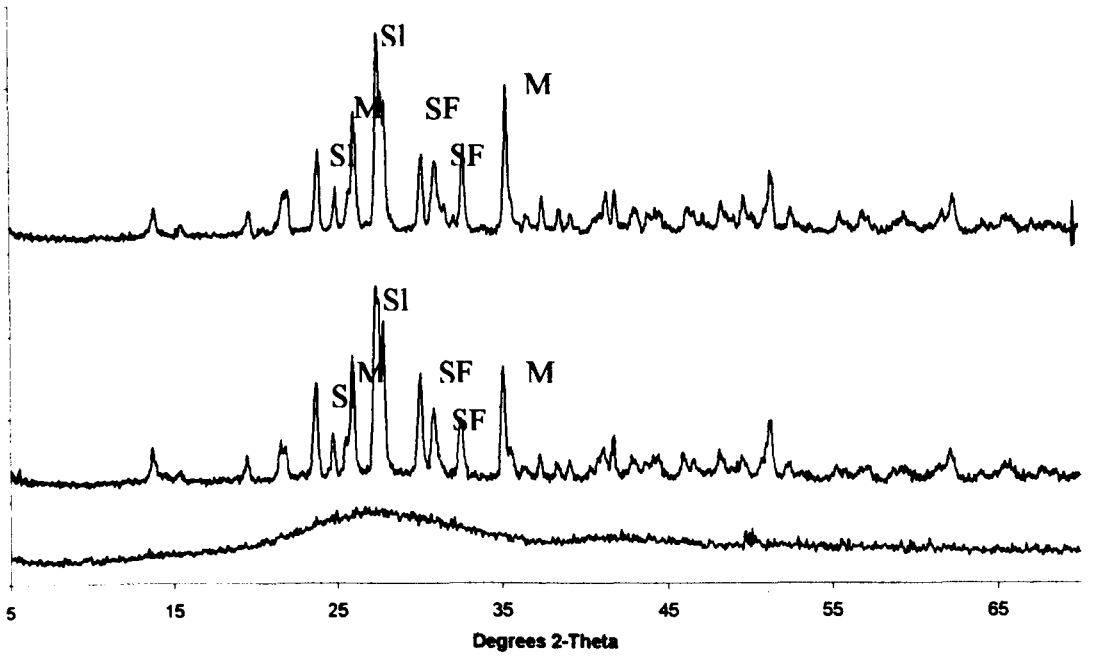

Figure 4.27: XRD curves for the as cast, 800 and 1000 °C heat-treated Glass (Sr5) ionomer glass samples.

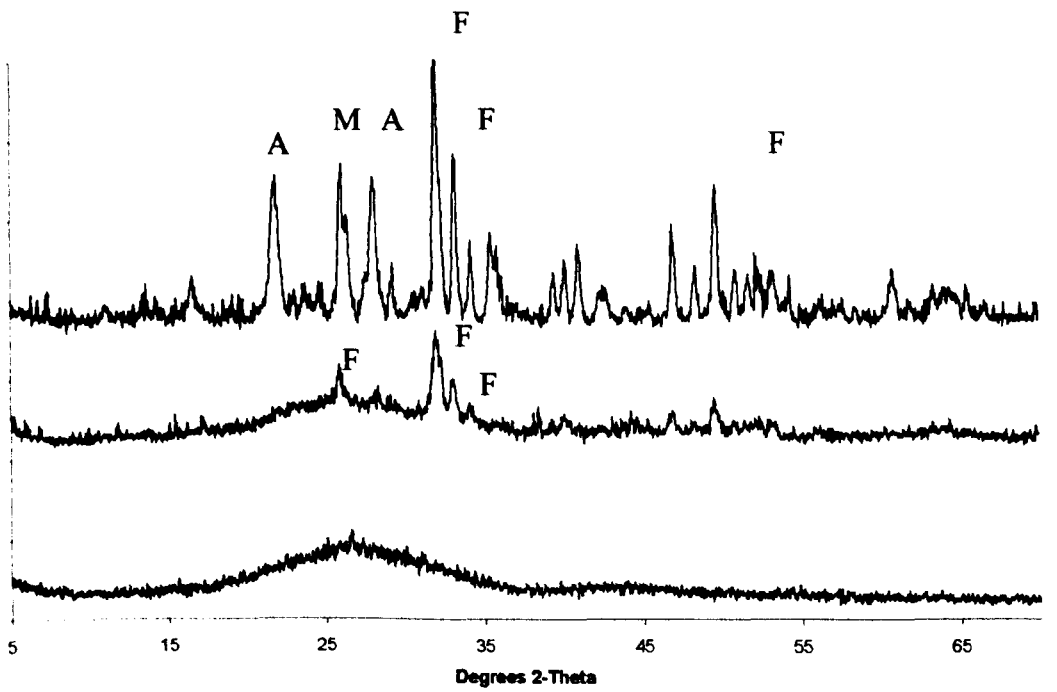

Figure 4.28: XRD curves for the as cast, 800 and 1000 °C heat-treated Glass (CaCa) ionomer glass samples.

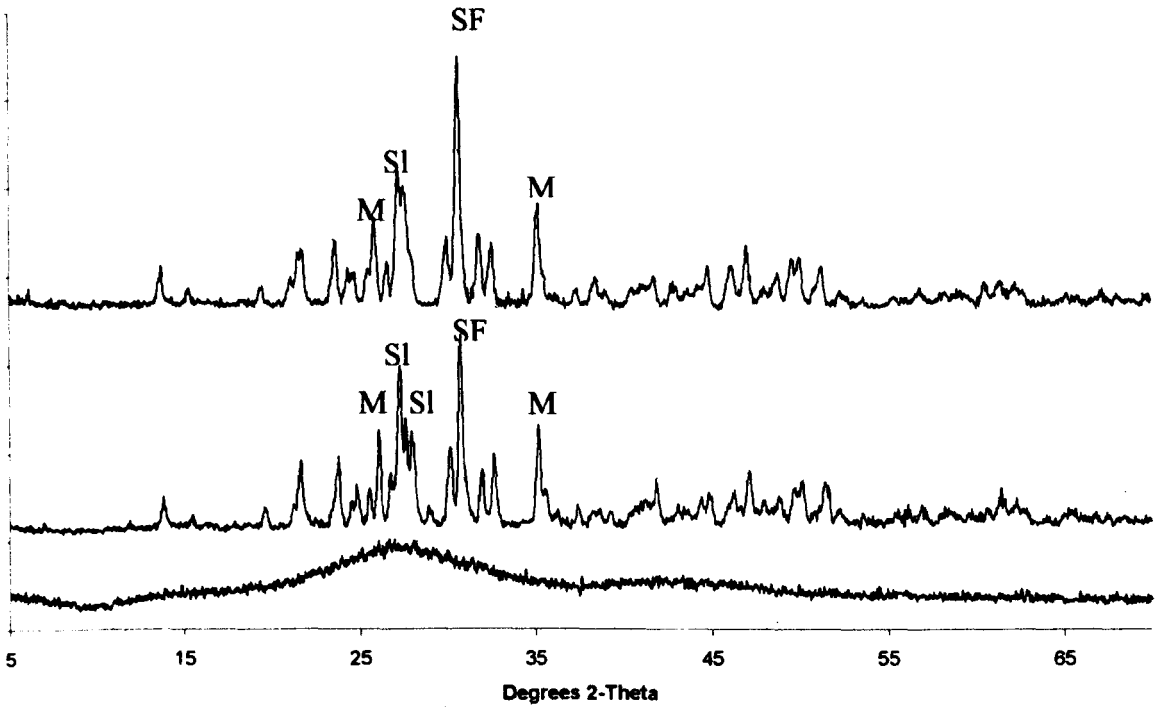

Figure 4.29: XRD curves for the as cast, 800 and 900 °C heat-treated Glass (SrSr) ionomer glass samples.

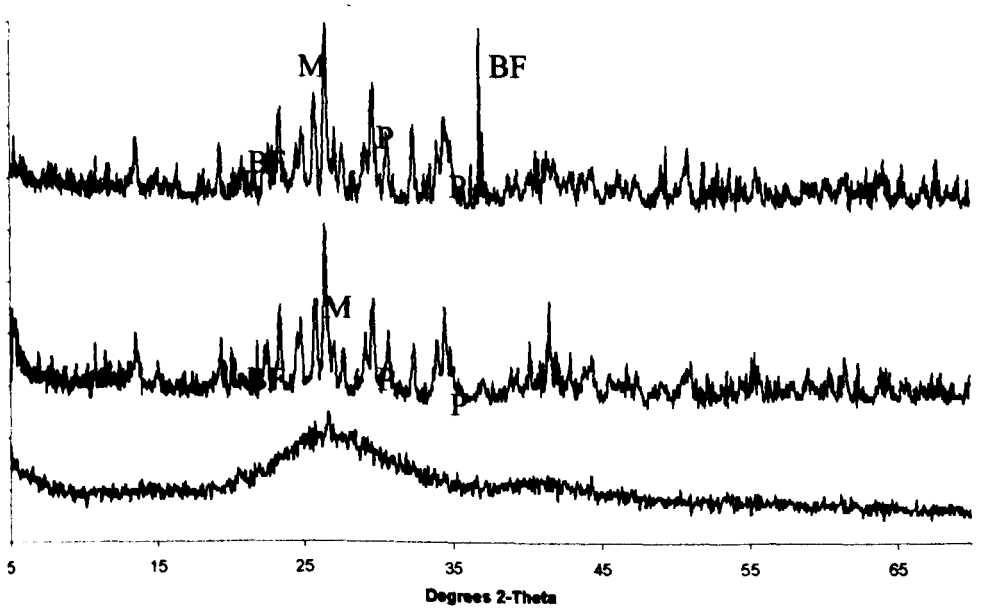

Figure 4.30: XRD curves for the as cast, 800 and 900 °C heat-treated Glass (BaBa) ionomer glass samples. **P** represents paracelsian and **BF** barium fluorapatite.

4.2.4 TEM and EDS

Milled glass powders of the strontium glasses Glass (Sr1-5) were prepared and viewed in a TEM to determine if any micro-crystallisation and phase separation of the glass powders had occurred upon quenching. Micrographs of the powders revealed a structure similar to that identified in the SEM. No phase separation or crystallisation was observed (an example is shown in *Figure 4.31*).

EDS of identified glass particles indicated that aluminium, silicon, calcium and phosphorus existed in all samples, while calcium, strontium and barium existed in their respective samples (see *Figure 4.32* and *4.33* for a comparison between a calcium and strontium based glass respectivly).

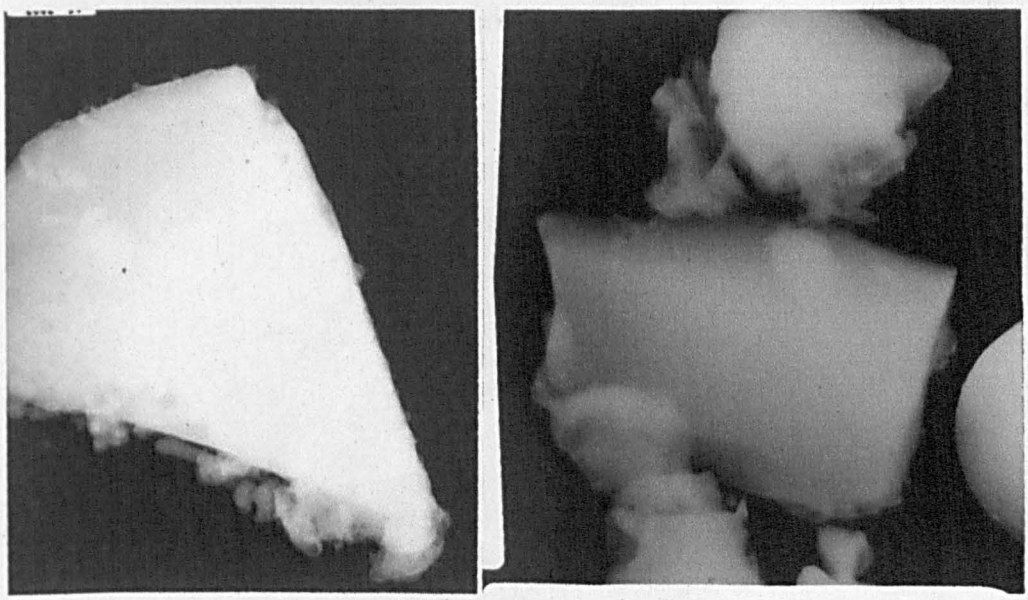

Figure 4.31: Transmission electron images of a typical glass particle of Glass (Sr1).

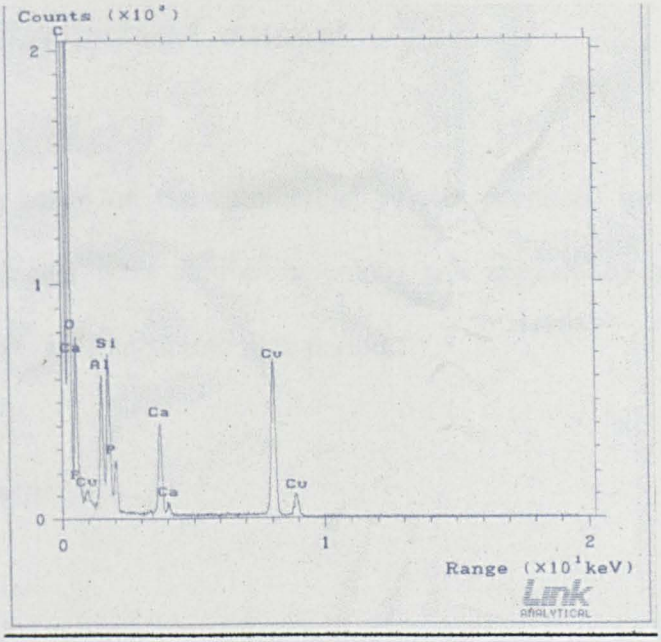

Figure 4.32: EDS trace of a calcium based ionomer glass (Glass (Ca)). Note the three calcium peaks present. Copper in the above trace is from the copper grid the samples are mounted on.

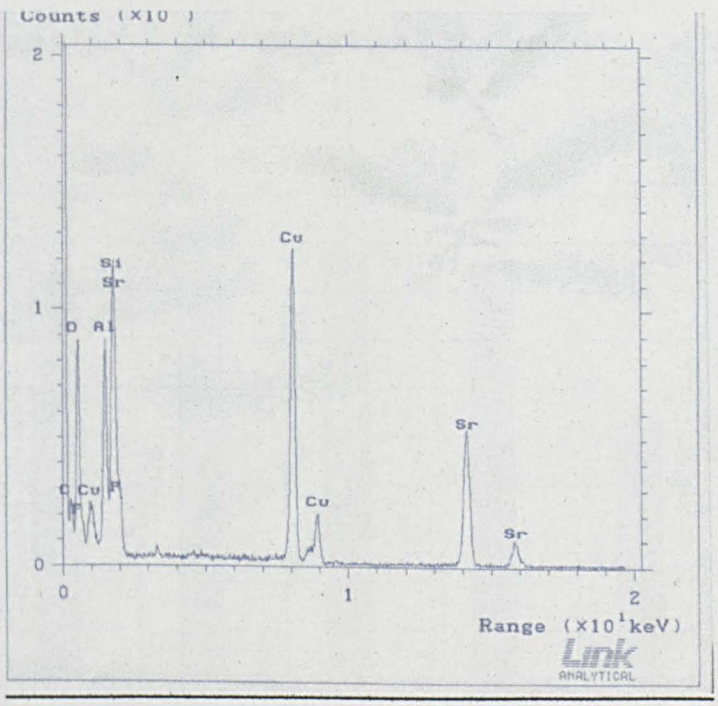

Figure 4.33: EDS trace of a strontium based ionomer glass (Glass (Sr5)). Note the three strontium peaks present. Copper in the above trace is from the copper grid the samples are mounted on.

4.3 Characterisation of Cements

All novel cements based on the commercial system produced in this study formed cements. The cements were similar in colour and appearance to the commercial material and set within a comparable time period.

4.3.1 Gilmore Needle

Freshly mixed cements of the ionomer compositions were tested using the Gilmore Needle indentation test to determine their feasibility to produce set cements in an analogous time to the commercial cement. Working and setting times of the strontium analogues provided by the Gilmore needle method are given in *Figure 4.34*. All the cements were found to be workable for between 1 and 3 minutes, and had set within 10 minutes.

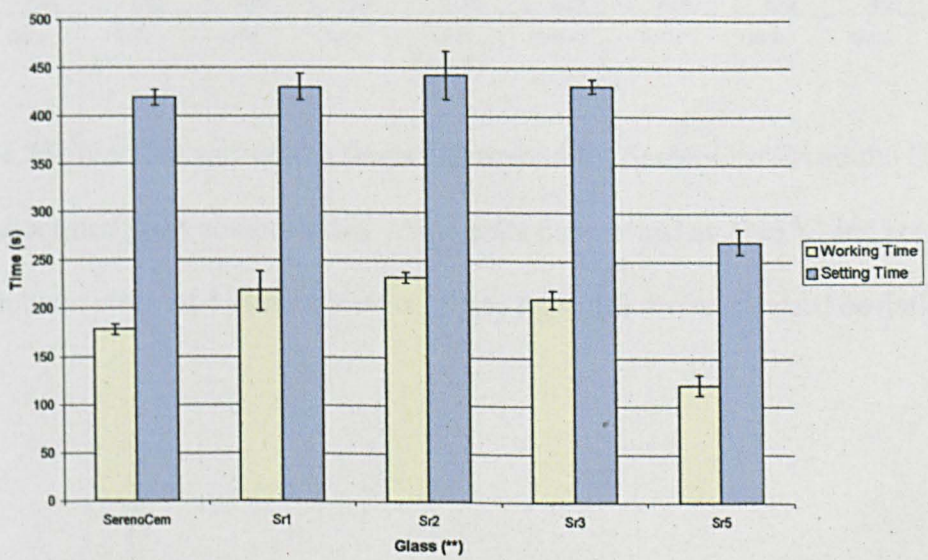

Figure 4.34: Working and setting times determined for SerenoCem® and the strontium analogues. All results determined at 23±1°C and are the arithmetic mean of 5 measurements. Error bars give ± one standard deviation.

A similar result was observed in the Group II substituted glasses where the change in concentration and ionic radius of the substituted ions affected the working and setting times of the cements, see *Figure 4.35*. The affect of tartaric acid on the working and setting times of SerenoCem® and the fully substituted strontium analogue Glass (Sr5) is given in *Figure 4.36*.

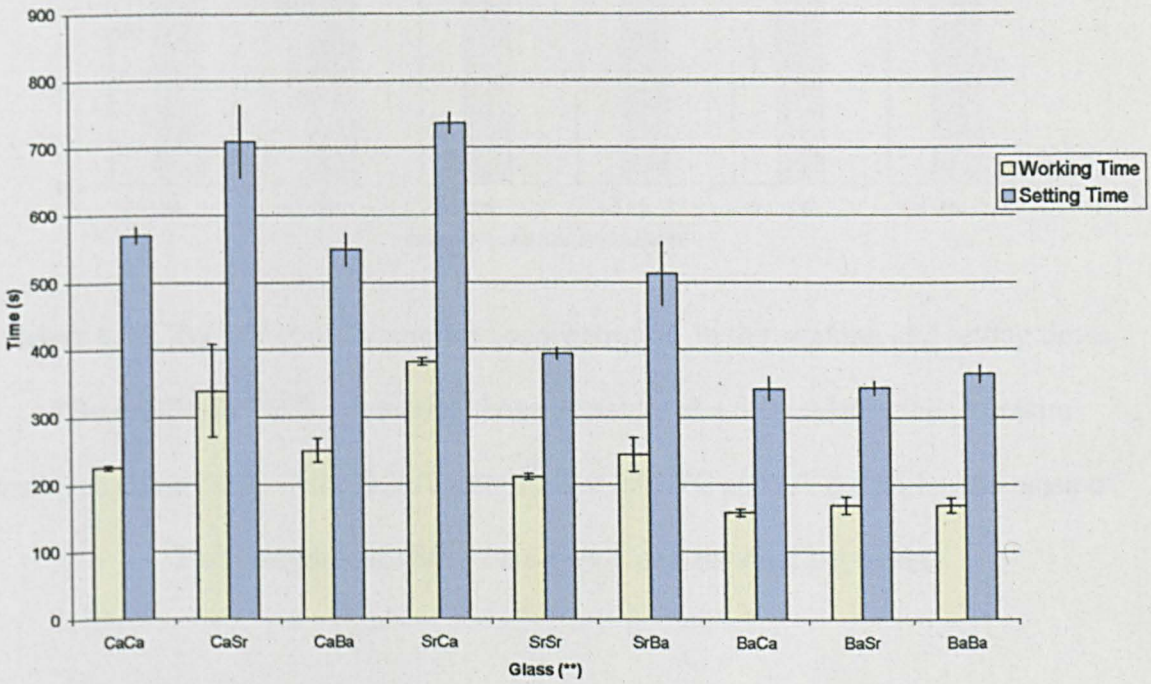

Figure 4.35: Working and setting times determined for SerenoCem® and the Group II A substituted glass compositions. All results determined at 23±1°C and are the arithmetic mean of 5 measurements. Error bars give ± one standard deviation.

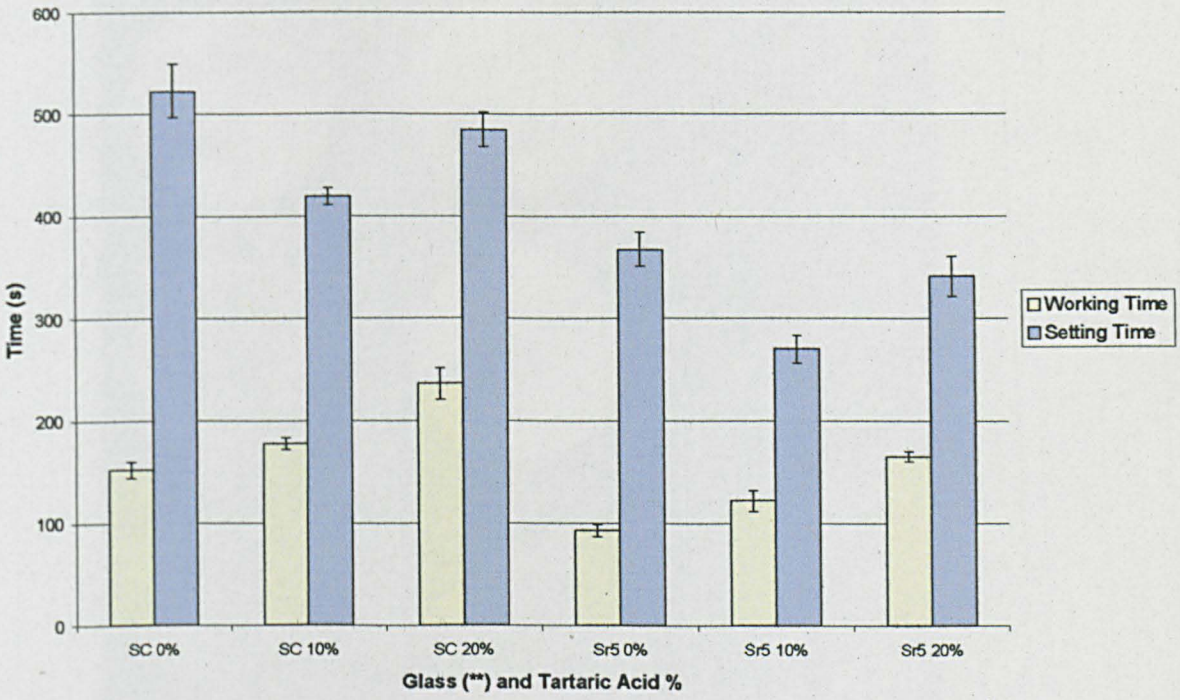

Figure 4.36: The affect of tartaric acid concentration on the working and setting times of SerenoCem® (SC) commercial bone cement and a fully substituted strontium analogue Glass (Sr5). All results determined at 23±1°C and are the arithmetic mean of 5 measurements. Error bars give ± one standard deviation.

4.3.2 Radiopacity

Radiopacity of SerenoCem®, the strontium cements GIC (Sr1-Sr5) were quantitatively measured using an aluminium step-wedge and a dental X-ray unit. A typical radiograph can be seen in *Figure 4.37*. SerenoCem® corresponded to a thickness of approx 1.5 mm aluminium while GIC (Sr5) gave three times the contrast of the commercial cement, approx 4.5 mm of aluminium.

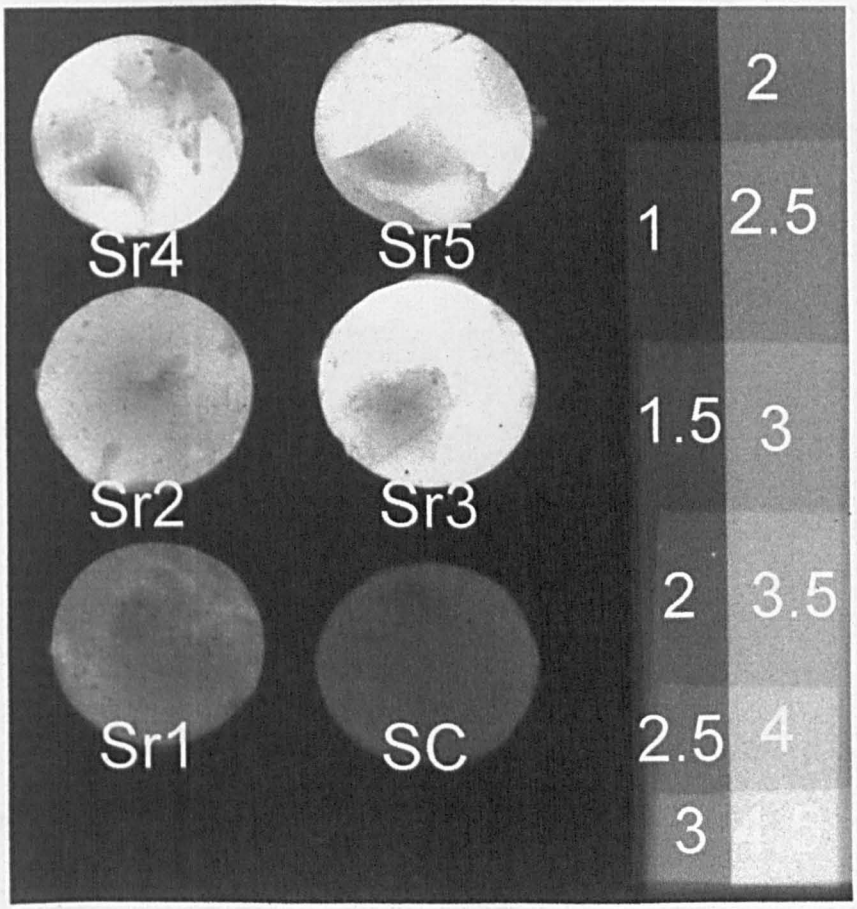

Figure 4.37: Radiograph of commercial SerenoCem® and the five strontium based cements compared to an aluminium step-wedge. Numbers indicate mm aluminium.

Radiographs were also taken of the Group II series. To give an indication of the increase in radiopacity with increasing ionic radius, a radiograph was taken with the end member in each series; see *Figure 4.38* as well as radiographs between the individual series, *Figure 4.39*. Results are consistent with increased concentrations of heavy metal ions giving greater contrast and therefore increased radiopacity.

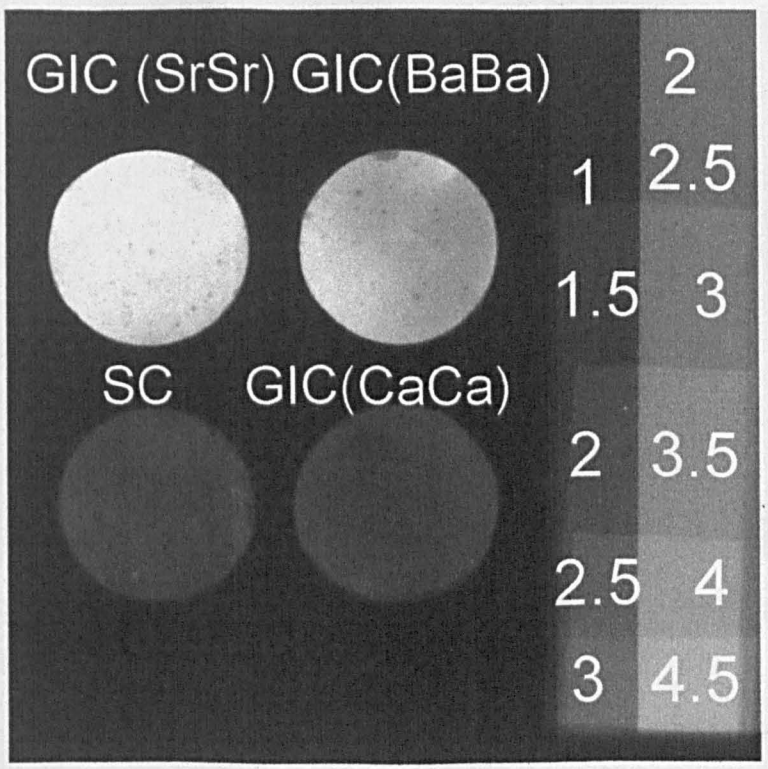

Figure 4.38: Radiograph of commercial SerenoCem®, GIC (CaCa), GIC (SrSr) and GIC (BaBa) cements compared to an aluminium step-wedge. Numbers indicate mm aluminium.

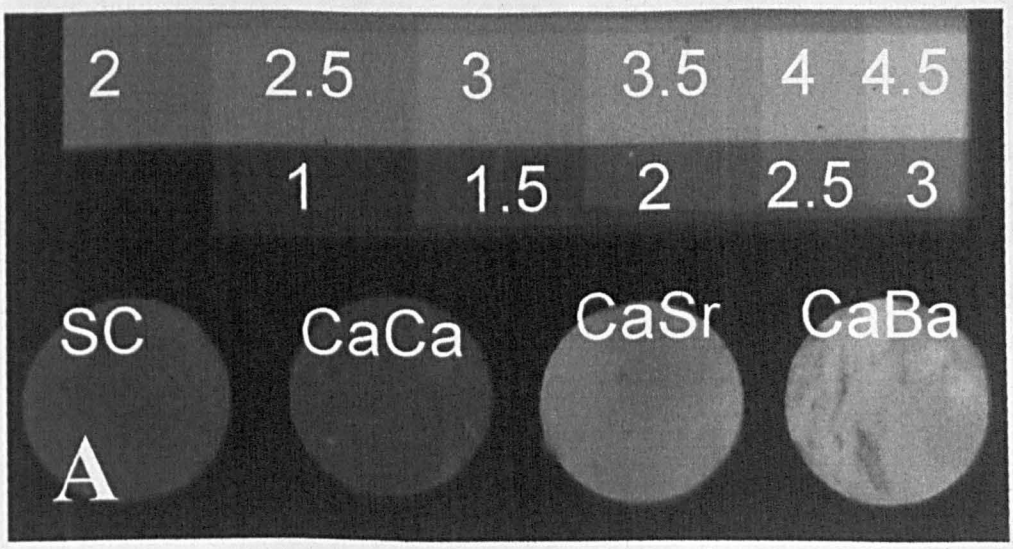

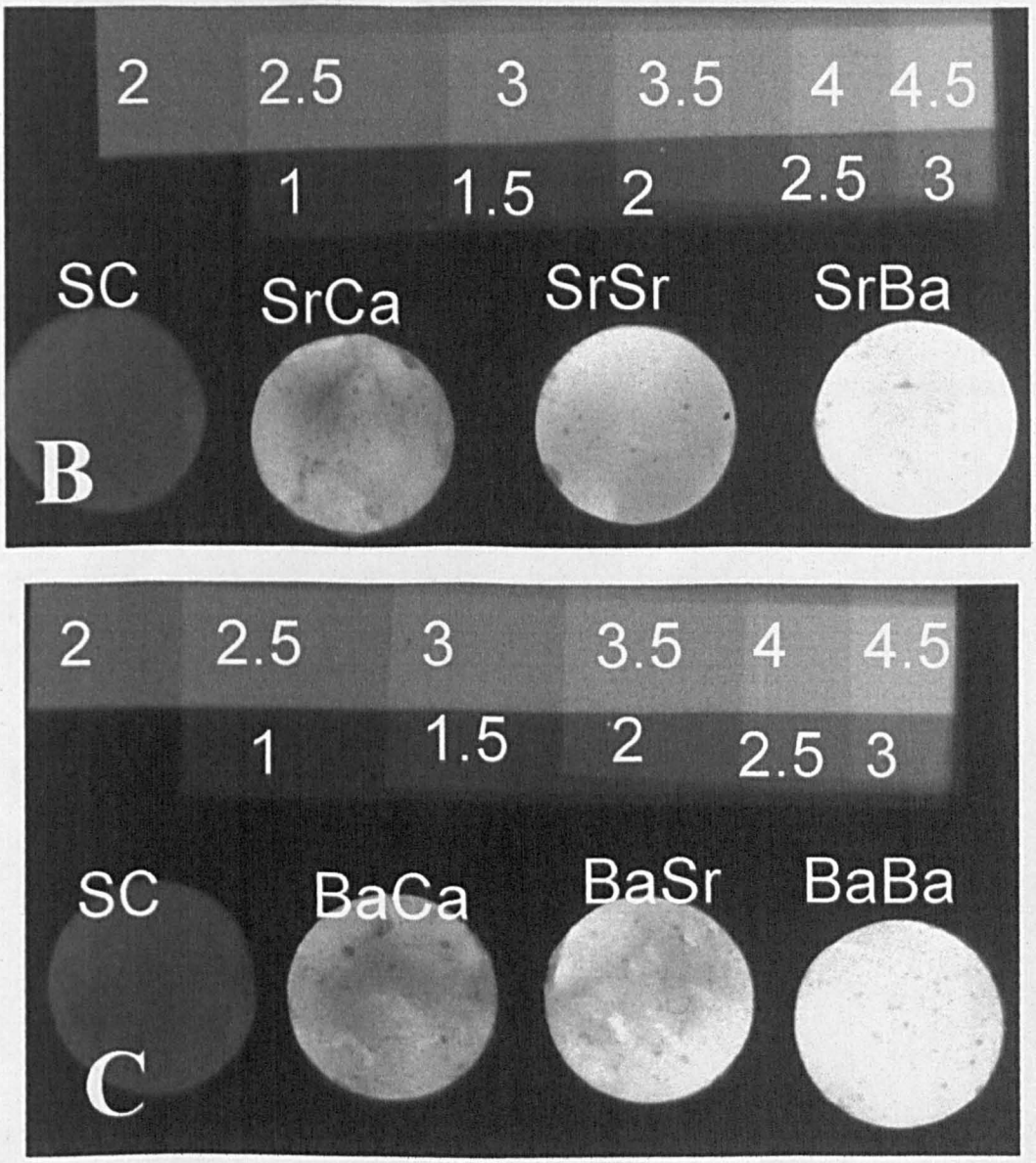

Figure 4.39: Radiograph of commercial SerenoCem® and three series of Group II cements compared to an aluminium step-wedge. **A** represents the change calcium based cements, **B** the strontium based cements and **C** the barium based cements. Numbers indicate mm aluminium.

4.3.3 Flexural Strength

Flexural strength measurements of cement rods aged for 1 and 28 days were taken. The results indicate that the substitution of strontium ions for the calcium ions in the ionomer glass had no statistically significant affect on the flexural strength of the resultant cements over 28 days (*Figure 4.40*). A similar result was observed in the Group II substituted series of cements (*Figure 4.41*).

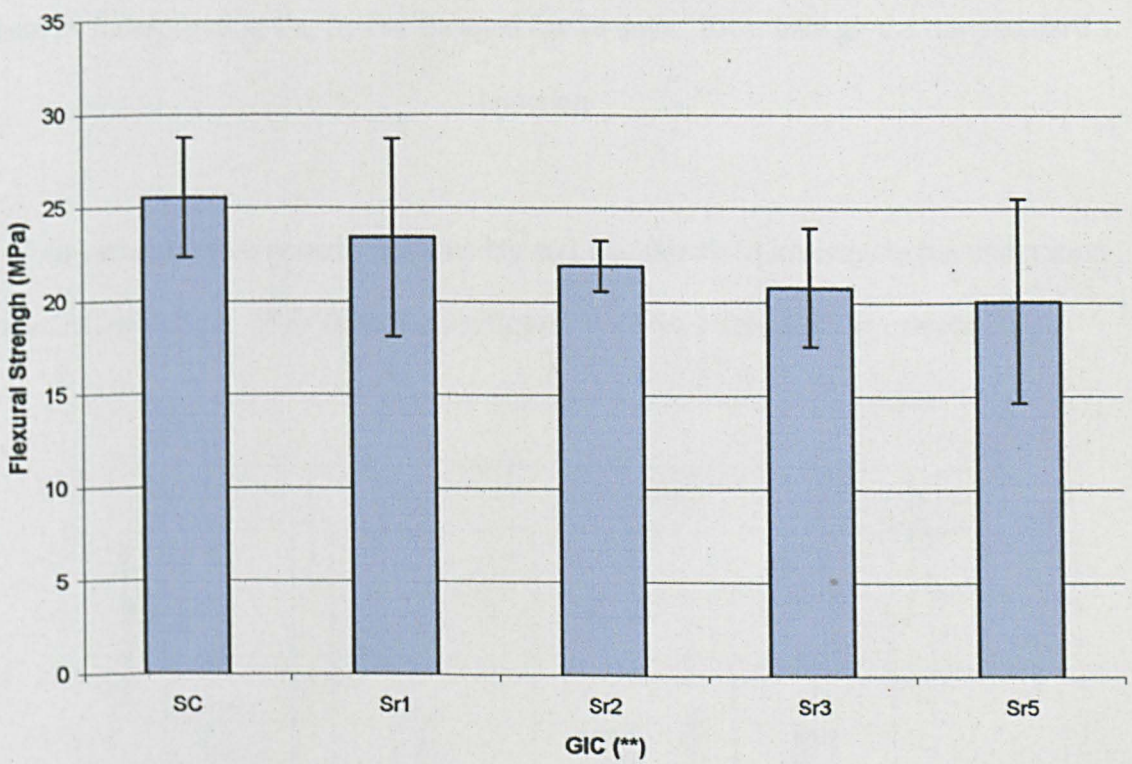

Figure 4.40: Flexural Strength measurements of SerenoCem® (SC) and the strontium analogues aged for 28 days. Error bars give ± one standard deviation.

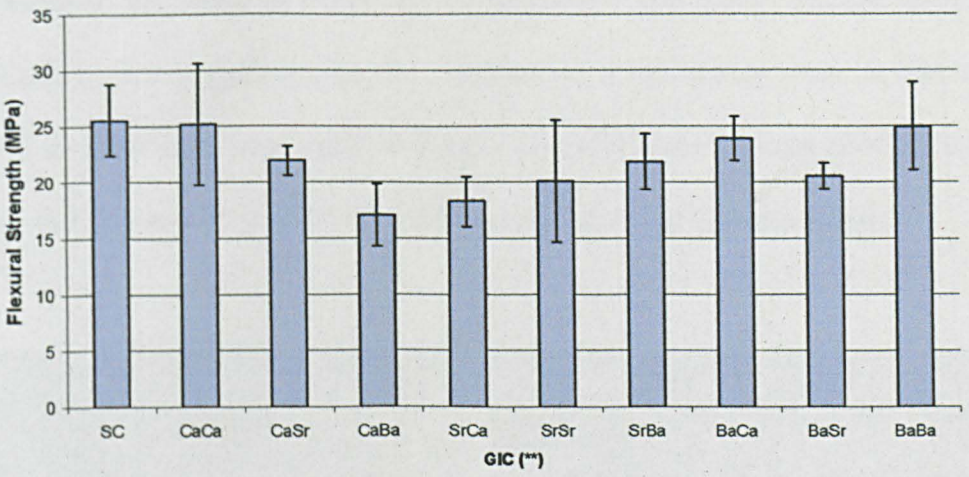

Figure 4.41: Flexural Strength measurements of SerenoCem® (SC) and the series of cements incorporating Ca, Sr and Ba aged for 28 days. Error bars give ± one standard deviation.

Four cements were tested after one day and one month to investigate the maturation of the GIC with time. This is shown in *Figures 4.42* for a series of the cements.

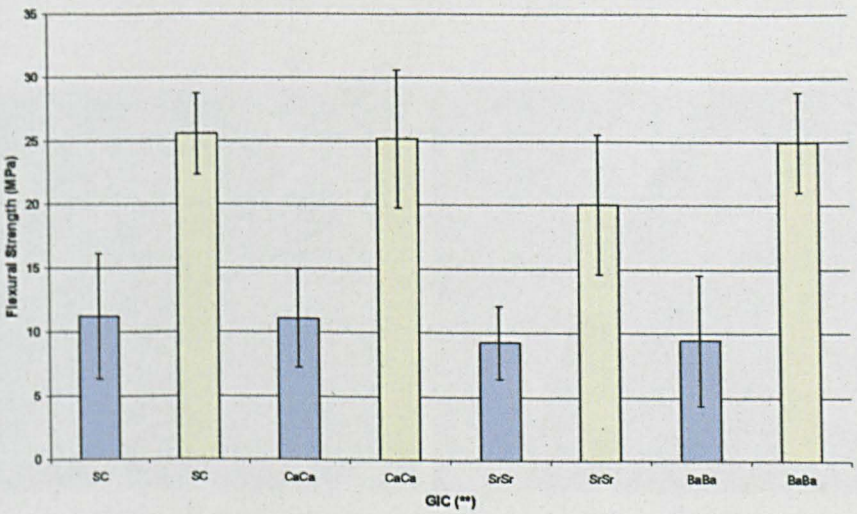

Figure 4.42: Flexural Strength measurements of SerenoCem® (SC) and a series of cements aged for one month. The blue bar represents the flexural strength after 1 day and the yellow bar the flexural strength after 28 days. Error bars give ± one standard deviation.

To ascertain the mode of failure of the cements in this study, fracture surfaces of GICs (CaCa), (SrSr), (BaBa) and the commercial bone cement were sectioned and viewed in an SEM after both 1 and 28 days. Secondary electron images of the cements are given in *Figures 4.43 to 4.46*. Marker bars represent the distance shown.

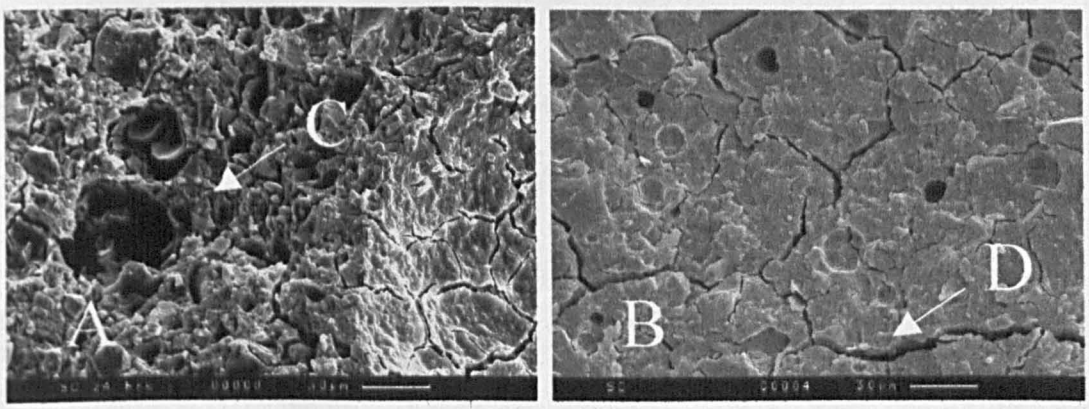

Figure 4.43: Photomicrographs of the fracture surface of SerenoCem® after 1 day (A) and 28 days (B). Feature (C) represents glass pullout in the surface of the sample and (D) a hydration or matrix fracture in the polymer matrix.

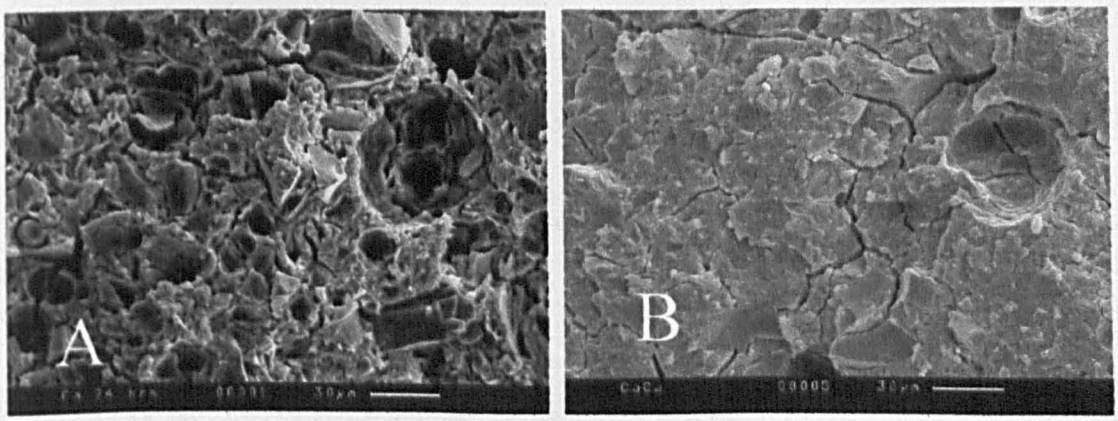

Figure 4.44: Photomicrographs of the fracture surface of GIC (CaCa) after 1 day (A) and 28 days (B).

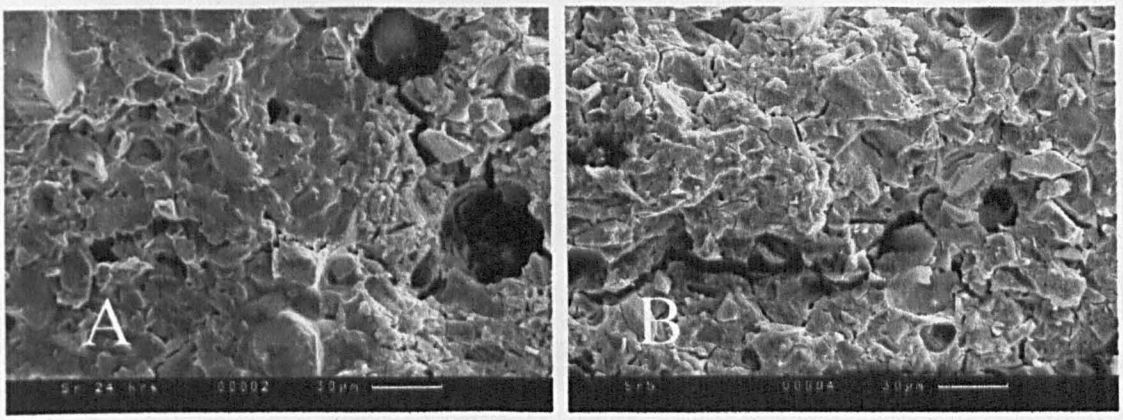

Figure 4.45: Photomicrographs of the fracture surface of GIC (SrSr) after 1 day (A) and 28 days (B).

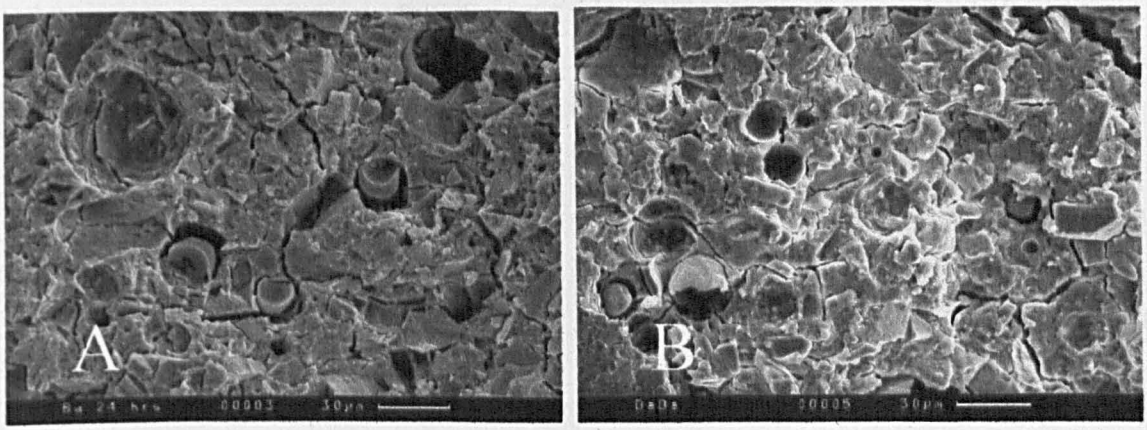

Figure 4.46: Photomicrographs of the fracture surface of GIC (BaBa) after 1 day (A) and 28 days (B).

4.3.4 Ion Release

Fluoride release rates of the cements were measured over a 28 day period. The elution of fluoride was detected using a fluoride ion electrode calibrated between two known limits. The cumulative fluoride ion release of the 100% substituted series of cements and the commercial control can be seen in *Figure 4.47*.

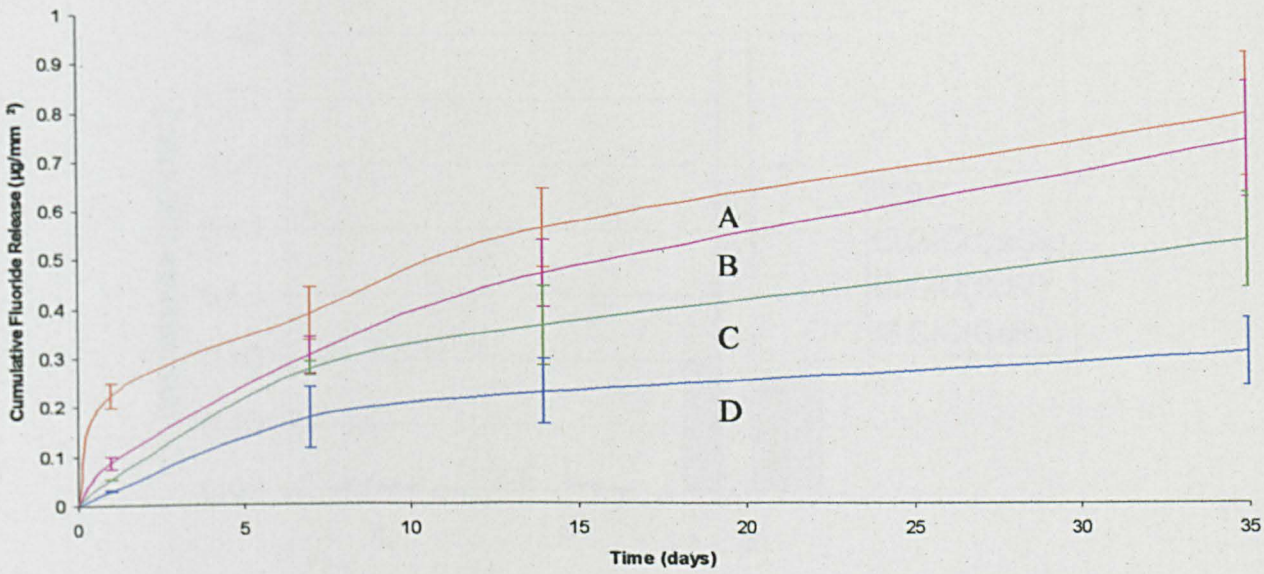

Figure 4.47: Cumulative elution of fluoride from the substituted ionomer and commercial cements over a four week period. (A-SerenoCem®, B-GIC(CaCa), C-GIC(SrSr), D-GIC(BaBa)). Error bars represent ± one standard deviation.

All cements released detectable levels of silicon, aluminium and phosphorus and their respective Group II ions. Aluminium, phosphorus and silicon release is shown for the 100% substitutions and the commercial material in *Figure 4.48*.

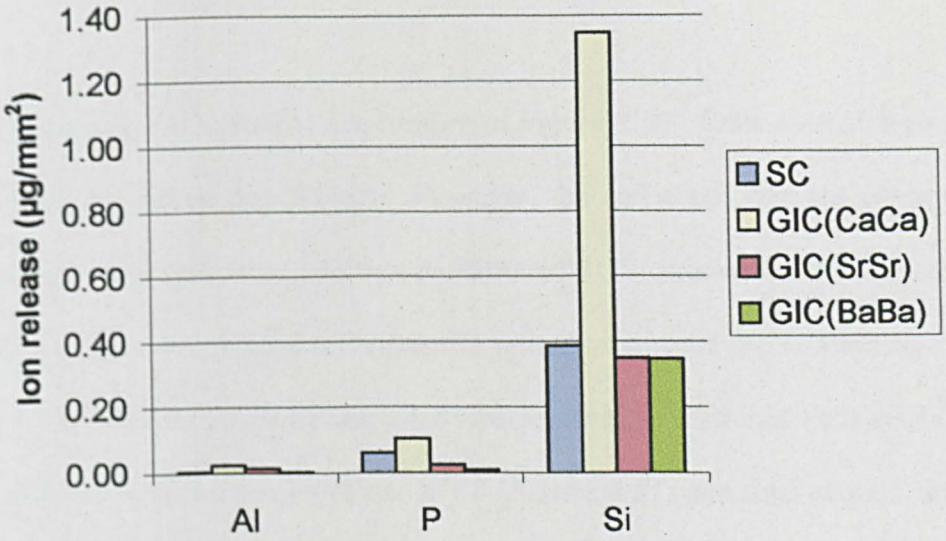

Figure 4.48: Aluminium, phosphorus and silicon ion release from the four GICs measured using ICP-ES. SC in the above figure is SerenoCem® bone cement.

Figure 4.49 shows the ion release of the Group II A ions. The cements released their respective Group II A ion. In addition, trace levels of strontium were detected in the calcium-based cement.

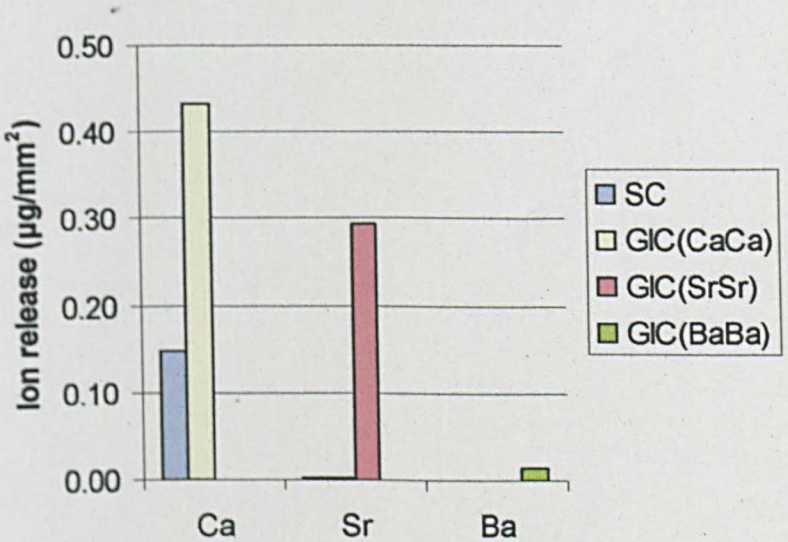

Figure 4.49: Group II A ion release from the four GICs measured using ICP-ES. SC in the above figure is SerenoCem® bone cement.

4.3.5 Biocompatibility

SEM micrographs of the results can be seen in *Figure 4.50*. Cells were able to grow on all the GICs studied in this project. However, the cell sheet was not confluent, and rounded cells were present in addition to flattened ROS cells with a normal osteoblast-like appearance. The poorest cell response was shown to be the commercial material (*Figures 4.50:A and 4.50:B*) having a few sparse sheets of flattened cells on its surface. This supported with the results of the MTT (*Figure 4.51*) and total protein assays. In both assays, the tissue culture plastic was used as the control (100%) (*Figure 4.50:F*).

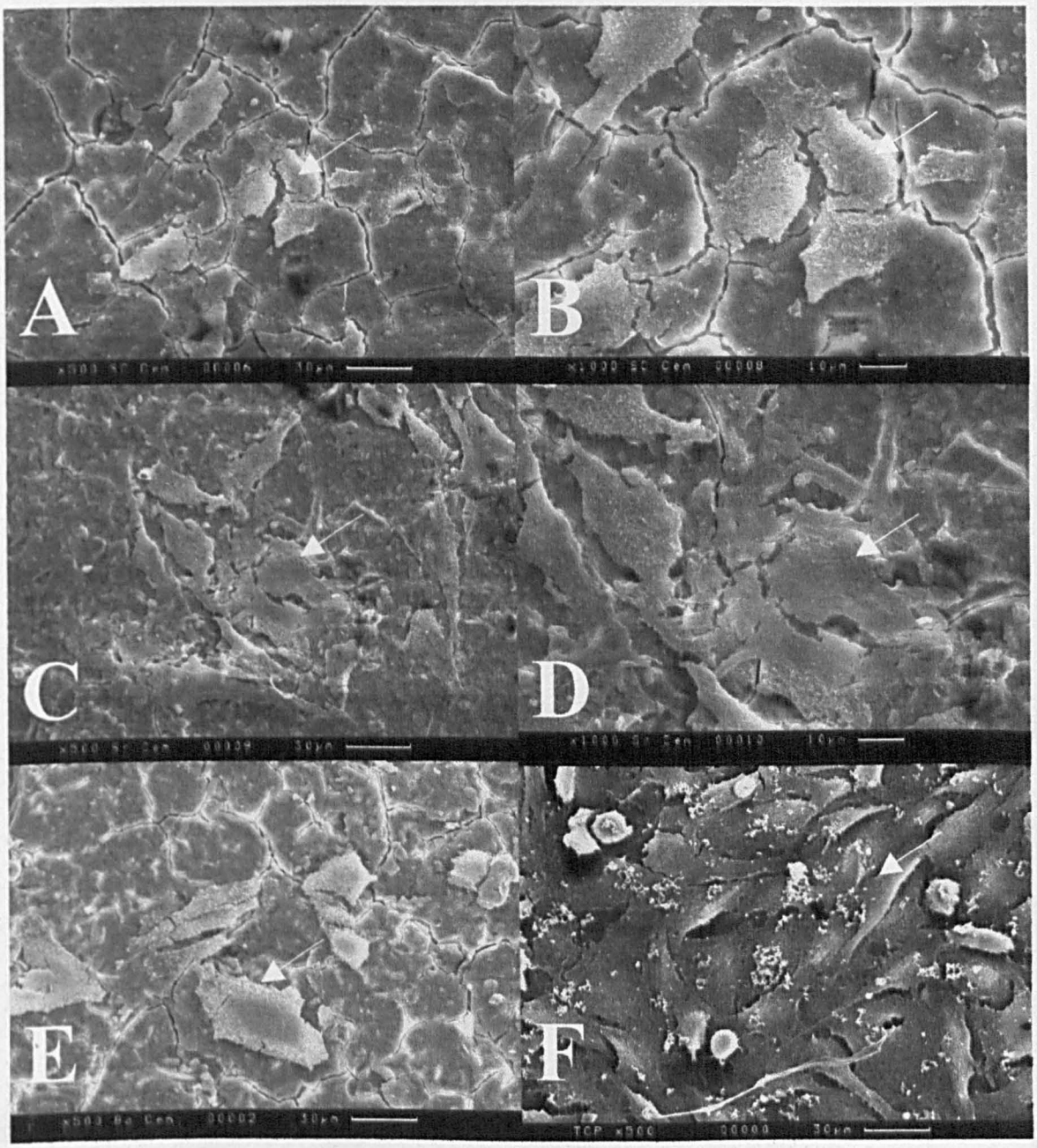

Figure 4.50: Secondary electron SEM images of cell cultured cements. Marker bars represent distance shown. A) Commercial SerenoCem® cement showing a few flattened cells attached to the surface B) Higher magnification micrograph of the cells on the commercial material showing the cells to be proliferating (note the surface deposits on the cells) C) GIC(SrSr) showing a proliferating sheet of flattened cells D) Higher magnification micrograph showing a semi-confluent sheet of flattened cells on the surface of GIC(SrSr) E) Micrograph of a section of cells proliferating on the surface of GIC(BaBa) F) Confluent sheet of flattened cells adhering to the surface of the tissue culture plastic control.

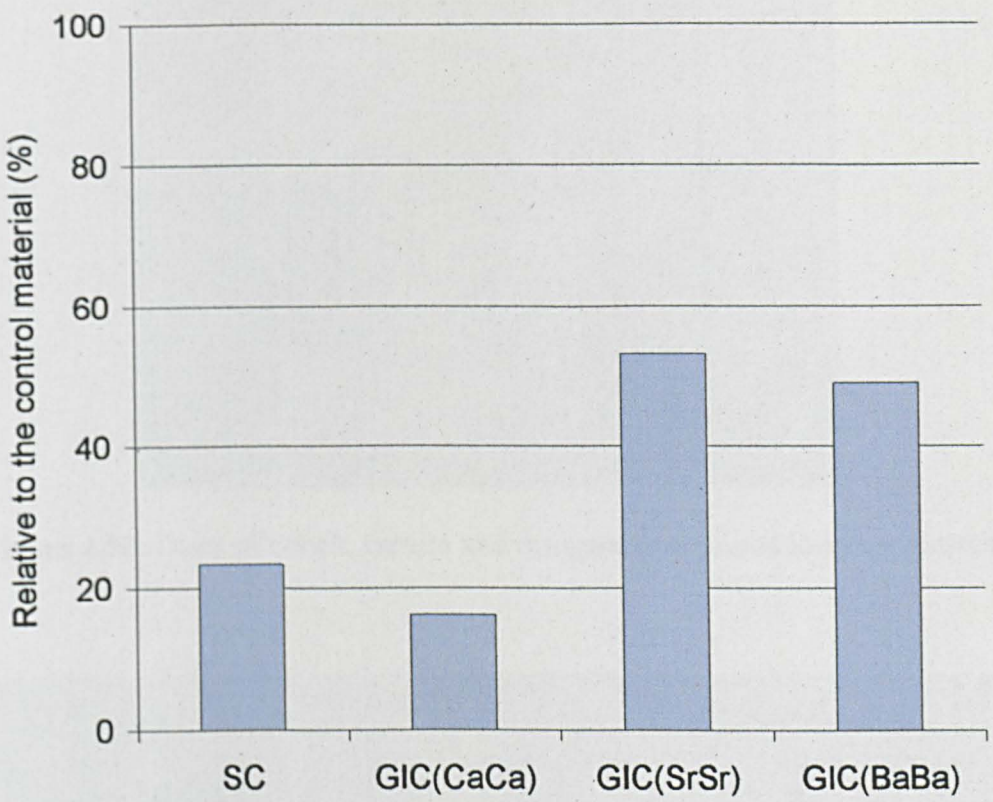

Figure 4.51: Bar chart displaying the MTT assay result for the end member cements.

4.3.6 Coloured GICs

Coloured glasses were successfully cast and were noticeably coloured on cooling, as shown in *figures 4.52 and 4.53*. Glasses were milled into <45 μm powders and only those containing cobalt oxide, manganese oxide and K2021 produced powders, were noticeably coloured. The remaining glass powders appeared white. The control containing no colouring agent produced a colourless glass and a white powder. Resultant glasses were mixed with poly(acrylic acid) and coloured cements formed.

Figure 4.52: Discs of cobalt, cerium and manganese coloured ionomer glasses.

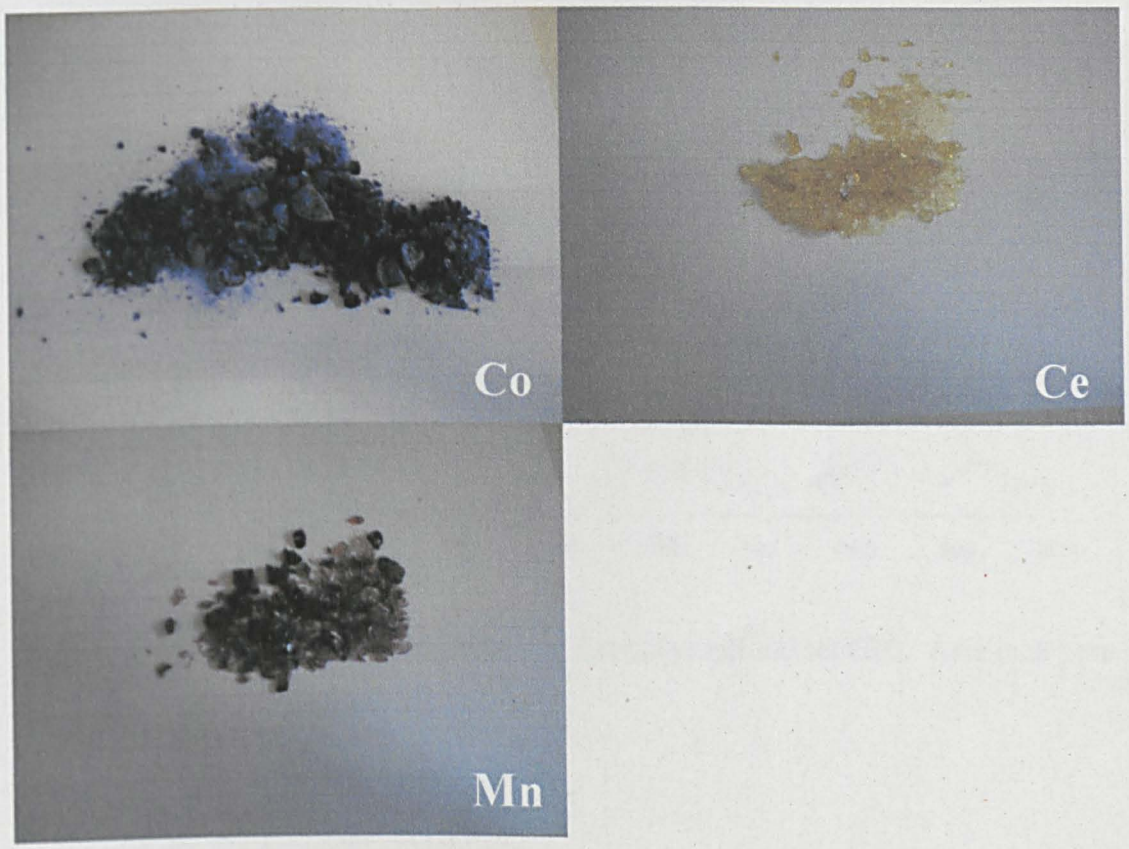

Figure 4.53: Ground up cobalt, cerium and manganese coloured ionomer glasses.

4.3.7 NMR

Solid state NMR was used to investigate the changes in micro-environment around the aluminium and silicon ions in the ionomer glass used in SerenoCem® as it sets upon the application of acrylic acid. ^{29}Si NMR was initially run on the basic glass composition and on set cements to obtain a control trace to compare with the cements with varying additive concentrations. This is shown in *Figure 4.54*. A trace showing the effect of tartaric acid on the silicon micro-environment can be seen in *Figure 4.55*.

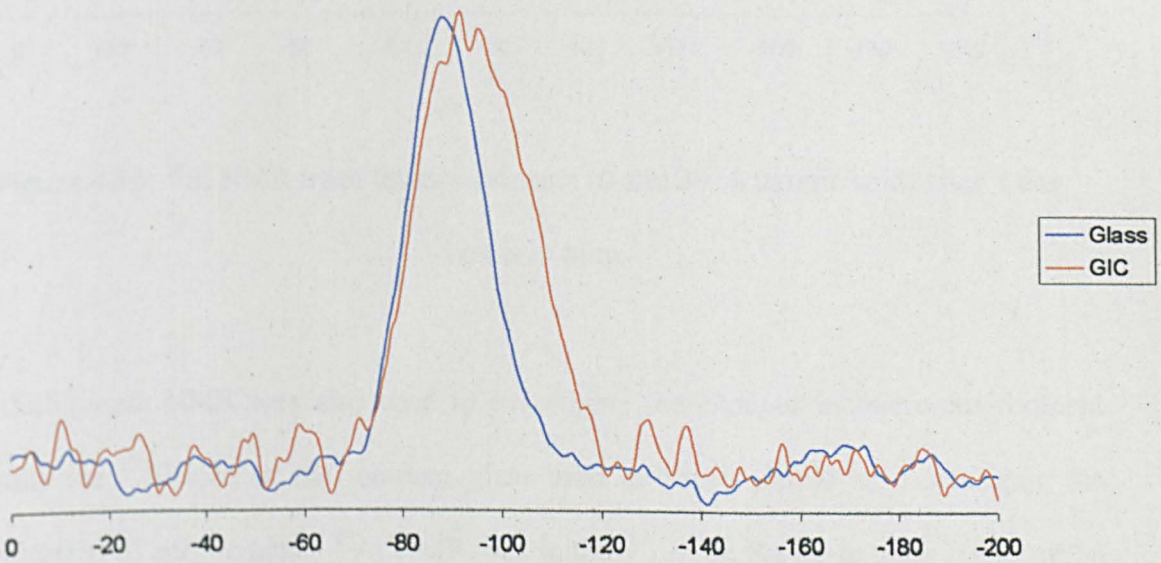

Figure 4.54: ^{29}Si NMR trace of the ionomer glass and the set GIC. Axis is in ppm.

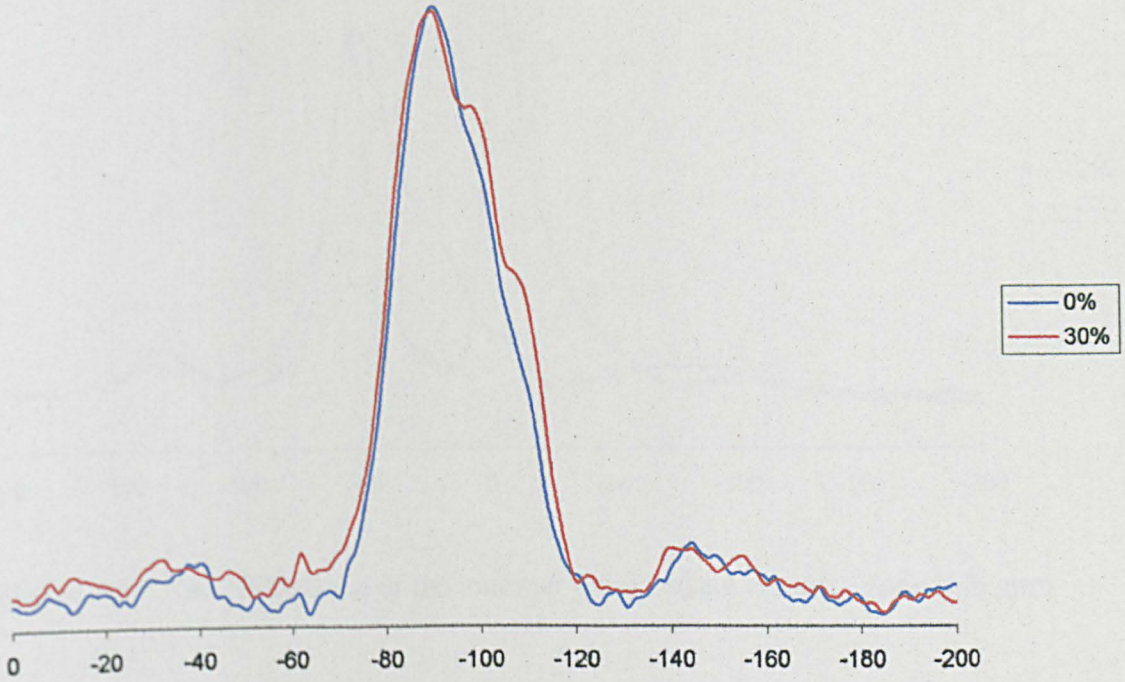

Figure 4.55: ^{29}Si NMR trace for two cements (0 and 30 % tartaric acid) after 1 day. Axis is in ppm.

Solid state NMR was also used to investigate the changes in micro-environment around the ^{27}Al ions in the ionomer glass used in SerenoCem® as it sets upon the application of acrylic acid. ^{27}Al NMR was initially run on the basic glass composition and set cements to obtain a control trace to compare with the cements with varying additive concentrations. This is shown in *Figure 4.56*. A trace showing the effect of tartaric acid on the aluminium micro-environment can be seen in *Figure 4.57*.

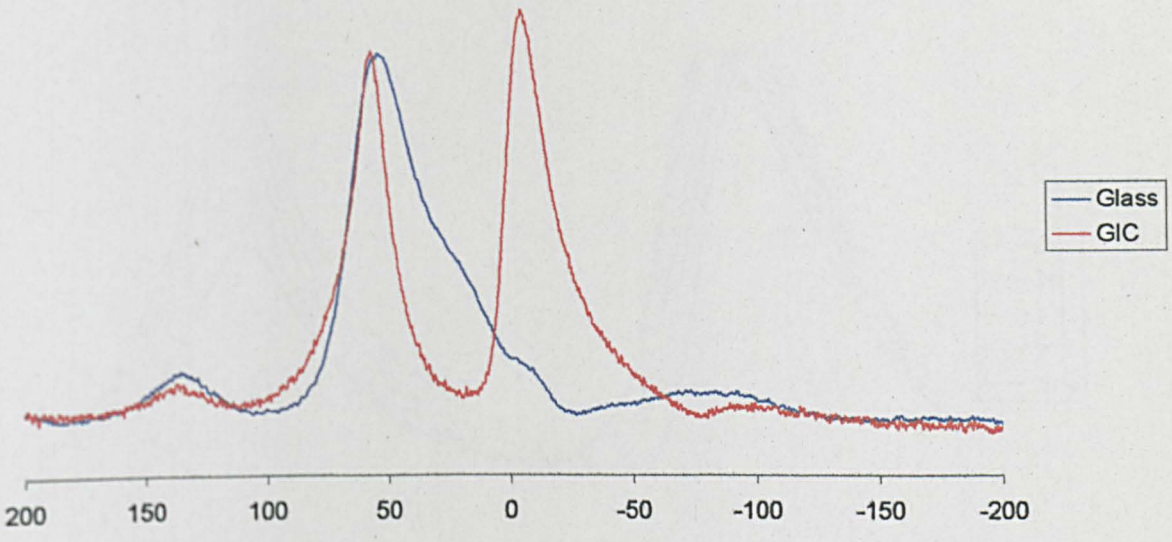

Figure 4.56: ^{27}Al NMR trace of the ionomer glass and set cement. Axis is in ppm.

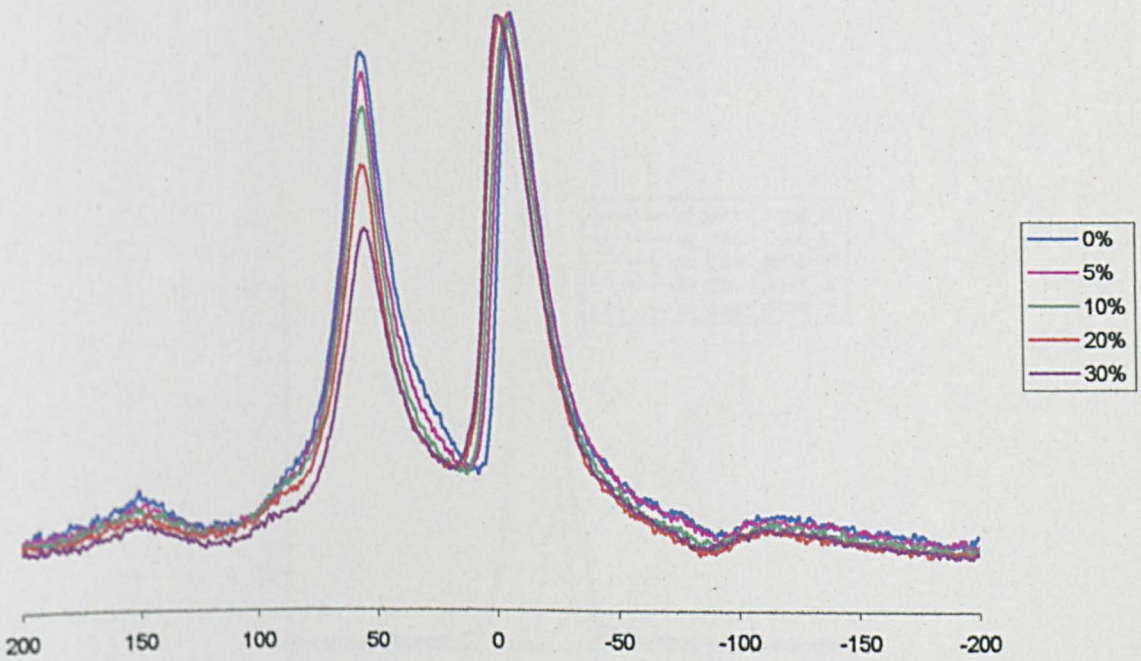

Figure 4.57: ^{27}Al NMR trace for the complete tartaric acid series after 1 day. Axis is in ppm.

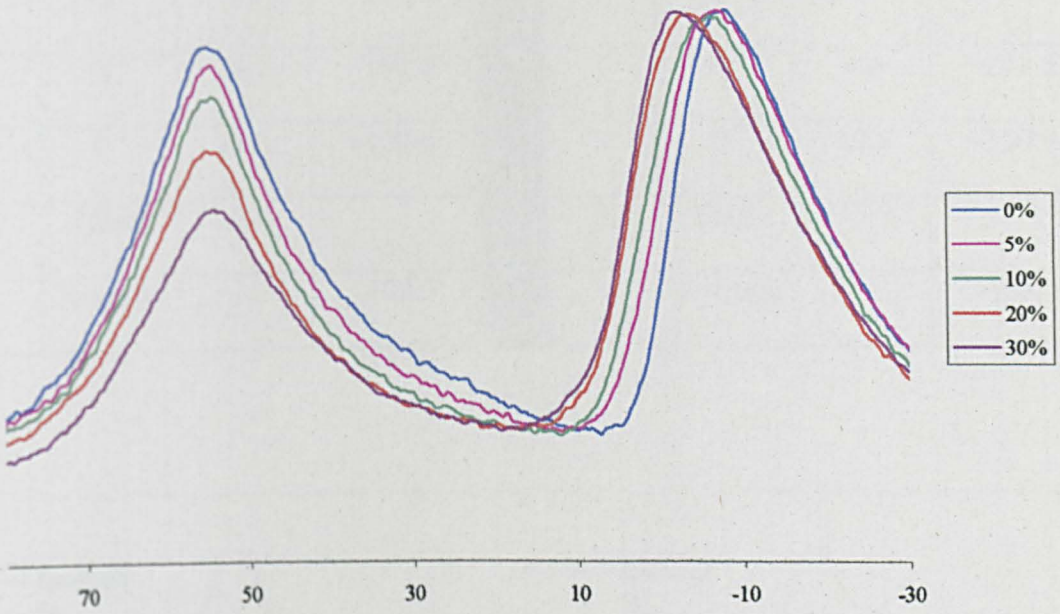

Figure 4.57b: ^{27}Al NMR trace of the region 80 to -30 ppm for the complete tartaric acid series after 1 day. Axis is in ppm.

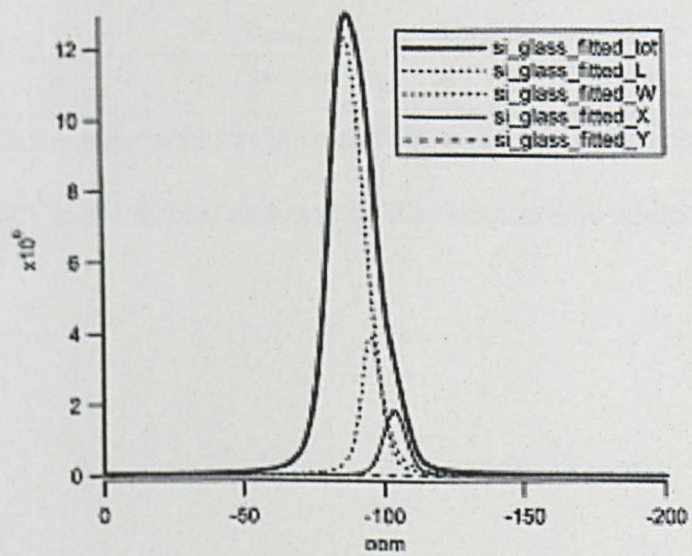

Figure 4.58: Silicon deconvolution trace of SerenoCem® glass powder.

Point	Peak	Percent	Shift/ppm
0	Q^2	9.5	-93.79
1	Q^3	18.5	-101.6
2	Q^4	12.1	-109.6
3	Glass	60	
4	Average		-102.3

Point	Peak	Percent	Shift/ppm
0	Q^2	58.1	-93
1	Q^3	6.4	-101.5
2	Q^4	19.8	-110.1
3	Glass	15.7	
4	Average		-103.4

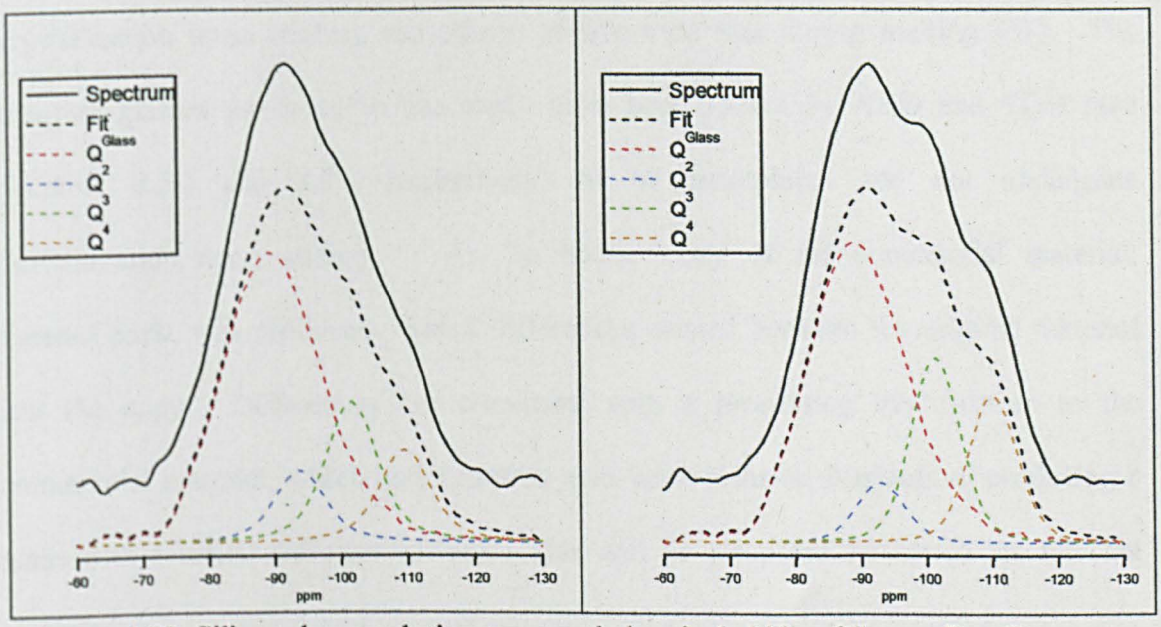

Figure 4.59: Silicon deconvolution trace and chemical shifts of SerenoCem® cement with a) 0% tartaric acid and b) 30% tartaric acid addition.

5. Discussion

5.1 Glass Preparation

All novel GIC compositions formed glasses that had an amorphous appearance upon shock cooling. No significant bulk or surface nucleation of crystals had occurred within the glass. The ionomer glass component of GICs are difficult to fabricate due to crystallisation upon cooling and silicon tetrafluoride loss during melting [61]. The ionomer glasses produced in this study have been shown by XRD and TEM (see *Sections 4.2.2* and *4.2.4* respectively) to be amorphous and not undergone devitrification upon cooling. An 'In house' copy of the commercial material, SerenoCem®, was produced. Small differences existed between the original material and the copy. Differences are consistent with a processing modification to the commercial material, which undergoes an acid wash prior to distribution, producing a glass with a cation deficient surface. This will be discussed further in the relevant sections.

Strontium and barium-based glasses appeared to be less viscous and more 'glass-like' upon pouring than the calcium-based glass compositions. This suggested that the replacement of calcium in the glass by the larger strontium and barium ions disrupted the glassy network more readily than in the commercial system. The addition of strontium or barium to the commercial ionomer glasses may allow the use of a decreased fusion temperature and as a result, reduce production costs.

Crucibles were sectioned and viewed using an optical microscope to determine if any chemical attack had occurred during the melt. Previous studies by K Hurrell-

Gilligham had shown the difficulty in manufacturing modified ionomer glasses of a similar basic composition to those used in this study and highlighted chemical attack as a problem [76]. *Figure 4.1* is a cross-sectional image of a crucible pre- and post-melting of Glass (Sr3). The presence of glass in the pores at the crucible surface suggested that a form of chemical attack may have occurred to a depth of 5-10 μm. The presence of fluorine and phosphate species in the glass melt have been shown to promote chemical attack of the crucible [76]. Phosphate has been found to modify the acid degradability of the ionomer glasses and removal of this species would therefore, result in shorter working times [65]. The attack was of limited depth and the crucible contained the same compositional species as the glass. It is unlikely to have a dramatic contamination effect on the glass composition. In conjunction with data on weight loss during the melt, it was concluded that the glass production methodology was appropriate for the glass compositions reported.

5.2 Glass Characterisation

5.2.1 Particle Size Analysis

Laser particle size analysis and scanning electron microscopy was undertaken to examine the size distribution and morphology of the glasses and provide a quantitative and qualitative representation of the milled ionomer glass powders. Distinct differences in particle size and morphology dramatically control the properties of a GIC, specifically the mechanical and setting characteristics of the cement.

5.2.1.1 Strontium Substituted Glasses

Photomicrographs of the strontium series showed the glass powders to be angular but spherical and not lathe shaped (shown clearly in *Section 4.2.1.1* and a typical photomicrograph reproduced below as *Figure 5.1*). Angular particles are a by-product of ball milling the as cast glasses. Lathe shaped particles would be evident if glass particles with a width of <45 μm but a length >45 μm had passed through the sieve aperture during processing. The presence of lathe shaped particles would modify the setting times of the respective cement. It is worth noting that all glasses exhibited a large number of smaller 'fine' (< 1μm) particles. The quantity of fines is important to the setting properties of a GIC due to the high surface area to volume ratio of the smaller particles. Cements mixed from an ionomer glass with a significant proportion of fines would set at a faster rate as the surface area of the fines will improve the reactivity of the cement. However, a distribution of particle sizes is required to achieve better mechanical properties [13]. Acid washing of the glass particles is used in industry to remove the effect of fines on the setting of commercial GICs. An optimal cement would have a good range of particle sizes so larger particles could improve the cement strength by slowing crack propagation and the smaller particles increase the ions available to crosslink the polymer matrix in reasonable working and setting times.

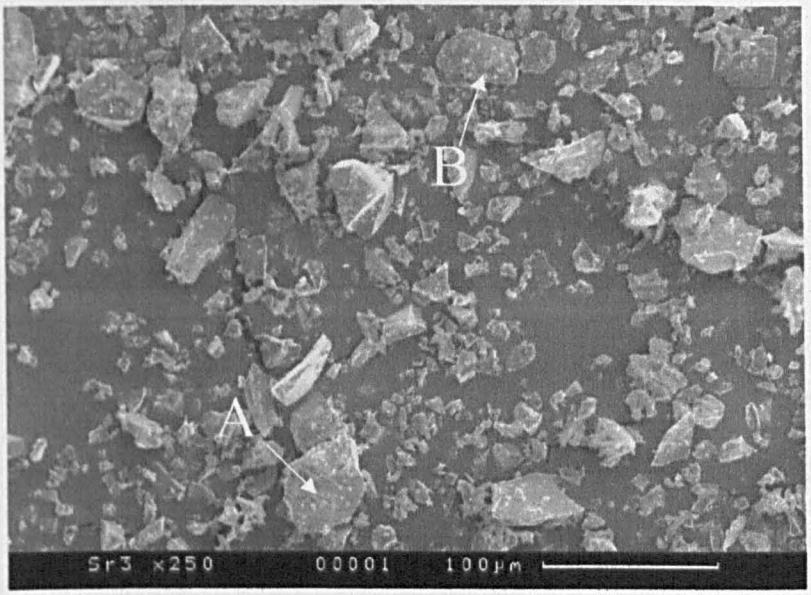

Figure 5.1: x250 magnification SEM photomicrographs of a range of Glass (Sr3) particles. Note a typical glass particle shown as **A** (approx 25 µm) and fines **B** on the surface of the larger particle.

Laser particle size analysis of Glass (Sr3) indicated 85% of particles were <45µm in size and the mean particle size was 26.46 µm. This correlated to the approximate glass particle size shown by SEM (labelled **A** above). Glass powders in the strontium series were found to have a similar particle size distribution and therefore, would display comparable properties in this study. Fines were noted, however, the average particle size suggested that the smaller particles are not over abundant. Mechanical properties and setting time studies would not be adversely effected by the presence of these small particles.

5.2.1.2 Substituted Glasses Incorporating Ca, Sr and Ba

Glass powders obtained were angular as seen previously and not lathe shaped after milling. A large proportion of 'fines' were observed within each glass powder distribution. All glasses incorporating Ca, Sr and Ba had a similar particle size distribution and would express comparable properties in this study. Laser particle size analysis of the glass powders indicated 95% or more of the particles were <45μm in size and the mean particle size was approximately 20 μm for the glasses incorporating Ca, Sr and Ba. This correlated to the approximate glass particle size shown by SEM (*Figures 4.9 to 4.17*).

5.2.2 DTA, Heat Treatment and XRD

XRD of the quenched glasses was used to determine crystallisation that had occurred during rapid cooling. Glasses were amorphous, as indicated by the glassy hump between 20 and 35 °2θ. Milled glass powders and the commercial material were heated at 10°C/min to 1050°C in a DTA7. The profiles for the thermal events of the glasses are given in *Section 4.2.2*. Glass transition and crystallisation temperatures obtained by DTA are tabulated in *Table 4.3*.

The change in glass transition temperature of the strontium substituted series of ionomer glasses (*Figure 4.19*) is shown graphically in *Figure 5.2*. Errors related to the calculation of the T_g and T_x exist between users. The determination of the temperatures is subjective and prone to operator error. However, results are generally consistent when carried out by the same operator. Increasing the strontium substitution in the parent composition led to distinct changes in the glass transition temperature of the

series. Glass (Sr1) with 20% substitution gave a minimum in the series indicating a sufficient disruption of the glassy network to cause a decrease in the transition temperature. Glass (Sr3) with 60% strontium substitution exhibits a maximum in the transition temperature suggesting a more ordered glass network. This can be partially explained by XRD of heat treated samples of the highly substituted glasses where a solid solution of calcium and strontium phases is evident. The fully substituted strontium glass had the lowest T_g as expected because strontium is a larger cation than calcium and would tend to disrupt the glass network more and therefore, decrease the T_g.

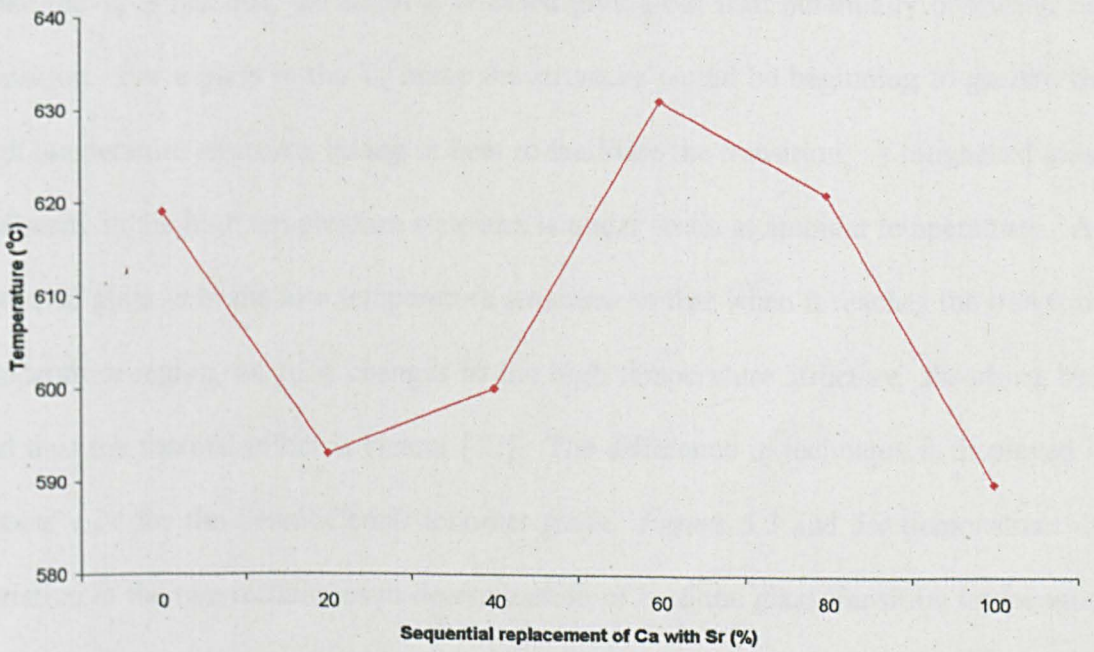

Figure 5.2: Glass transition temperature change with increasing strontium substitution.

Changes were evident in the crystallisation temperatures of the substituted glasses. In *Figure 4.19* T_{X1} clearly increases through the series and merges with the conversely decreasing T_{X2} peak. A distinct change in phase(s) occurs as the strontium substitution increases with respect to the strontium analogue of SerenoCem®. This is discussed

further in *Section 5.2.3* where heat treated samples of the ionomer glasses were reviewed by XRD.

Accurate determination of the glass transition temperatures by DTA was difficult to achieve with the ionomer glasses in this study. Glass transition temperatures calculated from the DTA traces in this study were reproducible but difficult to resolve with sufficient accuracy. It was decided to repeat the DTA experiments using a variation of the discussed method as suggested by Wilburn [72]. Strontium substituted glasses and the commercial GIC SerenoCem® were subjected to a series of prior heat-treatments before thermal analysis. Previous curves displayed a slight exothermic effect prior to the transition temperature range. Toughened or chilled glass is in a strained state and when the T_g is reached, the strain is released giving out heat potentially obscuring the transition. For a glass in the T_g range the structure would be beginning to go into the high temperature structure, taking in heat to facilitate the transition. A toughened glass is already in the high temperature state and is under strain at ambient temperatures. An annealed glass is in the low temperature structure so that when it reaches the transition temperature region, all of it changes to the high temperature structure, absorbing heat and thus the thermal effect is clearer [72]. The difference in technique is displayed in *Figure 4.24* for the SerenoCem® ionomer glass. *Figure 5.3* and *5.4* demonstrate the variation in the two techniques in determination of both the glass transition temperature and crytallisation temperature for the strontium series respectively. The correlation of the transition temperature remains constant the values are displaced to higher temperatures. *Figure 5.4* illustrates that this technique can be used to obtain improved transition temperatures without affecting the crystallisation temperatures as expected. As before determination of the temperatures is subjective and prone to operator error. However, results are generally consistent when carried out by the same operator.

DTA was carried out on the substituted glasses incorporating Ca, Sr and Ba. The 100% substituted glasses are shown in *Figure 4.20*. Glass transition temperature decreases with increasing ionic radius and therefore, increased disruption of the glass network. Analysis of the crystalline peaks of both series is reported in detail in *Section 5.2.3*.

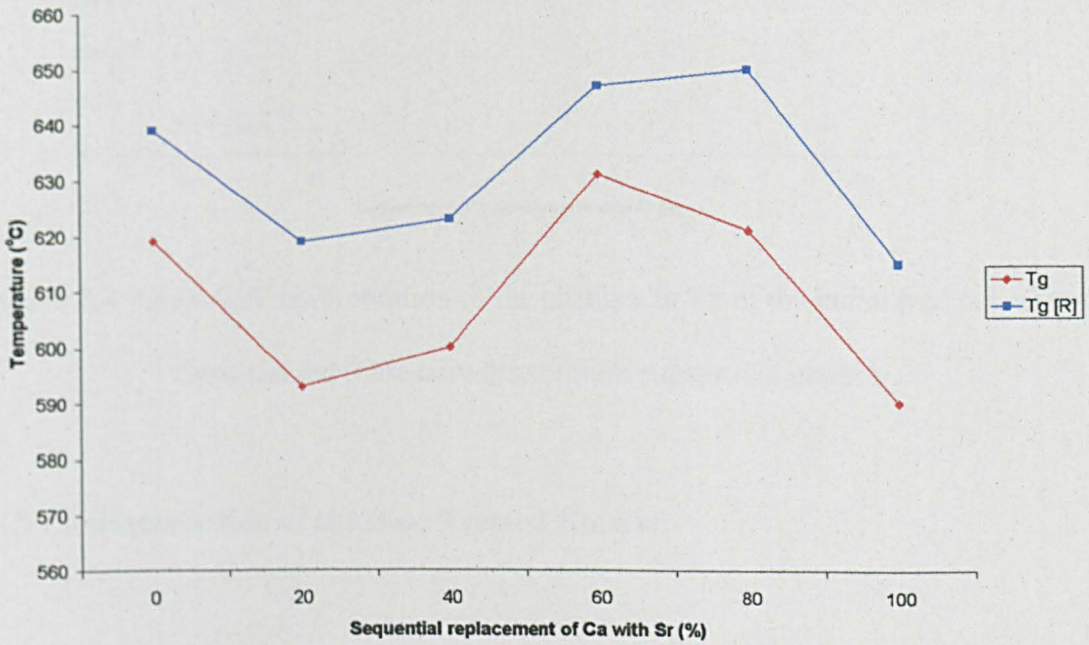

Figure 5.3: Graphical representation of the changes in T_g of the initial (red curve) and heat treated (blue curve) strontium substituted glasses.

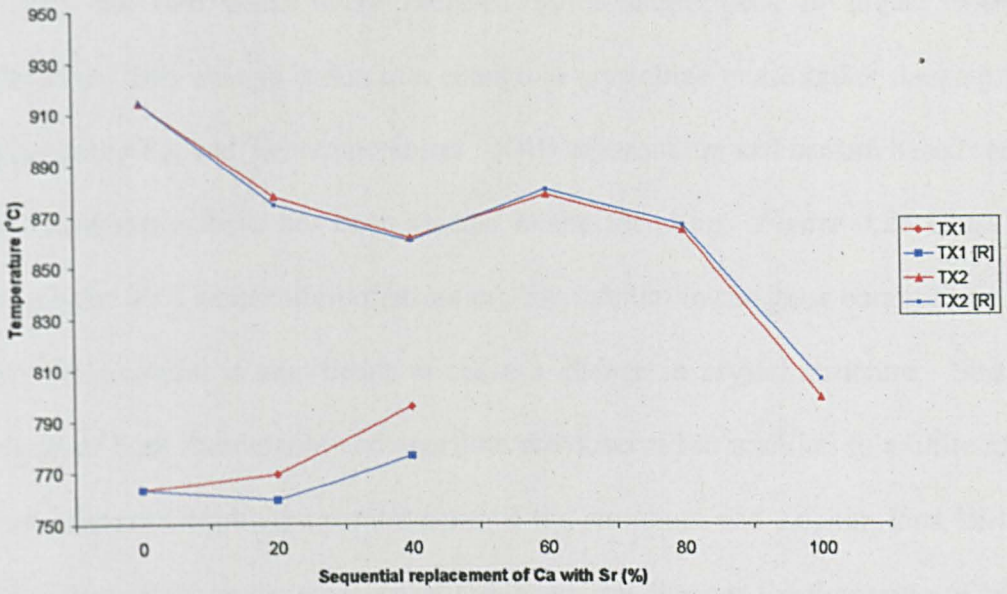

Figure 5.4: Graphical representation of the changes in Tx of the initial (red curve) and heat treated (blue curve) strontium substituted glasses.

5.2.3 Characterisation of the Heat Treated Glasses

Glass samples were subjected to a controlled heat treatment schedule at 700, 800, 900°C and if necessary 1000°C. Resultant crystalline samples were ground to a fine powder and the phases present identified using XRD. The data pertaining to SerenoCem® and the strontium substituted glasses can be found in *Table 4.6* and the data for the Group II A substitutions incorporating Ca, Sr and Ba in *Table 4.7*.

The SerenoCem® compositions displayed a similar thermal profile consistent with the published literature (*i.e.* phosphate containing glasses initially crystallise apatite most likely as fluorapatite with mullite as the second phase) see *Figure 4.25* [67]. However, the sequential substitution of calcium by strontium appeared to have a direct effect on the crystallisation of the novel glasses described in this study. DTA of the strontium based cements showed a gradual increase in the T_{X1} peak and decrease in T_{X2}

peak until the two peaks were replaced by a single peak at higher strontium substitutions. This change is due to a change in crystalline phase rather than a gradual variation in the T_{X1} and T_{X2} temperatures. XRD of strontium and barium based cements of this composition have not been studied in the literature. *Figure 4.26* Glass (Sr3) represents the 60% substitution of strontium for calcium in the glass composition. The amount of strontium is significant to cause a change in crystal structure. Strontium analogues of both fluorapatite and anorthite are observed in addition to mullite and the calcium phases. Despite the similar sizes of the strontium and calcium ions, there is a solid solution effect as the presence of the larger ion changes the d-spacing of the unit cell. Glass (Sr5) (*Figure 4.27*) represents the fully substituted strontium glass. XRD peaks for slawsonite and strontium fluorapatite are apparent in addition to mullite, analogous to the phases present in SerenoCem®. *Figure 4.30* represents the heat-treatment schedule for the fully substituted barium glass, Glass (BaBa). Phases analogous to those found in SerenoCem® were present (paracelsian and barium fluorapatite) in addition to mullite. Anorthite or analogous phases were identified in the substituted glasses contrary to those previously reported. The structural changes incurred by the larger Group II ions may be contributing to the crystallisation of anorthite or the analogous Group II based structure. The presence of anorthite has been reported in non-phosphate glasses but not phosphate glasses. Anorthite requires high temperatures for formation due to the requirement of bonds within the glass network to be broken [60, 67].

5.2.3 TEM and EDS

Milled glass powders of the strontium glasses Glass (Sr1-5) and the control material were prepared and viewed in a TEM to determine if any micro-crystallisation and phase separation of the glass powders had occurred upon quenching. No phase separation or crystallisation was observed consistent with XRD analysis of the as cast glass powders.

EDS of the identified glass particles indicated that aluminium, silicon, calcium and phosphorus existed in all samples, while calcium, strontium and barium existed in their respective samples. This is consistent with the glass compositions used.

5.3 Cement Characterisation

All novel cements based on the commercial system produced formed cements similar in colour and appearance to the commercial material and set within a comparable time period (*Section 5.3.1*). Cements were smooth on mixing and did not have a 'coarse' morphology. This correlates to the particle size analysis data (*Section 5.2.1*).

5.3.1 Gilmore Needle

The Gilmore Needle indentation test is a relatively simple method to perform, although relatively subjective and prone to operator interpretation. Repeatability between samples for the same user is achievable and allows a direct comparison of working and setting times. The Gilmore Needle indentation test is an important technique for surgeons as it gives a quick and direct result of the cements setting and handling characteristics achieved *in situ*. A number of factors are considered to effect the

working and setting times of a GIC including the particle size distribution, *in situ* temperature, glass composition, molecular weight and the number/stereochemistry of the side groups, and chelating additives.

GIC (Sr5) had statistically lower working and setting times than the control material (*Figure 4.34*). This can be partially explained by differences in the setting reaction caused by the strontium replacement. SerenoCem® and the 'in house' copy had comparable working and setting times. The commercial glass used in SerenoCem® bone cement undergoes an acid wash during processing. An acid wash procedure removes aluminium and calcium ions from the surface of the cement, thereby increasing its working time by slowing down the formation of the crosslinking bonds in the polymer matrix by the cations [8]. This is likely to have caused the difference seen in the samples and for a direct comparison an unprocessed SerenoCem® ionomer glass powder would be required. Cements, GIC (Sr1-Sr4) showed similar working and setting times to the commercial cement after its acid wash and would undergo a slower set than the control without the wash. This is indicative of an interaction of the strontium and calcium ions in the glass composition and complements the mixed cation effect also evident in the variation of glass transition temperatures in the strontium substituted glasses (*Figure 4.19*). The mobility of crosslinking ions during setting of the cement is a rate determining event and any factor that impedes the movement of ions either by increased bond strength or lack of ion mobility, working and setting times will be increased (see *Section 2.1.2.2*). Glasses incorporating Ca, Sr and Ba had a variety of different times ranging from between 2.5-7 minute working and 5.5–12 minute setting times. The range and pattern of times obtained may be due to the effect of the larger cations or a mixture of varying sized cations on the capability of the ionomer glasses to release the crucial crosslinking ions.

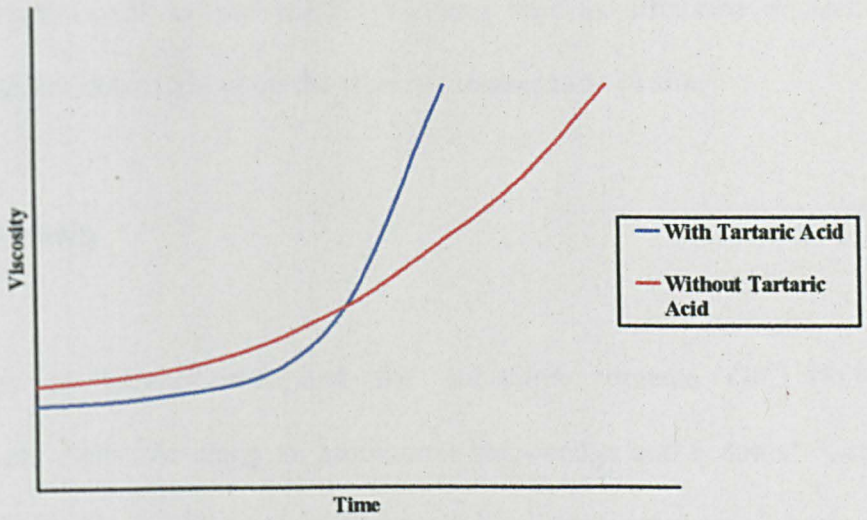

Figure 5.5: Schematic showing the effect of tartaric acid on the setting of a GIC [2].

The effect of adding *x* % of tartaric acid on the setting reaction of SerenoCem® and the 100% substituted strontium analogue, GIC (Sr5), was investigated (*Figure 4.36*). Working and setting times of SerenoCem® varied as reported in the dental literature for cements with the addition of tartaric acid [8, 12, 17, 18]. Tartaric acid extended the initial working time, allowing clinicians extra time to manipulate the cement, while still retaining the anticipated setting time, referred to as having a 'sharper' set (*Figure 5.5*). Varying the concentration of tartaric acid increased the working time at greater concentrations for both systems. Setting times increased with increasing concentration. A distinct minimum was observed at a concentration of ca 10 %. The addition of large concentrations of tartaric acid can make the cement brittle and effect its solubility and are not used clinically [18]. A further investigation of the effect of tartaric acid on the setting reaction of GICs can be found in *Section 5.3.7* where NMR and ion release data were used to improve the understanding of the mechanisms involved. All Gilmore indentation tests were carried out at ambient temperature 23°C. British standard

temperature for setting time is body temperature 37°C [74, 75]. The effect of a lower setting temperature is to increase the working time as discussed in *Section 2.1.2.2* setting times are dependant upon the working temperature *in situ*.

5.3.2 Radiopacity

Radiopacity of SerenoCem® and the strontium cements GIC (Sr1-Sr5) was quantitatively measured using an aluminium step-wedge and a dental X-ray unit. A typical radiograph can be seen in *Figure 4.37*. X-ray images were processed in a computer package to calculate the equivalent thickness of aluminium determined by the intensity of black on the image for the cements. Due to the inconsistency of GICs mixed by hand, an average was taken of a number of points on the image to give a more accurate determination of the actual thickness. This is shown below in the standard graph (*Figure 5.6*) and *Tables 5.1* for the strontium series.

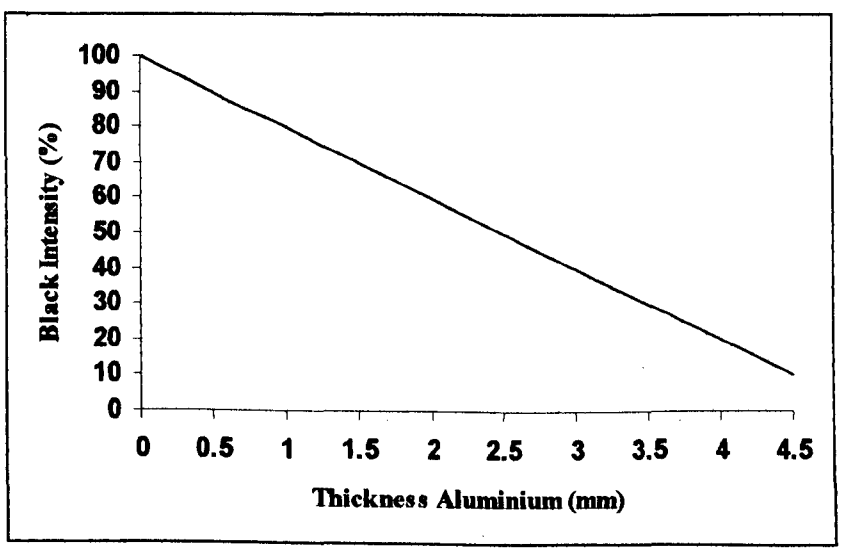

Figure 5.6: Calibration curve to determine the thickness of aluminium form the black intensity of the X-ray image.

Table 5.1: Derived aluminium thickness of the strontium based cements.

Cement	Black Intensity (%)	Al thickness equivalent (mm)
SC	75	1.0
GIC (Sr1)	63	1.8
GIC (Sr2)	52	2.4
GIC (Sr3)	25	3.7
GIC (Sr4)	12	4.3
GIC (Sr5)	0	4.5+

The radiopacity of SerenoCem® corresponded to a thickness of approx 1.0 mm aluminium while GIC (Sr5) gave three times the contrast of the commercial cement, approx 4.5+ mm of aluminium. Increasing the strontium content of the glass allowed the production of cements with significantly greater radiopacity than the control material. Bone has an approximate radiopacity of 2 mm of aluminium. Calcium based cements and the background bone tissue would have negligible contrast. The strontium and barium based cements would have sufficient radiopacity to aid postoperative detection.

Table 5.2: Derived aluminium thickness of the Group II substituted cements.

Cement	Black Intensity (%)	Al thickness equivalent (mm)
SC	75	1.0
GIC (CaCa)	82	0.9
GIC (SrSr)	5	4.5+

GIC (BaBa)	8	4.5+
Cement	**Black Intensity (%)**	**Al thickness equivalent (mm)**
SC	82	0.9
GIC (CaCa)	85	0.8
GIC (CaSr)	60	2.0
GIC (CaBa)	52	2.3
Cement	**Black Intensity (%)**	**Al thickness equivalent (mm)**
SC	80	0.9
GIC (SrCa)	50	2.5
GIC (SrSr)	14	4.2
GIC (SrBa)	3	4.5+
Cement	**Black Intensity (%)**	**Al thickness equivalent (mm)**
SC	80	0.9
GIC (BaCa)	50	2.5
GIC (BaSr)	27	3.7
GIC (BaBa)	8	4.5+

Radiographs were taken of the Group II substituted series incorporating Ca, Sr and Ba. To give an indication of the increase in radiopacity with increasing ionic radius, a radiograph was taken with the end member in each series (see *Figure 4.38*) as well as radiographs between the individual series, *Figure 4.39*. The equivalent thickness of aluminium for the substituted cements is found in *Table 5.2*.

Results were consistent with increased concentrations of the heavy metal ions giving greater contrast and therefore, increased radiopacity as used in trace amounts in dental

cements [7]. Production of radiopaque GICs may be achieved through substitution of Ca with either Sr or Ba, higher atomic number elements. Radiopaque cements would assist with post operative detection. Greater post operative detection and in certain cases removal of the implant could be improved by using coloured and radiopaque cements. Coloured GICs are reported in *Section 5.3.6*.

5.3.3 Flexural Strength

Flexural strength measurements of cement rods aged for 1 and 28 days were taken. Results indicated the substitution of strontium ions for calcium ions in the ionomer glass had no statistically significant effect on the flexural strength of the resultant cements over 28 days (*Figure 4.40*). However, the flexural strength of the strontium series appears to be decreasing with increased substitution. Using a larger sample set would decrease the degree of error and allow a more critical and accurate judgement of the results. Similar results were observed in the substituted series of cements incorporating Ca, Sr and Ba (*Figure 4.41*). *Table 5.3* gives the average flexural strength measurements for both 1 and 28 day samples (displayed graphically in *Figure 4.42*).

Table 5.3: Flexural strength measurements for 1 and 28 days showing the effect of cement maturation. Errors represent ± one standard deviation.

Cement	Flexural Strength after 1 day (MPa)	Flexural Strength after 28 days (MPa)
SerenoCem®	11.24 (±4.92)	25.56 (±3.19)
GIC (CaCa)	11.10 (±3.86)	25.18 (±5.44)
GIC (SrSr)	9.24 (±2.84)	20.08 (±5.45)
GIC (BaBa)	9.46 (±5.12)	24.98 (±3.91)

The gradual increase in flexural strength displayed by the cements with time corresponds to the slow maturation rate of the GIC [2]. As discussed in *Section 2.1.2.2* the maturation of a GIC corresponds to the formation of trivalent aluminium bridges between the dissociated carboxyl groups of the polymer. The crosslinking of the matrix by the aluminium ions results in a stronger bond than the initial calcium crosslinks and therefore, increased strength with time. However, as expected, there was a slight difference in flexural strength of the cements between 1 and 28 days as the cement matures slowly with increased aluminium crosslink formation.

To ascertain the mode of failure of the cements in this study, fracture surfaces of GICs (CaCa), (SrSr), (BaBa) and the commercial bone cement were sectioned and viewed in an SEM after both 1 and 28 days. Photomicrographs of the cements are given in *Figures 4.43 to 4.46*. The structure of the four glasses can be related to the theoretical structure of a GIC, as described by Hatton and Brook for dental GICs in 1992 [6]. Glass particles of varying particle size can be seen to exist in a polymer matrix. No differences existed between the two sample sets, suggesting that the failure

mechanism was the same in both unaged and aged samples. Fracture surfaces displayed a similar failure mechanism, with significant glass pullout and corresponding pores evident on the micrographs. The likely cause of cement failure is by matrix fracture at the glass-matrix interface, as reported in the literature, where a typical flexural strength for a GIC is given as 11 MPa [13]. Cracks in the microstructures are possibly caused by dehydration during SEM analysis, although, the paths of crack propagation generally linked microstructural features. Consequently, changes in the glass structure are unlikely to significantly increase the strength of the cements whereas changes to the matrix, such as in resin modified GICs, approximate strengths of 80 MPa are achievable [13]. Studies on the time dependence of a GICs set have suggested due to the in vivo long term set, fracture and mechanical studies should be done under appropriate environmental conditions and may differ as a result [77].

5.3.4 Ion Release

Ion release *in vivo* is an extremely important property in the study of GICs. Early models of ion release from cements during setting and the polymer matrix post setting have been investigated by a number of groups such as Hatton and Brook in 1992 [6, 46]. Fluoride release in dental GICs has been investigated comprehensively as a preventative measure in the spread of secondary caries [3, 10, 19-24]. Further studies using NMR, infrared spectroscopy and pH have focussed on the release of aluminium, calcium, phosphorus and silicon to determine their role in the setting reaction of GICs [8].

Ion release is a recognised important property for GICs *in vivo* [39]. Cell response to the presence of a GIC depends upon the dose and species of the eluted ions. Fluoride

release in GICs has been suggested to be a potential stimulator of bone formation, whereas fluoride and strontium have been postulated to prevent bone loss by depressing bone resorption and maintaining bone formation [43-51]. Conversely aluminium has potential neurotoxic effects and has been shown to inhibit bone mineralization [36, 39]. Therefore, it is important to have an understanding of the dynamics and dose of ions released from GICs to predict potential cell and environmental response [45, 48, 51].

Cumulative fluoride release profiles shown in *Figure 4.47* display an initial burst followed by a gradual decrease in the rate of elution to a limiting value. This indicated a change in release mechanism from an initial short-term surface washout followed by a long-term bulk diffusion process, in accordance with the literature [21]. The fluoride release rates were SerenoCem® > GIC(CaCa) > GIC(SrSr) > GIC(BaBa). Compounds of strontium and barium are less soluble than calcium compounds and therefore, this result is analogous with the glasses used in this study. As noted, SerenoCem® undergoes an acid wash stage during processing. This process retards the setting process by removing ions from the surface of the glass particles. A direct comparison of the fluoride release is not available. However, it is interesting to note that the release profile of SerenoCem® is higher than the materials that were not acid washed. Since ion mobility is paramount in fluoride release, this may be partially explained by fluoride ions from the bulk being more mobile through the ion depleted zone. For the other materials, the increased cationic radius is affecting the glass structure and stability thereby restricting ionic movement. The strength of the bond M-X increases with the sequence, M = Ca < Sr < Ba.

Phosphorus is released from the cements consistent with a phosphorus containing composition. Further analysis would be required to determine if this is from the glass or polymer network. Nicholson postulated that phosphorus and silicon may form an

inorganic network to aid the setting chemistry [8]. Silicon release from the GICs suggested that the calcium-based cements were more soluble than the strontium and barium based cements (*Figure 4.48*). Silicon release would suggest a break up of the glass network and therefore a greater release of ions from the structure would be evident. Another potential cause would be the debated theory that silicon is present as an inorganic network in the matrix [6, 8, 15]. The decrease in solubility of strontium and barium based cements would account for the apparent improved biocompatibility discussed in *Section 5.3.5*. *Figure 4.49* shows the ion release of the Group II A ions (Ca, Sr and Ba). The cements released their respective Group II A ion. In addition, trace levels of strontium were detected in the calcium-based cement. This was most likely due to contamination of the batch materials, however, was in trace amounts. As cationic radius increased ion release decreased. This was consistent with the resulting cements being less soluble and agrees with the observations described earlier. Low doses of strontium are beneficial at the implant site [45, 48, 51]. SerenoCem® was an exception to this case as it undergoes a special surface treatment on processing to provide a better working material but this also decreases ionic release from the material.

5.3.5 Biocompatibility

Biocompatibility of the 100 % substituted cements and the commercial control material were investigated. SEM and MTT assays were used to qualitatively and quantitatively measure the biocompatibility of the novel cements in relation to the commercial cement that is considered to have good biocompatibility [39]. SEM micrographs of the results can be seen in *Figure 4.50*. Cells were able to grow on all the GICs studied in this research. However, the cell sheet was not confluent, and rounded cells were present in

addition to flattened ROS cells with a normal osteoblast-like appearance. The observations were similar to those reported previously [68, 76]. Good biocompatibility is shown by a confluent sheet of cells on the surface of the test materials.

The poorest cell response was shown to be the commercial material (*Figures 4.50:A and 4.50:B*) and the 'in house' copy of the commercial cement, both exhibited few sparse sheets of flattened cells on the surface. This was quantitatively supported by the results of the MTT (*Figure 4.51*). Tissue culture plastic was used as the control material (100%) (*Figure 4.50:F*). Barium- and especially strontium- based novel GICs showed improved biocompatibility, with increased cell proliferation and adhesion compared to the commercial cement. This could be explained by an improved reaction between cells and the cement surface. The result is more consistent of materials with decreased solubility and therefore, decreased ion release into the cell medium. This was described in detail in *Section 5.3.4* and is consistent with the ion release profiles of the fully substituted cements. This was noted in a study by Lucksanasombool *et al* in the effect of ongoing metallic ion release in vivo but also the un-reacted acid component of improperly or difficult to mix cements [44]. A study by Johal *et al* concluded that strontium cements are osteoconductive and maybe beneficial as bone cements [51]. The release rate of strontium from strontium substituted glasses is of sufficiently low dose to enable osteointegration by depressing bone resorption and maintaining bone formation.

5.3.6 Coloured GICs

The aim of this section was to produce a range of coloured ionomer glasses, and demonstrate their ability to form brightly coloured cements. A selection of brightly coloured ionomer glasses was successfully produced, but the manufacture proved more

complicated than first anticipated. Preliminary glasses were based on the SerenoCem® ionomer glass composition with the addition of selected colouring agents. Initial attempts to produce coloured ionomer glasses based on the commercial composition were unsuccessful due to chemical attack of the sillimanite crucibles. A control glass based on the same composition but with no colouring agent was successfully produced. It is probable that the colouring agents reacted with a component in the glass, producing corrosive melt products leading to a chemical attack of the crucibles.

Melts were repeated under the same conditions but using a basic GIC glass composition that was free from both fluoride and phosphate [57]. Glass compositions would not completely melt at 1400°C due to the omission of fluoride. The presence of fluoride lowers the fusion temperature of the glass allowing the melt temperature to be reduced [62].

To determine the species involved in the chemical attack of the crucible, fluoride species were reintroduced to the ionomer glass composition to produce a glass suitable for dental applications [57]. The removal of the phosphate species from the glass composition prevented any attack of the crucible. It was possible that phosphate species were involved in the damage to the crucibles by producing corrosive melt products. Crucible attack in the presence of phosphate based GIC compositions has been noted in the literature [76]. Introduction of 1 wt % colouring agent to the basic ionomer glass composition enabled production of all six brightly coloured ionomer glasses (*Figures 4.52 and 4.53*). Cobalt, manganese and ionomer glass blended with a coloured glass K2021 produced coloured opaque glasses whilst the remaining glasses were coloured but translucent. Although fluoride content of these ionomer glasses was reduced from the standard 14 wt % in SerenoCem® to 10 wt % in the experimental glasses, it is still sufficient to produce a suitable GIC composition for dental applications [57].

Glass powders successfully formed cements although in a significantly shorter time period than conventional GICs. The decrease in working and setting times was due to the removal of phosphate species from the glass compositions. Phosphate has been found to modify the acid degradability of the ionomer glasses and removal of this species would result in shorter working times [65]. The opaque ionomer glasses, (Co), (Mn) and (K2021) produced blue, pink and green cements respectively, whereas the remaining translucent glass powders, including the control glass produced white cements. The combination of coloured cements and increased radiopacity will improve greater post operative detection and patient care.

5.3.7 NMR

Chelating agents have been widely used in commercial glass-ionomer systems since Wilson *et al* (1976) established the dramatic improvement conferred to the setting characteristics of the original ASPA cements [17]. L(+) tartaric acid is widely used in modern systems to improve the handling characteristics of the hardening cement without modifying the final set [2]. This can be seen in *Section 5.3.1* where working and setting times are modified by the addition of tartaric acid. Tartaric acid extends the initial working time, allowing clinicians extra time to manipulate the cement, while still retaining the anticipated setting time, referred to as having a 'sharper' set [2].

The higher acidic strength of tartaric acid is believed to preferentially attack the glass, decreasing its reactivity towards the polyacid. In addition it is believed that the chelating agent retards the cation incorporation in the matrix by modifying the rate of formation of the metal polyacrylates; calcium salts form more slowly, but the aluminium ones form more rapidly [8]. Increasing the concentration of tartaric acid

beyond a limiting percentage of the liquid component can lead to weaker cements with an increased solubility [18]. Changes in the structure of a mature GIC with increasing tartaric acid will show as variations in the chemical environments surrounding the aluminium and silicon ions found in the glass and matrix. The setting reaction of a mature commercial GIC, SerenoCem®, was investigated using ^{27}Al and ^{29}Si NMR to determine the chemical and structural changes in the glass and matrix with increasing concentration of tartaric acid in the liquid component of the ionomer cement.

^{29}Si NMR of the glass powder exhibited a NMR trace seen in a study (*Figure 4.54*). by Matsuya *et al* (1996) who used ^{27}Al and ^{29}Si NMR techniques on the setting reaction of a GIC to understand the reaction mechanism [14]. A peak at -90 ppm in the glass corresponds to the tetrahedral coordination of silicon to oxygen atoms in the glass network (SiO_4). Reacting the glass powder to the liquid component containing no tartaric acid exhibited a broader peak shifted towards a lower chemical shift of -100 ppm. Shoulders were observed on the trace. The addition of 30% tartaric acid to the liquid phase produced a distinctly different trace when investigated (*Figure 4.55).* A number of distinct shoulders on the trace are apparent indicating that the peak could be an amalgamation of a number of smaller peaks representing silicon in varying coordination states in the glass, cation deficient zone, and possibly crosslinked in the matrix. Matsuya *et al* deconvoluted the ^{29}Si trace and attributed the chemical shift as reconstruction of the silicate network and elimination of aluminium from the network. Deconvolution of the original glass and the cements set with 0 and 30% were deconvoluted. *Figures 4.58 and 4.59* illustrate that the peaks are an amalgamation of a number of smaller peaks as expected. Changes in the intensity of the smaller peaks with increasing concentrations of tartaric acid indicate a modification to the setting mechanism or a structural difference between the two concentrations. The ^{29}Si peak

representing silicon in the tetrahedral coordination increases in the mature cement reacted in the presence of a higher acid concentration. Average shifts in the peaks of the various Q species between the two tartaric acid concentrations differ by an average 1 ppm with the 30% tartaric acid based cement being more polymerised (lower in Al). The small shift between samples is not significant. Average Q numbers (Q^n) of the systems can be calculated as 3.10 and 3.25 respectively, assuming no aluminium which would cause notable shifts in the Q species. For example, Q^4 in this system is -110 ppm, breaking a bond to give Q3 will give a shift to the left of 8 ppm for each bond broken. An adjacent Al would give a shift of 4-5 ppm per bond. Therefore, interpretation of this data is unambiguous without detailed knowledge of the position of aluminium in relation to the GIC structure. A study by Stamboulis *et al* commented that the shift depends upon the number of non-bridging and bridging oxygens in addition to the number of next nearest neighbour aluminium species. Increasing the number of non bridging oxygens was theorised to move the peak in a positive direction while increasing the aluminium species neighbouring the silicon would move it to a negative value [16]. Further determination of the mechanisms involved in the setting of SerenoCem® using ^{29}Si NMR is difficult due to the presence of additional peaks not fitted being present and distorting the fitted peaks, depolymerisation or aluminium species interaction and a degree of baseline noise (see further work section). However, the apparent shoulders present on *Figure 4.55* would indicate a change in mechanism brought about by the addition of higher concentrations of tartaric acid. Further work would be required to identify the mechanism involved.

Aluminium ions in the glass powder (*Figure 4.56*) have a broad peak at 60 ppm attributed to tetrahedrally coordinated aluminium in the glass network (Al[4]). Griffin and Hill (1999) suggested that aluminium could be found as $AlPO_7$ in the glass network

as well as AlO_4 where it is charge balanced by calcium ions [61]. Shoulders on the trace exist around 0 ppm indicated decreased amounts of higher coordination aluminium ions. ^{27}Al NMR of the mature GIC can be seen on the same trace and the result is similar to the previous study [14]. Peaks can be seen at 60 ppm as seen previously but also at 0 ppm corresponding to octahedral aluminium (Al[6]). The relative peak sizes indicate a significant amount of aluminium in the set cement is in the octahedral coordination suggested by Matsuya *et al* is free hydrated aluminium or aluminium crosslinking the polymer matrix [14]. A 2004 study by Stamboulis *et al* used ^{27}Al and ^{29}Si MAS NMR to characterise five commercial ionomer glasses [16]. The authors identified the presence of Al(IV), Al(V) and Al(VI) at 45-60, 20 and 0 ppm respectively and consistent with other previous studies [14, 16, 78]. The study went on to further and investigated the ^{19}F and ^{31}P NMR of the commercial cements. The presence of these species as the next nearest neighbours was shown to have an important influence on the ^{27}Al spectra and the peak shift [16]. Further work on the influence of ^{19}F and ^{31}P on SerenoCem®, a phosphor-fluoro-alumino-silicate glass, would help further the understanding of the setting reaction and GIC structure. A study by Pires *et al* (2004) used ^{1}H and ^{19}F techniques to monitor the curing kinetics of a setting strontium containing cement and determine its gelation and maturation stages. In combination with MAS NMR of aluminium and silicon, the authors quantified the aluminium in the glass component and the cement. They indicated that 32% of the 4-coordinate aluminium, 100% of the 5-coordinate and 41% of the 6-coordinate aluminium is leeched during the setting reaction. 5-coordinate aluminium was only present in the surface layer created by the acid attack [78].

The addition of tartaric acid to the liquid component modifies the intensity and position of and Al[4] and Al[6] peaks (see *Figure 4.57b*). An increase in the

concentration of tartaric acid increased the ratio of Al[6] to Al[4] and caused a shift of the octahedral aluminium peak to a higher ppm (*Figure 4.57*). The increased ratio of Al[6] in the cements formed with higher tartaric acid concentration would suggest the presence of tartrate is increasing the proportion of aluminium taking part in the setting reaction and therefore, 'protecting' the silicon in the glass during maturation. An increase in aluminium ions removed from the glass is consistent with the views of a number of studies [8, 17, 18].

Table 5.4: Peak area of the ^{27}Al NMR traces with respect to the tartaric acid concentration.

Tartaric Acid Concentration %	Tetrahedral Peak	Octahedral Peak
0	0.094	0.086
5	0.076	0.083
10	0.068	0.086
20	0.051	0.084
30	0.043	0.090

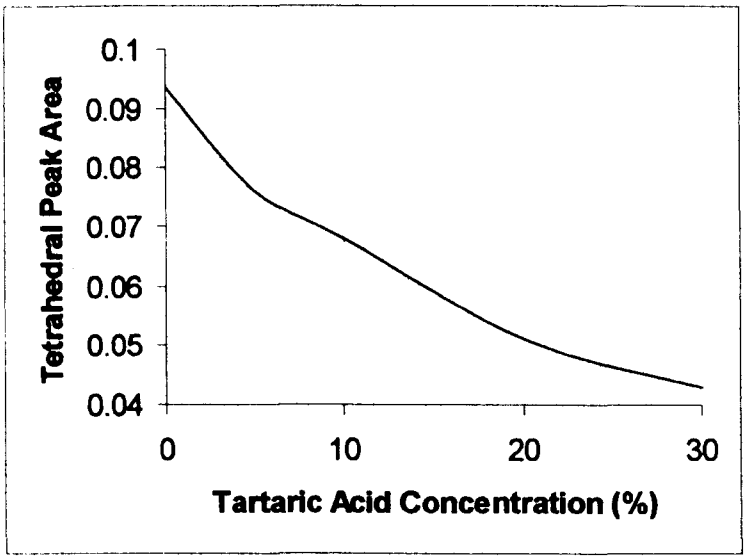

Figure 5.7: Tetrahedral peak area for increasing tartaric acid concentration.

The peak area of the tetrahedral and octahedral peaks for the five tartaric acid concentrations was estimated using a weighing technique. The results are shown in *Figure 5.7* and *Table 5.4*. From the above figure it can be seen that although a rough estimate, the tetrahedral peak decreases with increasing tartaric acid. This is consistent with the presence of tartrate increasing the proportion of aluminium taking part in the setting reaction. The octahedral peak does not vary significantly between samples although the peak shifts to a higher ppm. However, the combination of broad components not being picked up by the receiver, the effect of noise and baseline variation decrease the accuracy of the results obtained and quantitative interpretation would be invalid. Improved accuracy is possible with more runs and variations on the technique used.

6. Conclusions

This study has increased our knowledge of ionomer glasses and GICs, and has provided information to improve their formulation for medical applications. The principal conclusions are:

1) Production of radiopaque GICs, achieved by substitution of Ca by Sr or Ba, higher atomic number Group II elements. Radiopaque cements will assist with post operative detection.

2) Substitution of Ca by Sr and Ba in the glass composition had no detrimental effects on the handling characteristics, flexural strength and biocompatibility of experimental cements.

3) Differential thermal analysis demonstrated that substitution did influence crystallisation behaviour in ionomer glasses. Substitution of Ca with Sr resulted in a reduction in T_g, with the lowest observed for the 20 and 100% substitutions of Ca. A similar result was observed when Ca was substituted by Ba. This suggested a form of mixed cation effect in the glass, indicating that this may provide a route for reducing the liquidus temperature of ionomer glasses.

4) Coloured ionomer glasses based on the SerenoCem® composition have been fabricated by the addition of transition metal ions and these allow the production of coloured ionomer cements. Coloured cements are easier to place, manipulate and remove from the surgical field improving post operative detection further.

5) Preliminary NMR studies have provided a greater understanding of the setting reaction ion release from set GICs, in particular with regard to the effects of tartaric acid. Tartrate appears to increase the proportion of aluminium taking

part in the acid-base reaction during the setting, therefore "protecting" the Si in the glass.

Completion of this study has demonstrated routes to provide surgeons with GICs optimised for use as bone cements.

7. Further Work

- Carry out NMR time study of the silicon and aluminium environments during the set and contrast data with the mature cements. Changes in the silicon and aluminium environment would be likely to vary as complexes are formed and ultimately crosslinks the polycarboxylate groups.
- Measure ion release of silicon, phosphorus and the representative Group II ions over time. This could be combined with the NMR study to further understand the setting reaction of a GIC in the presence of tartaric acid.
- Improve the accuracy of the NMR data obtained by increasing acquisition time and number of runs to more accurately determine the position of the aluminium in the glass and matrix.
- Produce glasses with a larger proportion of smaller 'fine' particles. Increasing the surface area would allow improved hydration and give spectra with less unreacted glass overlapping.
- Biological testing of the cements incorporating mixed compositions of calcium, strontium and barium.
- Solubility measurements of the fully substituted cements to ascertain the method of improved strontium biocompatibility *in vitro*.

8. References

[1] FDA Approval 510k for SerenoCem® medical grade bone cement, http://www.fda.gov/cdrh/pdf/k003567.pdf, accessed Sept 2004.

[2] R.V.Noort, *Introduction to Dental Materials*, 1994, Mosby, London.

[3] E.A.M.Kidd *et al*, *Essentials of Dental Caries: 2nd Edition*, 1997, Oxford University Press, Oxford.

[4] Biology of the Human Dentition Website, http://www.uic.edu/classes/orla/orla312/BHDI.html, accessed April 2005.

[5] MyDr Website, http://www.mydr.com.au/default.asp?article=3728, accessed April 2005.

[6] P.V.Hatton and I.M.Brook, *Characterisation of the ultrastructure of glass-ionomer (poly-alkenoate) cement.* British Dental Journal, 1992. 173: p. 275-277.

[7] A.D.Wilson, J.W.Nicholson, *Acid-base Cement: Their Biomedical and Industrial Applications*, 1993, University Press, Cambridge.

[8] J.W.Nicholson, *Chemistry of glass-ionomer cements: a review.* Biomaterials, 1998. 19: p. 485-494.

[9] S.Griffin, R.Hill, *Influence of poly(acrylic acid) molar mass on the fracture properties of glass polyalkenoate cements.* Journal of Materials Science, 1998. 33: p. 5383-5396.

[10] V.H.W.Khouw-Lui, H.M.Anstice, G.J.Pearson, *An in vitro investigation of a poly(vinyl phosphonic acid) based cement with four conventional glass-ionomer cements. Part 1: flexural strength and fluoride release*. Journal of Dentistry, 1999. 27: p. 351-357.

[11] J. Ellis *et al*, *The Glass Polyphospohonate Cement: A Novel Glass-Ionomer Cement Based on Poly(Vinyl Phosphonic Acid)*. Clinical Materials, 1991. 7: p. 341-346.

[12] H.J.Prosser, S.M.Jerome, A.D.Wilson, *The Effect of Additives on the Setting Properties of a Glass-Ionomer Cement*. J Dent Res, 1982. 61(10) p. 1195-1198.

[13] D.Xie *et al*, Mechanical properties and microstructures of glass-ionomer cements, Dental Materials, 2000. 66: p 129-138.

[14] S.Matsuya, T.Maeda, M.Ohta, *IR and NMR Analysis of Hardening and Maturation of Glass-ionomer Cement*. J Dent Res, 1996. 75(12): p. 1920-1927.

[15] T.Maeda *et al*, *Ion Distribution in Matrix Parts of Glass-Polyalkenoate Cement by SIMS*. J Dent Res, 1999. 78(1): p 86-90.

[16] A. Stamboulis *et al*, *Characterisation of commercial ionomer glasses using magic angle nuclear magnetic resonance (MAS-NMR)*. Biomaterials, 2004. 25: p 3907-3913.

[17] A.D.Wilson, S.Crisp, and A.J.Ferner, *Reactions in Glass-Ionomer Cements: IV. Effect of Chelating Comonomers on Setting Behaviour*. Journal of Dental Research, 1976. 55(3): p. 489-495.

[18] S. Crisp *et al*, *Characterisation of glass-ionomer cements: 5. The effct of the tartaric acid concentration in the liquid component*. Journal of Dentistry, 1979. 7(4): p. 304-312.

[19] L.Forsten, *Fluoride release and uptake by glass-ionomers and related materials and its clinical effect.* Biomaterials, 1998. 19: p. 503-508.

[20] A.M.Diaz-Arnold *et al, Short-term fluoride release/uptake of glass ionomer restoratives.* Dent Materials, 1995. 11: p. 96-101.

[21] W.M.Tay, M.Braden, *Fluoride ion diffusion from polyalkenoate (glass-ionomer) cements.* Biomaterials, 1988. 9: p. 454-456.

[22] L.Forsten, *Fluoride release and uptake by glass ionomers.* Scand J Dent Res, 1991. 99: p 241-245.

[23] An M.J.C.De Witte *et al, Fluoride release profiles of mature restorative glass ionomer cements after fluoride application.* Biomterials, 2000. 21: p. 475-482.

[24] A.J.Preston *et al, Fluoride recharge of aesthetic dental materials.* J. Oral Rehabil, 1999. 26(12): p. 936-40.

[25] W.A.J.Higgs *et al, Evaluating acrylic and glass-ionomer cement strength using the biaxial flexure test.* Biomaterials, 2001. 22: p. 1583-1590.

[26] D.Brune, D.Smith, *Microstructure and strength properties of silicate and glass ionomer cements.* Acta Odontol. Scand, 1982. 40: p. 389-396.

[27] H.J.Prosser *et al, Glass-ionomer cements of improved flexural strength.* J Dent Res, 1986. 65: p. 146-148.

[28] L.M.Jonck, *Biological Evaluation of Glass-Ionomer Cement (Ketac-0) as an Interface Material in Total Joint Replacement. A Screening Test.* Clinical Materials, 1989. 4: p. 201-224.

[29] I.M.Brook, G.T.Craig, D.J.Lamb, *Initial In-Vivo Evaluation of Glass-Ionomer Cements for use as Alveolar Bone Substitutes*, Clinical Materials, 1991. 7: p. 295-300.

[30] I.M.Brook *et al, Bone cell interactions with a granular glass-ionomer bone substitute material: in vivo and in vitro culture models*, Biomaterials, 1992. 13(10): p. 721-725.

[31] G.Babighian, *Use of a glass ionomer cement in otological surgery. A prelininary report.* The Journal of Laryngology and Otology, 1992. 106: p. 954-959.

[32] G.Geyer, J.Helms, *Ionomer-based bone substitute in otologic surgery.* Eur Arch Otorhinolaryngol, 1993. 250: p. 253-256.

[33] G.Geyer, S.Dazert, J.Helms, *Performance of ionomeric cement (Ionocem®) in the reconstruction of the posterior meatal wall after curative middle-ear surgery.* The Journal of Laryngology and Otology, 1997. 111: p. 1130-1136.

[34] Description of Altzheimer's disease. Medical information and evaluation, http://www.medicinenet.com/alzheimers_disease/article.htm, accessed Sept 2004.

[35] J.L.Renard *et al. Post-otoneurosurgery aluminium encephalopathy.* The Lancet, 1994. 344: p. 64-65.

[36] O.H.Andersson, J.E.Dahl, *Aluminium release from glass ionomer cements during early water exposure in vitro.* Biomaterials, 15(11): p. 882-888.

[37] MSN Encarta Website, http://encarta.msn.com/media_461550661_761563171_-1_1/Structure_of_the_Ear.html, accessed Sept 2004.

[38] SerenoCem® commerical brochure. Corinthian Medical Ltd, Nottingham, UK.

[39] I.M.Brook and P.V.Hatton, *Glass-ionomers: bioactive implant materials.* Biomaterials, 1998. 19: p. 565-571.

[40] P.Sasanaluckit *et al, Biocompatibility of glass ionomer cements.* Biomaterials, 1993. 14(12): p. 906-917.

[41] A.Oliva *et al*, *Biocompatibility studies on glass ionomer cements by primary cultures of human osteoblasts*. Biomatierlas, 1996. 17(13): p. 1351-1356.

[42] L.G.Brentegani *et al*, *Histological evaluation of the biocompatibility of a glass-ionomer cement in rat alveolus*. Biomaterials, 1997. 18(2): p. 137-140.

[43] S.Mehta *et al*, *Effects of high levels of fluoride on bone formation: an in vitro model system*. Biomaterials, 1995. 16(2): p. 97-102.

[44] Lucksanasombool *et al*, *Effects of glass ionomer cements on bone tissue*. J Mater Sci Mater Med, 2002. 13(2): p 203-210.

[45] M.D.Grynpas *et al*, *Strontium Increases Vertebral Bone Volume in Rates at a Low Dose That Does Not Induce Detectable Mineralization Defect*, Bone, 1996. 18(3): p. 253-259.

[46] D.H.Carter *et al*, *Role of exchanged ions in the intergration of ionomeric (glass polyalkenoate) bone substitutes*. Biomaterials, 1997. 18: p. 459-466.

[47] A.J.Devlin, P.V.Hatton, I.M.Brook, *Dependance of in vitro biocompatibility of ionomeric cements on ion release*. Journal of Materials Science: Materials in Medicine, 1998. 9: p. 737-741.

[48] E.Rokita *et al*, *Bone mineralisation after strontium and fluoride treatment in osteoporosis*. Nuclear Instruments and Methods in Physics Research B, 1999. 158: p. 412-417.

[49] S.G. Dahl *et al*, *Incorporation and distribution of strontium in bone*. Bone, 2001. 28(4): p 446-453.

[50] Verberckmoes *et al*, *Dose-dependant effects of strontium on osteoblast function and mineralization*. Kidney Int, 2003. 64(2): p 534-543.

[51] K.K.Johal *et al*, *In vivo responce of strontium and zinc-based ionomeric cement implants in bone*. Journal of Materials Science: Materials in Medicine, 2002. 13: p. 375-379.

[52] J.Christoffersen *et al*, *Effects of strontium ions on growth and dissolution of hydroxyapatite and on bone mineral detection*. Bone, 1997. 20(1): p 47-54.

[53] D. Guo *et al*, *Development of a strontium-containing hydroxyapatite bone cement*. Biomaterials, 2005. 26(19): 4073-4083.

[54] Verberckmoes *et al*, *Effects of strontium on the physiochemical characteristics of hydroxyapatite*. Calcif Tissue Int, 2004. 75(5): p 405-415.

[55] Wong *et al*, *In vivo cancellous bone remodeling on a strontium-containing hydroxyapaitie (sr-HA) bioactive cement*. J Biomed Mater Res A, 2004. 68(3): p 513-521.

[56] Wong *et al*, *Ultrastructural study of mineralization of a strontium-containing hydroxyapatite (sr-HA) cement in vivo*. J Biomed Mater Res A, 2004. 70(3): p 428-435.

[57] A.D.Wilson, *The Chemistry of Dental Cements*. Chemical Society Reviews, 1978. 7(2): p. 265-296.

[58] S.Deb, J.W.Nicholson, *The effect of strontium oxide in glass-ionomer cements*. Journal of Materials Science: Materials in Medicine, 1999. 10: p. 471-474.

[59] R.J.Hand, A.B.Seddon, *An hypothesis on the nature of Griffith's cracks in alkali silicate and silica glasses*. Phys. Chem. Glasses, 1997. 38(1): p. 11-14.

[60] D.Wood and R.Hill, *Glass Ceramic approach to controlling the properties of a glass-ionomer bone cement.* Biomaterials, 1991. 12: p. 164-170.

[61] S.G.Griffin, R.G.Hill, *Influence of glass composition in the properties of glass polyalkenoate cements. Part I: influence of aluminium to silicon ratio.* Biomaterials 1999. 20: p. 1579-1586.

[62] S.G.Griffin, R.G.Hill, *Influence of glass composition in the properties of glass polyalkenoate cements. Part IV: influence of fluorine content.* Biomaterials 2000. 21: p. 693-698.

[63] E.De Barra, R.G.Hill, *Influence of glass composition in the properties of glass polyalkenoate cements. Part III: influence of fluorite content.* Biomaterials 2000. 21: p. 563-569.

[64] N.B.Mohialdin, *A TMS study of some acid soluble glasses.* MSc Thesis, University of Greenwich, 1996.

[65] S.G.Griffin, R.G.Hill, *Influence of glass composition in the properties of glass polyalkenoate cements. Part II: influence of phosphate content.* Biomaterials 2000. 21: p. 399-403.

[66] P.W.McMillan, *Glass Ceramics: 2nd Edition*, 1979, Academic Press, London.

[67] D.Wood, R.Hill, *Structure-Property Relationships in Ionomer Glasses.* Clinical Materials, 1991. 7: p. 301-312.

[68] K.Hurrell-Gillingham *et al*, *Devitrification of ionomer glass and its effect on the in vitro biocompatibility of glass-ionomer cements.* Biomaterials, 2003. 24: p. 3153-3160.

[69] Coloured glass theory and additives, Glassworks Services Limited Website, http://www.glassworksservices.co.uk/html/melting_advice.html#B, accessed Sept 2004.

[70] Theodore *et al*, *Multi-colored dual-cured compomer*. Pediatr Dent, 2004. 26: p 273-276.

[71] Co*loured GIC company website*. http://www.voco.de/usa/twinky/twinky.htm. Accessed April 2005.

[72] Personal communication with Dr F.W.Wilburn.

[73] JCPDS Powder Diffraction Files, http://www.icdd.com/, accessed Sept 2004.

[74] British Standard EN29917, *Dental water-based cements*, 1994, British Standards Institution.

[75] British Standard BS6039, *Dental glass ionomer cements*, 1981, British Standards Institution.

[76] K.Hurrell-Gillingham, *Novel Glass Ionomer Cements for Biomedical Applications*. PhD Thesis, University of Sheffield, 2004.

[77] Lucksanasombool *et al*, *Time dependence of the mechanical properties of GICs in simulated physiological conditions*. J Mater Sci Mater Med, 2002. 13(8): p 745-750.

[78] R. Pires *et al*, *Stray-field imaging and multimuclear magnetic resonance spectroscopy studies on the setting of a commmercial glass-ionomer cement*. J Mater Sci Mater Med, 2004. 15: p 201-208.

[79] Lloyd *et al*, *Solid state spatially resolved H and F nuclear magnetic resonance spectroscopy of dental materials by stray-field imaging*. J Mater Sci Mater Med, 1999. 10(6): p 369-373.

9. Appendices

Appendix I –

Batch Calculations for the Substituted Ionomer Glasses.

Strontium Series Batch Calculations

SerenoCEM Glass **Commercial**

Material	Weight	Oxides in the glass				
		SiO_2	Al_2O_3	P_2O_5	CaO	CaF_2
SiO_2	2160	2160				
Al_2O_3	1190		1190			
$AlPO_4$	2984		1247.492	1736.903		
$CaCO_3$	2420				1355.742	
CaF_2	1247					1247
Total	10001	**2160**	**2437.492**	**1736.903**	**1355.742**	**1247**
					Total	**8937.137**

$2AlPO_4 = Al_2O_3 + P_2O_5$

$2AlPO_4 = Al_2O_3$ **Raw material factor = 2.392**

$2AlPO_4 = P_2O_5$ **Raw material factor = 1.718**

$CaCO_3 = CaO + CO_2$

$CaCO_3 = CaO$ **Raw material factor = 1.785**

Oxide	Wt %
SiO_2	24.16881
Al_2O_3	27.27374
P_2O_5	19.43467
CaO	15.16976
CaF_2	13.95301
Total	100

New SerenoCEM Glass

$2Al(OH)_3 = Al_2O_3 + 3H_2O$

$2Al(OH)_3 = Al_2O_3$ **Raw material factor = 1.530012**

$2CaHPO_4 = 2CaO + P_2O_5 + H2O$

$2CaHPO_4 = 2CaO$ **Raw material factor = 2.426129**

$2CaHPO_4 = P_2O_5$ **Raw material factor = 1.917148**

Raw Mat	Wt Oxide x Raw Mat Factor	Wt %	For 200g	For 300g
SiO_2	24.169 x 1	24.1688	48.3376	72.5064
$Al(OH)_3$	27.274 x 1.530	41.7292	83.4583	125.1875
$CaHPO_4$	19.434 x 1.917	37.2591	74.5183	111.7774
$CaCO_3$	-	-	-	-
CaF_2	13.953 x 1	13.9530	27.9060	41.8590
	Total	117.1101	234.2202	351.3304

nb 37.2593g of $CaHPO_4$ gives 15.3575g of CaO and therefore no $CaCO_3$ is added.

Oxide	Mol	Mol %	
SiO_2	0.402	**31.945**	
Al_2O_3	0.267	**21.242**	
P_2O_5	0.137	**10.875**	
CaO	***0.274***	**21.747**	**Due to above slight excess**
CaF_2	0.179	**14.191**	
Total	**1.259**	**100**	

Strontium Substituted SerenoCEM Glass

$2SrHPO_4 = 2SrO + H_2O + P_2O_5$

$2SrHPO_4 = 2SrO$ **Raw material factor = 1.771859**

$2SrHPO_4 = P_2O_5$ **Raw material factor = 2.587373**

Original Mol Ratio **$4.50SiO_2$-$2.99Al_2O_3$-$1.53P_2O_5$-$3.07CaO$-$2.00CaF_2$**

SC(Al 5Ca/0Sr)

Oxide	Mol	Mol %	Mol ratio	RMM	Wt	Wt %
SiO_2	0.402	**31.945**	4.50	60.08	1919.282	24.124
Al_2O_3	0.267	**21.242**	2.99	101.96	2165.849	27.223
P_2O_5	0.137	**10.875**	1.53	141.92	1543.337	19.398
CaO	0.274	**21.747**	3.06	56.08	1219.558	15.329
CaF_2	0.179	**14.191**	2.00	78.08	1108.03	13.927
Total	**1.259**	**100**			**7956.056**	**100**

Raw Mat	Wt for 100g		
SiO_2	24.124		
$Al(OH)_3$	41.651		
$CaHPO_4$	37.189	**Giving CaO**	15.32868
$CaCO_3$	0.000		
CaF_2	13.927		
Total	116.891		

SC(Al 4Ca/1Sr)

Oxide	Mol	Mol %	Mol ratio	RMM	Wt	Wt %
SiO_2	0.402	**31.945**	4.50	60.08	1919.282	23.142
Al_2O_3	0.267	**21.242**	2.99	101.96	2165.849	26.115
P_2O_5	0.137	**10.875**	1.53	141.92	1543.337	18.609
CaO	0.274	**21.747**	3.06	56.08	1219.558	14.705
CaF_2	0.089	**7.095**	1.00	78.08	554.015	6.680
SrF_2	0.089	**7.095**	1.00	125.62	891.334	10.748
Total	**1.259**	**100**			**8293.375**	**100**

Raw Mat	Wt for 100g		
SiO_2	23.142		
$Al(OH)_3$	39.957		
$CaHPO_4$	35.677	**Giving CaO**	14.705
$CaCO_3$	0.000		
CaF_2	6.680		
SrF_2	10.748		
Total	116.204		

SC(Al 3Ca/2Sr)

Oxide	Mol	Mol %	Mol ratio	RMM	Wt	Wt %
SiO_2	0.402	**31.945**	4.50	60.08	1919.282	22.238
Al_2O_3	0.267	**21.242**	2.99	101.96	2165.849	25.095
P_2O_5	0.137	**10.875**	1.53	141.92	1543.337	17.882
CaO	0.274	**21.747**	3.06	56.08	1219.558	14.130
CaF_2	0	**0**	0.00	78.08	0	0
SrF_2	0.179	**14.191**	2.00	125.62	1782.668	20.655
Total	**1.259**	**100.000**			**8630.694**	**100**

Raw Mat	Wt for 100g		
SiO_2	22.238		
$Al(OH)_3$	38.395		
$CaHPO_4$	34.282	**Giving CaO**	14.130
$CaCO_3$	0.000		
CaF_2	0.000		
SrF_2	20.655		
Total	115.570		

SC(Al 2Ca/3Sr)

Oxide	Mol	Mol %	Mol ratio	RMM	Wt	Wt %
SiO_2	0.402	**31.945**	4.50	60.08	1919.282	21.384
Al_2O_3	0.267	**21.242**	2.99	101.96	2165.849	24.131
P_2O_5	0.137	**10.875**	1.53	141.92	1543.337	17.195
CaO	0.183	**14.498**	2.04	56.08	813.039	9.059
SrO	0.091	**7.249**	1.02	103.62	751.133	8.369
CaF_2	0	**0**	0.00	78.08	0	0
SrF_2	0.179	**14.191**	2.00	125.62	1782.668	19.862
Total	**1.259**	**100**			**8975.308**	**100**

Raw Mat	Wt for 100g		
SiO_2	21.384		
$Al(OH)_3$	36.921		
$SrHPO_4$	14.830	**Giving SrO**	8.370
$CaHPO_4$	21.977	**Giving CaO**	9.059
SrO	0.000		
CaF_2	0.000		
SrF_2	19.862		
Total	114.975		

SC(Al 1Ca/4Sr)

Oxide	Mol	Mol %	Mol ratio	RMM	Wt	Wt %
SiO_2	0.402	**31.945**	4.50	60.08	1919.282	20.593
Al_2O_3	0.267	**21.242**	2.99	101.96	2165.849	23.239
P_2O_5	0.137	**10.875**	1.53	141.92	1543.337	16.560
CaO	0.091	**7.249**	1.02	56.08	406.519	4.362
SrO	0.183	**14.498**	2.04	103.62	1502.266	16.119
CaF_2	0	**0**	0	78.08	0	0
SrF_2	0.179	**14.191**	2.00	125.62	1782.668	19.128
Total	**1.259**	**100**			**9319.922**	**100**

Raw Mat	Wt for 100g		
SiO_2	20.593		
$Al(OH)_3$	35.556		
$SrHPO_4$	28.564	**Giving SrO**	16.121

$CaHPO_4$	10.582	Giving CaO	4.362
SrO	0.000		
CaF_2	0.000		
SrF_2	19.128		
Total	114.423		

SC(Al 0Ca/5Sr)

Oxide	Mol	Mol %	Mol ratio	RMM	Wt	Wt %
SiO_2	0.402	**31.945**	4.50	60.08	1919.282	19.859
Al_2O_3	0.267	**21.242**	2.99	101.96	2165.849	22.410
P_2O_5	0.137	**10.875**	1.53	141.92	1543.337	15.969
CaO	0	**0**	0	56.08	0	0
SrO	0.274	**21.747**	3.06	103.62	2253.399	23.316
CaF_2	0	**0**	0	78.08	0	0
SrF_2	0.179	**14.191**	2.00	125.62	1782.668	18.445
Total	**1.259**	**100**			**9664.535**	**100**

Raw Mat	Wt for 100g		
SiO_2	19.859		
$Al(OH)_3$	34.288		
$SrHPO_4$	41.318	Giving SrO	23.319
$CaHPO_4$	0.000		
SrO	0.000		
CaF_2	0.000		
SrF_2	18.445		
Total	113.910		

100%x **x=Calcium, Strontium or Barium**

Calcium

Oxide	Mol	Mol%	Mol ratio	RMM	m=nxRMM	Wt%
SiO_2	0.402	31.930	4.50	60.0843	1918.4979	24.1142
Al_2O_3	0.267	21.207	2.99	101.9612	2162.3225	27.1789
P_2O_5	0.137	10.882	1.53	141.9446	1544.5918	19.4145
CaO	0.274	21.763	3.07	56.0774	1220.4295	15.3400
CaF_2	0.179	14.218	2.00	78.0748	1110.0389	13.9524
Totals	**1.259**	**100**			**7955.8805**	

Raw Mat	Wt for 100g	150g
SiO_2	24.114	36.171
$Al(OH)_3$	41.585	62.378
$NH_4H_2PO_4$	31.465	47.198
$CaCO_3$	27.379	41.068
CaF_2	13.952	20.929
Total	**138.496**	**207.744**

Strontium

Oxide	Mol	Mol%	Mol ratio	RMM	m=nxRMM	Wt%
SiO_2	0.402	31.930	4.50	60.0843	1918.4979	19.8469
Al_2O_3	0.267	21.207	2.99	101.9612	2162.3225	22.3693
P_2O_5	0.137	10.882	1.53	141.9446	1544.5918	15.9788
SrO	0.274	21.763	3.07	103.6194	2255.1005	23.3291
SrF_2	0.179	14.218	2.00	125.6168	1785.9736	18.4759
Totals	**1.259**	**100**			**9666.4863**	

Raw Mat	Wt for 100g	150g
SiO_2	19.847	29.770
$Al(OH)_3$	34.226	51.340
$NH_4H_2PO_4$	25.897	38.846
$SrCO_3$	33.237	49.856
SrF_2	18.476	27.714
Total	**131.684**	**197.525**

Barium

Oxide	Mol	Mol%	Mol ratio	RMM	m=nxRMM	Wt%
SiO_2	0.402	31.930	4.50	60.0843	1918.4979	16.7481
Al_2O_3	0.267	21.207	2.99	101.9612	2162.3225	18.8767
P_2O_5	0.137	10.882	1.53	141.9446	1544.5918	13.4840
BaO	0.274	21.763	3.07	153.3264	3336.8891	29.1304
BaF_2	0.179	14.218	2.00	175.3238	2492.6895	21.7607
Totals	**1.259**	**100**			**11454.991**	

Raw Mat	Wt for 100g	150g
SiO_2	16.748	25.122
$Al(OH)_3$	28.882	43.324
$NH_4H_2PO_4$	21.854	32.780
$BaCO_3$	37.492	56.238
BaF_2	21.761	32.641
Total	**126.737**	**190.105**

60%x40%Ca

Strontium

Oxide	Mol	Mol%	Mol ratio	RMM	m=nxRMM	Wt%	Raw Mat	Wt for 100g	150g
SiO_2	0.402	31.930	4.50	60.0843	1918.4979	21.3390	SiO_2	21.339	32.009
Al_2O_3	0.267	21.207	2.99	101.9612	2162.3225	24.0511	$Al(OH)_3$	36.800	55.199
P_2O_5	0.137	10.882	1.53	141.9446	1544.5918	17.1802	$NH_4H_2PO_4$	27.844	41.766
SrO	0.274	21.763	3.07	103.6194	2255.1005	25.0830	$SrCO_3$	35.736	53.604
CaF_2	0.179	14.218	2.00	78.0748	1110.0389	12.3467	CaF_2	12.347	18.520
Totals	**1.259**	**100**			**8990.5515**		**Total**	**134.066**	**201.099**

Barium

Oxide	Mol	Mol%	Mol ratio	RMM	m=nxRMM	Wt%	Raw Mat	Wt for 100g	150g
SiO_2	0.402	31.930	4.50	60.0843	1918.4979	19.0472	SiO_2	19.047	28.571
Al_2O_3	0.267	21.207	2.99	101.9612	2162.3225	21.4679	$Al(OH)_3$	32.847	49.271
P_2O_5	0.137	10.882	1.53	141.9446	1544.5918	15.3350	$NH_4H_2PO_4$	24.854	37.280
BaO	0.274	21.763	3.07	153.3264	3336.8891	33.1292	$BaCO_3$	42.638	63.958
CaF_2	0.179	14.218	2.00	78.0748	1110.0389	11.0207	CaF_2	11.021	16.531
Totals	**1.259**	**100**			**10072.34**		**Total**	**130.407**	**195.611**

60%x40%Sr

Calcium

Oxide	Mol	Mol%	Mol ratio	RMM	m=nxRMM	Wt%	Raw Mat	Wt for 100g	150g
SiO_2	0.402	31.930	4.50	60.0843	1918.4979	22.2259	SiO_2	22.226	33.339
Al_2O_3	0.267	21.207	2.99	101.9612	2162.3225	25.0506	$Al(OH)_3$	38.329	57.493
P_2O_5	0.137	10.882	1.53	141.9446	1544.5918	17.8942	$NH_4H_2PO_4$	29.001	43.502
CaO	0.274	21.763	3.07	56.0774	1220.4295	14.1387	$CaCO_3$	25.235	37.852

SrF_2	0.179	14.218	2.00	125.6168	1785.9736	20.6906	SrF_2	20.691	31.036
Totals	**1.259**	**100**			**8631.8153**		**Total**	**135.481**	**203.222**

Barium

Oxide	Mol	Mol%	Mol ratio	RMM	m=nxRMM	Wt%	Raw Mat	Wt for 100g	150g
SiO_2	0.402	31.930	4.50	60.0843	1918.4979	17.8494	SiO_2	17.849	26.774
Al_2O_3	0.267	21.207	2.99	101.9612	2162.3225	20.1179	$Al(OH)_3$	30.782	46.172
P_2O_5	0.137	10.882	1.53	141.9446	1544.5918	14.3706	$NH_4H_2PO_4$	23.291	34.936
BaO	0.274	21.763	3.07	153.3264	3336.8891	31.0458	$BaCO_3$	39.957	59.935
SrF_2	0.179	14.218	2.00	125.6168	1785.9736	16.6164	SrF_2	16.616	24.925
Totals	**1.259**	**100**			**10748.275**		**Total**	**128.495**	**192.742**

60%x40%Ba

Calcium

Oxide	Mol	Mol%	Mol ratio	RMM	m=nxRMM	Wt%	Raw Mat	Wt for 100g	150g
SiO_2	0.402	31.930	4.50	60.0843	1918.4979	20.5439	SiO_2	20.544	30.816
Al_2O_3	0.267	21.207	2.99	101.9612	2162.3225	23.1548	$Al(OH)_3$	35.428	53.142
P_2O_5	0.137	10.882	1.53	141.9446	1544.5918	16.5400	$NH_4H_2PO_4$	26.807	40.210
CaO	0.274	21.763	3.07	56.0774	1220.4295	13.0688	$CaCO_3$	23.325	34.988
BaF_2	0.179	14.218	2.00	175.3238	2492.6895	26.6925	BaF_2	26.693	40.039
Totals	**1.259**	**100**			**9338.5311**		**Total**	**132.796**	**199.195**

Strontium

Oxide	Mol	Mol%	Mol ratio	RMM	m=nxRMM	Wt%	Raw Mat	Wt for 100g	150g
SiO_2	0.402	31.930	4.50	60.0843	1918.4979	18.4948	SiO_2	18.495	27.742
Al_2O_3	0.267	21.207	2.99	101.9612	2162.3225	20.8453	$Al(OH)_3$	31.895	47.842
P_2O_5	0.137	10.882	1.53	141.9446	1544.5918	14.8902	$NH_4H_2PO_4$	24.133	36.199

SrO	0.274	21.763	3.07	103.6194	2255.1005	21.7397	**$SrCO_3$**	30.973	46.460
BaF_2	0.179	14.218	2.00	175.3238	2492.6895	24.0301	**BaF_2**	24.030	36.045
Totals	**1.259**	**100**			**10373.202**		**Total**	**129.525**	**194.288**

100%xNOF_2

Strontium

Oxide	Mol	Mol%	Mol ratio	RMM	m=nxRMM	Wt%	Raw Mat	Wt for 100g	150g
SiO_2	0.402	31.930	4.50	60.0843	1918.4979	20.5105	**SiO_2**	20.511	30.766
Al_2O_3	0.267	21.207	2.99	101.9612	2162.3225	23.1172	**$Al(OH)_3$**	35.371	53.056
P_2O_5	0.137	10.882	1.53	141.9446	1544.5918	16.5131	**$NH_4H_2PO_4$**	26.763	40.144
SrO	0.453	35.981	5.07	103.6194	3728.3231	39.8592	**$SrCO_3$**	56.788	85.182
Totals	**1.259**	**100**			**9353.7353**		**Total**	**139.432**	**209.149**

Raw Materials Factors

$2NH_4H_2PO_4 = P_2O_5 + 3H_2O + 2NH_3$
Factor = 2 x (115.0255)/141.9446 **1.62071**

$CaCO_3 = CaO + CO_2$
Factor = 100.0869/56.0774 **1.78480**

$SrCO_3 = SrO + CO_2$
Factor = 147.6289/103.6194 **1.42472**

$BaCO_3 = BaO + CO_2$
Factor = 197.3359/153.3264 **1.28703**

$2Al(OH)_3 = Al_2O_3 + 3H_2O$
Factor= 2 x (78.0034)/101.9612 **1.53006**

RMM's

CaO	56.0774	**$NH_4H_2PO_4$**	115.0255
Al_2O_3	101.9612	**$SrCO_3$**	147.6289
SiO_2	60.0843	**$CaCO_3$**	100.0869
P_2O_5	141.9446	**$BaCO_3$**	197.3359
SrO	103.6194	**CO_2**	44.0095
BaO	153.3264	**H_2O**	18.0152
CaF_2	78.0748	**NH_3**	17.0304
BaF_2	175.3238	**$Al(OH)_3$**	78.0034
SrF_2	125.6168		

Appendix II –

Molar Cement Weight Calculations for Cement Fabrication.

Molar Equivalents Calculation for Cement Fabrication

Molar Equivalents:

$4.5SiO_2.3Al_2O_3.1.5P_2O_5.3CaO.2CaF_2$

Si	28.0855
O	15.9994
Al	26.98154
P	30.97376
Ca	40.08
F	18.9984
Sr	87.62
Ba	137.34

	SC/100 Ca	100 Sr	100 Ba	No F	CaSr
Si	9	9	9	9	9
Al	12	12	12	12	12
P	6	6	6	6	6
Gr II	10	10	10	10	6:4
F	8	8	8	0	8
O	57	57	57	61	57
Mw Total	2227.1435	2702.544	3199.744	2614.554	2417.304
Weight	1	1.213457	1.436703	1.173949	1.085383
No Moles	0.000449	0.000449	0.000449	0.000449	0.000449

n=m/MW

CaBa	SrCa	SrBa	BaCa	BaSr	Sr1	Sr2	Sr3	Sr4
9	9	9	9	9	9	9	9	9
12	12	12	12	12	12	12	12	12
6	6	6	6	6	6	6	6	6
6:4	6:4	6:4	6:4	6:4	8:2	6:4	4:6	2:8
8	8	8	8	8	8	8	8	8
57	57	57	57	57	57	57	57	57
2616.184	2512.384	2901.424	2810.704	3000.8635	2322.224	2417.304	2512.384	2607.464
1.174681	1.128074	1.302756	1.262022	1.3474046	1.042691	1.085383	1.128074	1.170766
0.000449	0.000449	0.000449	0.000449	0.000449	0.000449	0.000449	0.000449	0.000449

Sr5
9
12
6
10
8
57
2702.544
1.213457
0.000449

Appendix III

JCPDS Data.

[10-352] PDF-2 Sets 1-86 Quality: I Wavelength: 1.540598

Barium Aluminum Silicate
Paracelsian
Ba Al2 Si2 O8

Rad.: CuKa (1.5418) Filter: d-sp:
I/Icor.: Cutoff: Int.: Diffractometer
Ref.: Smith., Acta Crystallogr., 6, (1953), 613

Sys.: Monoclinic S.G.: P21/a (14) V(redu): 746.0
a: 9.076 b: 9.583 c: 8.578 A: 0.9471 C: 0.8951
A: B: 90.00 C: Z: 4 mp:
Dx: 3.342 Dm: 3.315 SS/FOM: F30= 9.7 (0.038, 81)

ea: 1.5702 nwB: 1.5824 ey: 1.5869 Sign: - 2V: 53deg
Color: Colorless
Ref.: Deer, W., Howie, R., Zussman, J., Rock Forming Minerals, 4, 160

Specimen from Benallt mine, Rhiw, Caernarvonshire, Wales, UK.

Hanawalt: 4.00/X 3.80/7 2.99/5 2.73/5 2.56/5 3.59/5 2.37/5 2.19/5 3.29/4 3.01/4
Max-d: 6.58/2 6.38/2 5.22/1 4.00/X 3.80/7 3.70/1 3.59/5 3.29/4 3.19/2 3.12/1

d[A]	2Theta	Int.	h k l	d[A]	2Theta	Int.	h k l
6.5800	13.446	20	-1 1 0	2.3700	37.934	45	-1 2 3
6.3800	13.869	20	0 1 1	2.2800	39.492	4	4 0 0
5.2200	16.972	8	1 1 1	2.2300	40.416	20	2 3 2
4.0000	22.206	100	-2 0 1	2.1900	41.187	45	-4 0 1
3.8000	23.391	70	-1 2 1	2.1600	41.786	6	-2 2 3
3.7000	24.032	6	-2 1 1	2.1400	42.195	16	-4 1 1
3.5900	24.780	45	-1 1 2	2.0500	44.142	8	-4 2 0
3.2900	27.081	35	-2 2 0	2.0300	44.600	8	3 1 3
3.1900	27.947	16	0 2 2	1.8740	48.541	20	1 5 0
3.1200	28.587	8	-2 0 2	1.8490	49.241	10	4 3 0
3.0700	29.063	8	2 2 1	1.8310	49.757	6	1 5 1
3.0100	29.655	35	-1 3 0	1.8070	50.464	6	-4 3 1
2.9900	29.858	50	0 3 1	1.7980	50.735	8	-2 2 4
2.9600	30.168	30	2 1 2	1.7820	51.223	8	5 1 0
2.8800	31.027	6	3 1 0	1.7440	52.423	8	-3 3 3
2.7300	32.778	50	3 1 1	1.7180	53.278	14	1 5 2
2.6200	34.196	20	1 1 3	1.6640	55.151	14	-5 2 1
2.6100	34.331	35	2 3 0	1.5900	57.955	20	-1 2 5
2.5600	35.023	50	0 3 2	1.5510	59.557	16	5 3 1
2.3900	37.604	20	-3 1 2				

[15-776] PDF-2 Sets 1-86 Quality: I Wavelength: 1.540598

Aluminum Silicate
Mullite, syn
Al6 Si2 O13

Rad.: CuKa1 (1.54056) Filter: Beta Ni d-sp:
I/Icor.: Cutoff: Int.: Diffractometer
Ref.: Natl. Bur. Stand. (U.S.) Monogr. 25, 3, (1964), 3

Sys.: Orthorhombic S.G.: Pbam (55) V(redu): 167.3
a: 7.5456 b: 7.6898 c: 2.8842 A: 0.9812 C: 0.3751
A: B: C: Z: .75 mp:
Dx: 3.170 Dm: 3.000 SS/FOM: F30= 59.9 (.0135, 37)

---

ca: 1.637 nwB: 1.641 ey: 1.652 Sign: + 2V: 45-50deg
Color: Colorless
Ref.: Winchell., Elements of Optical Mineralogy, 2, 401

Sample was prepared from stoichiometric mixture of \Al2 O3\ and \Si O2 !x H2 O\. Sample was repeatedly ground and heated up to // temperature of 1725 C. Spectrographic analysis: 0.01 to 0.1% Fe, and 0.001 to 0.01% each // of Ca, Cr, Mg, Mn, Ni, Ti and Zr. // Pattern taken at 25 C. // Chemical analysis showed \Al2 O3\ 61.6, \Si O2\ 38 (mole%).

Hanawalt: 3.39/X 3.43/X 2.21/6 5.39/5 2.54/5 2.69/4 1.52/4 2.12/3 2.89/2 2.29/2
Max-d: 5.39/5 3.77/1 3.43/X 3.39/X 2.89/2 2.69/4 2.54/5 2.43/1 2.39/1 2.31/1

---

d[A]	2Theta	Int.	h k l	d[A]	2Theta	Int.	h k l
5.3900	16.433	50	1 1 0	1.3932	67.132	< 2	1 1 2
3.7740	23.554	8	2 0 0	1.3494	69.618	6 U	2 0 2
3.4280	25.971	95	1 2 0	1.3462	69.808	6 U	4 4 0
3.3900	26.268	100	2 1 0	1.3356	70.444	12	1 5 1
2.8860	30.961	20	0 0 1	1.3290	70.846	5 U	1 2 2
2.6940	33.229	40	2 2 0	1.3266	70.993	5 U	2 1 2
2.5420	35.279	50	1 1 1	1.3172	71.578	4	5 1 1
2.4280	36.994	14	1 3 0	1.3120	71.906	3	3 5 0
2.3930	37.555	< 2	3 1 0	1.3004	72.649	4	5 3 0
2.3080	38.993	4	0 2 1	1.2814	73.903	7	0 6 0
2.2920	39.277	20	2 0 1	1.2771	74.193	13	2 5 1
2.2060	40.875	60	1 2 1	1.2714	74.582	6	2 2 2
2.1210	42.591	25	2 3 0	1.2630	75.164	12	5 2 1
2.1060	42.909	8	3 2 0	1.2574	75.557	< 2	6 0 0
1.9690	46.060	2	2 2 1	1.2396	76.838	6	1 3 2
1.9230	47.228	2	0 4 0	1.2349	77.185	2	3 1 2

1.8870	48.185	8	4	0	0	1.2199	78.314	2	4	4	1
1.8630	48.846	< 2	1	4	0	1.2131	78.838	< 2	2	6	0
1.8410	49.469	10	3	1	1	1.1924	80.482	4	2	3	2
1.7954	50.813	< 2	3	3	0	1.1855	81.048	3	5	3	1
1.7125	53.463	6	2	4	0	1.1457	84.496	< 2	4	0	2
1.7001	53.884	14	3	2	1	1.1190	87.004	1	2	6	1
1.6940	54.094	10	4	2	0	1.1032	88.572	4	2	4	2
1.5999	57.563	20	0	4	1	1.0981	89.092	5	4	2	2
1.5786	58.414	12	4	0	1	1.0548	93.820	< 2	2	7	0
1.5644	58.996	2	1	4	1	1.0172	98.449	4	1	7	1
1.5461	59.765	2	4	1	1	1.0133	98.962	4	2	5	2
1.5242	60.713	35	3	3	1	1.0065	99.872	8	3	7	0
1.5067	61.494	< 2	1	5	0						
1.4811	62.676	< 2	5	1	0						
1.4731	63.055	< 2	2	4	1						
1.4605	63.663	8	4	2	1						
1.4421	64.573	18	0	0	2						
1.4240	65.495	4	2	5	0						
1.4046	66.516	8	5	2	0						

|15-876| PDF-2 Sets 1-86 Quality: * Wavelength: 1.540598

Calcium Fluoride Phosphate
Fluorapatite, syn
Ca5 (P O4)3 F

Rad.: CuKa1 (1.54056) Filter: Beta Ni d-sp: Diffractometer
I/Icor.: 1.50 Cutoff: Int.:
Ref.: Natl. Bur. Stand. (U.S.) Monogr. 25, 3, (1964), 22

Sys.: Hexagonal S.G.: P63/m (176) V(redu): 523.2
a: 9.3684 b: c: 6.8841 C: 0.7348
A: B: C: Z: 2 mp:
Dx: 3.201 Dm: 3.150 SS/FOM: F30= 73.0 (.0121, 34)

---

ea: 1.628 nwB: 1.633 ey: Sign: - 2V:
Ref.: Dana's System of Mineralogy, 7th Ed., II, (1951), 879

Prepared at NBS, Gaithersburg, MD, USA, from \Ca3 (P O4)2\. Spectroscopic analysis: 0.1 to 1.0% each of Mg and Na; and 0.01 to // 0.1% each of Al, Ba, Ge, Fe, Si, and Sr. // Pattern taken at 25 C. // To replace 3-736, 34-11 and 35-496. See ICSD 1709, 1710, 9444, 9445, 24236, 27829, 27830, 30261, 34228, 34229, 34230, 66453 and 66454 (PDF 70-796, 70-797, 71-880, 71-881, // 73-1727, 75-915, 76-558, 76-559, 76-560 and 79-1459).

Hanawalt: 2.80/X 2.70/6 2.77/6 3.44/4 2.62/3 1.84/3 1.94/3 2.25/2 3.07/2 1.80/2
Max-d: 8.12/1 5.25/1 4.68/1 4.06/1 3.87/1 3.49/1 3.44/4 3.17/1 3.07/2 2.80/X

---

d[A]	2Theta	Int.	h k l	d[A]	2Theta	Int.	h k l
8.1200	10.887	8	1 0 0	2.0280	44.647	2	4 0 0
5.2500	16.874	4	1 0 1	1.9970	45.378	4	2 0 3
4.6840	18.931	< 1	1 1 0	1.9370	46.866	25	2 2 2
4.0550	21.901	8	2 0 0	1.8840	48.267	14	3 1 2
3.8720	22.950	8	1 1 1	1.8620	48.874	4	3 2 0
3.4940	25.473	< 1	2 0 1	1.8370	49.584	30	2 1 3
3.4420	25.864	40	0 0 2	1.7970	50.765	16	3 2 1
3.1670	28.154	14	1 0 2	1.7710	51.564	14	4 1 0
3.0670	29.092	18	2 1 0	1.7480	52.294	14	4 0 2
2.8000	31.937	100	2 1 1	1.7220	53.145	16	0 0 4
2.7720	32.268	55	1 1 2	1.6840	54.442	< 1	1 0 4
2.7020	33.128	60	3 0 0	1.6370	56.141	6	3 2 2
2.6240	34.142	30	2 0 2	1.6070	57.285	4	3 1 3
2.5170	35.641	6	3 0 1	1.5800	58.357	2	5 0 1
2.2890	39.330	8	2 1 2	1.5620	59.096	< 1	3 3 0
2.2500	40.041	20	3 1 0	1.5340	60.285	6	4 2 0

2.2180	40.644	4	2	2	1	1.5240	60.722	4	3 3 1
2.1400	42.195	6	3	1	1	1.5010	61.753	4	2 1 4
2.1280	42.444	4	3	0	2	1.4970	61.936	4	4 2 1
2.0610	43.894	6	1	1	3	1.4680	63.300	8	5 0 2

|17-609| PDF-2 Sets 1-86 Quality: I Wavelength: 1.540598

Strontium Fluoride Phosphate
Sr5 (P O4)3 F

Rad.: CuKa1 (1.5405) Filter: Beta Ni d-sp: 114.6
I/Icor.: Cutoff: Int.: Densitometer
Ref.: Central Research Laboratory, The General Electric Company Limited, Wembly, England., Private Communication, (1964)

Sys.: Hexagonal S.G.: P63/m (176) V(redu): 596.7
a: 9.776 b: c: 7.210 C: 0.7375
A: B: C: Z: 2 mp:
Dx: Dm: SS/FOM: F30= 34.1 (.0163, 54)

ca: nwB: ey: Sign: 2V:

A phosphor incorporating 1.0% Mn as activator; prepared from mixture of \Sr H P O4\, \Sr C O3\ and \Sr F2\ by heat treatment at // 1200 C in nitrogen atmosphere. D=2.92 deliberately not chosen as second Hanawalt line because of // proximity to d=2.90.

Hanawalt: 2.90/X 2.93/X 2.82/6 3.32/3 2.02/3 1.92/3 3.20/3 2.03/3 1.85/3 4.23/2
Max-d: 4.23/2 4.05/1 3.61/2 3.32/3 3.20/3 2.93/X 2.90/X 2.82/6 2.75/1 2.40/1

d[A]	2Theta	Int.	h k l	d[A]	2Theta	Int.	h k l
4.2300	20.985	16	2 0 0	1.8030	50.584	16	0 0 4
4.0500	21.929	8	1 1 1	1.7100	53.547	4	3 2 2
3.6100	24.641	16	0 0 2	1.6480	55.733	2	5 0 1
3.3200	26.832	30	1 0 2	1.6000	57.559	4	4 2 0
3.2000	27.858	25	2 1 0	1.5880	58.035	4	4 0 3
2.9250	30.538	95	2 1 1	1.5710	58.724	6	2 1 4
2.9010	30.797	100	1 1 2	1.5620	59.096	6	4 2 1
2.8220	31.681	55	3 0 0	1.5330	60.328	4	5 0 2
2.7450	32.594	4	2 0 2	1.5210	60.854	10	5 1 0
2.4040	37.377	6	2 1 2	1.5110	61.300	4	3 2 3
2.3480	38.303	10	3 1 0	1.4880	62.353	10	5 1 1
2.2320	40.378	10	3 1 1	1.3670	68.596	4	4 3 1
2.1570	41.846	10	1 1 3	1.3490	69.642	6	3 3 3
2.0310	44.577	25	4 0 1	1.3320	70.662	6	4 2 3
2.0230	44.763	30	2 2 2	1.3150	71.716	10	2 1 5
1.9670	46.110	15	3 1 2	1.2900	73.329	10	4 1 4
1.9220	47.254	30	2 1 3	1.2710	74.610	10	6 1 1
1.8750	48.513	16	3 2 1				
1.8470	49.297	25	4 1 0				
1.8250	49.932	16	4 0 2				

[37-462] PDF-2 Sets 1-86 Quality: * Wavelength: 1.540598

Strontium Aluminum Silicate
Slawsonite
Sr Al2 Si2 O8

Rad.: CuKa1 (1.54060) Filter: d-sp: Diffractometer
I/Icor.: Cutoff: Int.: Diffractometer
Ref.: Erd. R., U.S. Geological Survey, Menlo Park, California, USA., Private Communication. (1984)

Sys.: Monoclinic S.G.: P21/a (14) V(redu): 693.7
a: 8.895(1) b: 9.359(1) c: 8.333(1) A: 0.9504 C: 0.8904
A: B: 90.23(1) C: Z: 4 mp:
Dx: 3.044 Dm: 3.050 SS/FOM: F30= 22.4 (.0137, 98)

---

ea: 1.573(2) nwB: 1.581(2) ey: 1.587(2) Sign: - 2V: 83deg
Color: Colorless

Specimen from Triassic Martin Bridge Formation, Wallowa Mountains. // Wallowa County, Oregon, USA. Chemical analysis (wt.%): \Si O2\ 38.68, \Al2 O3\ 29.32, \Fe2 O3\ 1.14, CaO 2.26, SrO 26.60, minor \Ti O2\, MgO, FeO, \Na2 O\, \K2 O\, \H2 O\@+, \H2 O\@-: \(Na0.01 K0.01 Ca0.13 Sr0.82 Mg0.02) // (Al1.85 Fe0.04 Ti0.01) Si2.07 O8\. // Dx for the empirical formula = 3.044. // To replace 17-140 and 29-1296.

Hanawalt: 3.22/X 3.93/8 3.71/8 2.92/5 2.94/4 2.67/4 2.68/4 2.55/4 1.83/3 3.50/3
Max-d: 6.45/3 6.23/2 5.11/1 4.68/1 4.17/1 3.93/8 3.71/8 3.63/2 3.50/3 3.22/X

---

d[A]	2Theta	Int.	h k l	d[A]	2Theta	Int.	h k l
6.4500	13.718	30	1 1 0	1.8120	50.315	15	-4 2 2 M
6.2300	14.205	15	0 1 1	1.8120	50.315	15	4 3 0 M
5.1050	17.357	3	-1 1 1	1.7910	50.947	11	0 4 3 M
4.6770	18.960	3	0 2 0	1.7910	50.947	11	-1 5 1 M
4.1680	21.300	9	0 0 2	1.7690	51.627	6	4 3 1
3.9320	22.595	81	-2 0 1	1.7480	52.294	18	5 1 0 M
3.7100	23.967	75	-1 2 1	1.7480	52.294	18	2 2 4 M
3.6250	24.537	20	-2 1 1	1.7100	53.547	7	-4 1 3 M
3.5040	25.399	31	-1 1 2	1.7100	53.547	7	5 1 1 M
3.2240	27.646	100	2 2 0	1.7030	53.785	9	4 1 3 M
3.1100	28.681	12	0 2 2	1.7030	53.785	9	-3 3 3 M
3.0340	29.416	8	2 0 2	1.6800	54.582	4	3 4 2
2.9390	30.389	43	-1 2 2	1.6320	56.328	7	-5 2 1
2.9230	30.559	51	0 3 1	1.6090	57.207	5	5 1 2
2.8880	30.939	22	2 1 2	1.5560	59.346	21	0 4 4 M

2.8270	31.624	7	3 1 0	1.5560	59.346	21	-3 5 1 M
2.6800	33.408	39	-3 1 1	1.5520	59.515	27	0 5 3
2.6730	33.498	40	3 1 1	1.5430	59.897	7	5 2 2
2.5530	35.122	37	2 3 0 M	1.5200	60.899	11	-4 3 3
2.5530	35.122	37	-1 1 3 +	1.4790	62.775	8	2 2 5 M
2.5050	35.818	21	3 2 0	1.4790	62.775	8	3 5 2 M
2.3360	38.507	29	3 1 2	1.4690	63.252	8	-2 4 4 M
2.3050	39.046	23	1 2 3	1.4690	63.252	8	0 3 5 M
2.1770	41.444	19	-2 3 2 M	1.4480	64.278	5	5 3 2
2.1770	41.444	19	2 3 2 M	1.4320	65.084	5	4 5 0
2.1470	42.050	25	4 0 1	1.4160	65.912	8	5 4 0
2.1070	42.888	8	-2 2 3	1.3940	67.089	7	2 3 5 M
2.0960	43.124	12	-4 1 1	1.3940	67.089	7	-6 2 1 M
2.0830	43.407	12	0 0 4 M	1.3900	67.307	7	-3 2 5
2.0830	43.407	12	-3 3 1 M	1.3420	70.058	8	-1 4 5 M
2.0080	45.116	9	2 4 1 M	1.3420	70.058	8	-5 4 2 M
2.0080	45.116	9	4 2 0 M	1.3390	70.238	6	6 3 0
1.9860	45.643	6	-3 1 3 M	1.3320	70.662	5	0 2 6 M
1.9860	45.643	6	-1 1 4 M	1.3320	70.662	5	4 0 5 M
1.9670	46.110	5	-4 0 2	1.3100	72.032	6	-6 0 3
1.8630	48.846	10	-3 2 3 M	1.3100	72.032	6	3 6 2 M
1.8630	48.846	10	-1 2 4 M	1.2900	73.329	11	5 5 0
1.8560	49.043	14	3 2 3 M	1.2750	74.336	7	-5 5 1
1.8560	49.043	14	-2 4 2 M				
1.8330	49.699	33	1 5 0				

[41-1486] PDF-2 Sets 1-86 Quality: * Wavelength: 1.540598

Calcium Aluminum Silicate
Anorthite, ordered
Ca Al2 Si2 O8

Rad.: CuKa1 (1.54051) Filter: Beta Ni d-sp: Diffractometer
I/Icor.:0.41 Cutoff: 22.1 Int.: Diffractometer
Ref.: Sanc, I., Polytechna, Foreign Trade Corporation, Panska, Czechoslovakia.,
ICDD Grant-in-Aid, (1990)

Sys.: Triclinic S.G.: P-1 (2) V(redu): 1338.7
a: 8.1756(10) b: 12.8720(13) c: 14.1827(17) A: 0.6351 C: 1.1018
A: 93.172(8) B: 115.911(9) C: 91.199(13) Z: 8 mp:
Dx: 2.725 Dm: 2.760 SS/FOM: F30= 9.0 (.0157,212)
Ref.: Angel, R., Carpenter, M., Finger, L., Am. Mineral., 75, (1990), 150

---

ca: 1.577 nwB: 1.585 ey: 1.590 Sign: - 2V: 78deg
Color: Colorless
Ref.: Deer, W., Howie, R., Zussman, J., Rock Forming Minerals, 4, (1963), 94

Chemical analysis (wt.%): \Si O2\ 44.3, \Al2 O3\ 34.8, CaO 19.4, \Na2 O\ 1.2,
\K2 O\ 0.3: \(Ca0.89 Na0.09 K0.02) (Al1.92 Si0.08) // Si2 O8\. // Specimen
from anorthosite dike, Stare Ransko, Czechoslovakia. // Pattern taken at 25(1)
C. // To replace 12-301 and validated by calculated pattern 20-20.

Hanawalt: 3.18/X 3.21/9 3.20/7 4.04/2 3.26/2 2.95/2 3.62/2 3.12/2 3.78/1 2.14/1
Max-d: 6.53/1 5.91/1 4.69/1 4.61/1 4.04/2 3.91/1 3.78/1 3.75/1 3.62/2 3.47/1

---

d[A]	2Theta	Int.	h k l	d[A]	2Theta	Int.	h k l
6.5292	13.551	4	-1 1 0	1.8363	49.603	5	0 -6 4
5.9129	14.971	1	0 -2 1	1.7957	50.803	9	1 1 6
4.6889	18.911	9	0 -2 2	1.7694	51.613	8	-2 0 8
4.6116	19.231	2	1 2 -2	1.7618	51.853	4	2 -4 4
4.0404	21.981	22	-2 0 2	1.7565	52.023	2	-2 6 4
3.9105	22.721	5	1 -1 2	1.7314	52.833	2	2 2 -8
3.7792	23.521	14	-1 3 0	1.7182	53.273	3	0 6 4
3.7525	23.691	10	1 1 2	1.7131	53.443	3	0 4 6
3.6230	24.551	15	1 3 0	1.6811	54.543	1	4 4 -2
3.4660	25.681	4	-1 -1 4	1.6050	57.364	2	0 8 0
3.3631	26.482	10	-1 1 4	1.6009	57.524	1	5 1 -5
3.2581	27.352	20	-2 2 0	1.5873	58.064	1	-5 1 2
3.2086	27.782	88	0 4 0	1.5708	58.734	1	0 -2 8
3.1962	27.892	69	-2 0 4	1.5410	59.984	1	-4 2 8
3.1806	28.032	100	0 0 4	1.5356	60.214	2	-3 1 9

3.1249	28.542	15	2 2 0	1.5187	60.954	2	1 1 -9
3.0384	29.372	9	2 1 1	1.4988	61.854	3	1 2 -9
2.9520	30.252	17	0 -4 2	1.4895	62.284	2	2 -7 3
2.9340	30.442	11	0 -2 4	1.4763	62.904	2	5 3 -6
2.8886	30.932	3	1 4 0	1.4541	63.974	2	1 8 2
2.8289	31.602	12	-2 2 4	1.4095	66.254	1	1 1 8
2.8073	31.852	3	1 3 -4	1.3873	67.454	4	1 9 0
2.6557	33.722	7	-1 3 4	1.3621	68.874	2	-5 4 0
2.5565	35.072	1	2 -2 2	1.3506	69.545	1	6 1 -5
2.5439	35.252	3	2 2 -5	1.3416	70.085	3	1 7 5
2.5238	35.542	10	-2 4 2	1.2977	72.825	1	1 7 -8
2.5054	35.812	9	-3 1 4	1.2753	74.315	1	0 -1 10
2.4358	36.872	2	-2 -4 3	1.2699	74.685	1	-6 3 2
2.4049	37.362	1	1 5 -2	1.2614	75.275	2	0 4 9
2.3840	37.702	2	1 -5 1	1.2329	77.335	1	5 3 2
2.3593	38.112	2	2 4 0	1.2246	77.955	1	3 0 7
2.3229	38.732	2	-3 3 2	1.2120	78.925	2	2 10 -1
2.2646	39.772	3	-1 1 6	1.2074	79.285	1	0 9 5
2.2365	40.292	2	1 -5 2	1.1689	82.446	1	1 -9 6
2.1851	41.282	1	-1 -4 5	1.1630	82.956	1	2 -1 9
2.1741	41.503	1	-3 3 0	1.1449	84.566	1	2 8 5
2.1401	42.193	14	2 -4 2	1.1265	86.286	1	2 2 9
2.1190	42.633	7	2 4 -5	1.0675	92.366	1	2 10 -8
2.0961	43.123	6	1 5 2				
2.0239	44.743	2	-4 1 3				
1.9860	45.643	3	0 6 2				
1.9317	47.003	4	-4 2 4				
1.9236	47.213	2	4 2 -4				
1.8772	48.453	3	-1 -6 4				
1.8468	49.303	4	-4 0 6				

[71-1316] PDF-2 Sets 1-86 Quality: C Wavelength: 1.540598

Barium Fluoride Phosphate
Ba5 (P O4)3 F

Rad.: CuKa1 (1.54060) Filter: d-sp: calculated
I/Icor.:3.66 Cutoff: 17.7 Int.: calculated
Ref.: Calculated from ICSD using POWD-12++, (1997)

Sys.: Hexagonal S.G.: P63/m (176) V(redu): 690.3
a: 10.15300(200) b: c: 7.73300(100) C: 0.7616
A: B: C: Z: 2 mp:
Dx: 4.765 Dm: SS/FOM: F30= 461.4 (.0020, 32)
ICSD: 010029
Ref.: Mathew, M., Mayer, I., Dickens, B., Schroeder, L.W., J. Solid State Chem., 28, (1979), 79

ca: nwB: ey: Sign: 2V:

Hanawalt: 3.05/G 3.08/G 2.93/G 3.54/G 3.32/G 2.04/G 4.40/G 2.12/G 1.91/G 2.06/G
Max-d: 8.79/3 5.81/1 5.08/5 4.40/G 4.24/G 3.87/G 3.82/2 3.54/G 3.32/G 3.08/G

d[A]	2Theta	Int.	h k l	d[A]	2Theta	Int.	h k l
8.7928	10.052	31	1 0 0	1.4398	64.687	12	6 0 1
5.8068	15.246	2	1 0 1	1.4209	65.656	16	3 4 1
5.0765	17.455	46	1 1 0	1.4146	65.986	13	3 3 3
4.3964	20.182	279	2 0 0	1.4080	66.336	23	2 5 0
4.2438	20.916	215	1 1 1	1.4022	66.645	65	1 2 5
3.8665	22.983	166	0 0 2	1.3966	66.946	38	4 2 3 +
3.8219	23.255	16	2 0 1	1.3966	66.946	38	2 3 4 +
3.5394	25.140	411	1 0 2	1.3852	67.572	37	5 2 1
3.3233	26.804	374	1 2 0	1.3703	68.405	45	6 0 2
3.0759	29.006	862	1 1 2	1.3678	68.548	26	3 0 5
3.0533	29.225	999	1 2 1	1.3619	68.892	109	4 1 4
2.9309	30.475	500	3 0 0	1.3540	69.349	33	3 4 2
2.9034	30.771	57	2 0 2	1.3466	69.784	37	1 5 3
2.7407	32.647	1	3 0 1	1.3409	70.125	22	1 6 0
2.5382	35.333	19	2 2 0	1.3230	71.217	78	5 2 2
2.5203	35.593	2	1 2 2	1.3212	71.330	35	1 6 1 +
2.4736	36.289	3	1 0 3	1.3212	71.330	35	2 2 5 +
2.4387	36.827	89	3 1 0	1.3061	72.282	1	3 1 5
2.4117	37.254	5	2 2 1	1.3009	72.618	1	5 0 4
2.3357	38.513	37	3 0 2	1.2888	73.407	5	0 0 6
2.2984	39.164	122	1 1 3	1.2752	74.322	15	1 0 6
2.2236	40.536	23	2 0 3	1.2733	74.452	12	6 0 3 M

2.1982	41.027	35	4 0 0	1.2733	74.452	12	3 3 4 M
2.1219	42.572	274	2 2 2	1.2691	74.739	37	4 4 0
2.1144	42.730	155	4 0 1	1.2669	74.896	20	1 6 2
2.0627	43.857	247	3 1 2	1.2601	75.364	46	2 4 4
2.0368	44.443	296	1 2 3	1.2561	75.649	26	3 5 0
2.0172	44.899	68	2 3 0	1.2524	75.914	5	4 4 1
1.9519	46.488	184	2 3 1	1.2492	76.141	48	1 1 6
1.9332	46.962	131	3 0 3 M	1.2399	76.819	3	7 0 1
1.9332	46.962	131	0 0 4 M	1.2356	77.129	25	5 2 3
1.9187	47.339	202	4 1 0	1.2274	77.747	30	2 3 5
1.9109	47.544	267	4 0 2	1.2230	78.074	30	1 5 4
1.8881	48.154	4	1 0 4	1.2193	78.356	17	6 2 0
1.8623	48.867	7	1 4 1	1.2058	79.407	2	4 4 2
1.8067	50.474	16	2 2 3 M	1.2045	79.516	3	6 2 1 +
1.8067	50.474	16	1 1 4 M	1.2045	79.516	3	1 4 5 +
1.7884	51.025	11	3 2 2	1.2016	79.739	3	2 1 6
1.7697	51.605	32	1 3 3 +	1.1947	80.300	54	3 5 2
1.7697	51.605	32	2 0 4 +	1.1896	80.714	11	1 6 3
1.7187	53.254	32	1 4 2	1.1798	81.522	2	3 0 6
1.7148	53.387	18	5 0 1	1.1679	82.537	4	6 0 4
1.6922	54.157	9	3 3 0	1.1646	82.815	30	7 1 0
1.6711	54.898	94	1 2 4	1.1614	83.100	16	5 0 5
1.6617	55.235	48	4 2 0	1.1577	83.423	1	4 3 4
1.6530	55.548	38	3 3 1	1.1492	84.181	28	2 2 6
1.6246	56.608	19	4 2 1	1.1416	84.869	9	3 3 5
1.6138	57.021	96	3 0 4	1.1395	85.064	31	3 1 6
1.6008	57.529	61	5 0 2	1.1381	85.191	18	2 5 4
1.5886	58.012	81	2 3 3	1.1321	85.751	5	4 2 5
1.5792	58.388	29	1 5 0	1.1292	86.029	4	3 5 3
1.5502	59.590	67	3 3 2	1.1258	86.349	2	5 4 0
1.5473	59.714	88	1 5 1	1.1151	87.381	21	1 7 2
1.5380	60.114	10	4 1 3 +	1.1141	87.488	13	5 4 1
1.5380	60.114	10	2 2 4 +	1.1118	87.709	35	4 0 6
1.5267	60.605	2	2 4 2	1.1050	88.393	19	1 5 5
1.5232	60.756	1	1 0 5	1.1018	88.714	27	1 6 4
1.5150	61.123	7	1 3 4	1.0991	88.991	15	8 0 0
1.4795	62.753	11	1 1 5	1.0966	89.248	17	6 3 1 +
1.4655	63.422	3	6 0 0	1.0966	89.248	17	1 0 7 +
1.4620	63.591	8	5 1 2				
1.4590	63.738	4	2 0 5				
1.4517	64.095	17	5 0 3 M				
1.4517	64.095	17	4 0 4 M				
1.4455	64.401	3	4 3 0				